Novel Exposure Monitoring for FAIS Prevention in Sport: Identifying High-risk Hip Motions in Soccer

By

Harvey John Marchant

A thesis

presented to the University of Waterloo

in fulfillment of the

thesis requirement for the degree of

Master of Applied Science

in

Systems Design Engineering

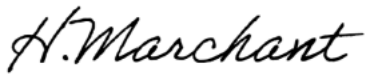
Waterloo, Ontario, Canada, 2026

© Harvey John Marchant 2026

Author's Declaration

I hereby declare that I am the sole author of this thesis. This is a true copy of the thesis, including any required final revisions, as accepted by my examiners.

I understand that my thesis may be made electronically available to the public.



Harvey Marchant

Abstract

Hip osteoarthritis (OA) is a leading cause of pain and disability worldwide and is more prevalent among former elite athletes, particularly those who participated in high-impact sports during adolescence. Femoroacetabular impingement syndrome (FAIS), a common cause of hip and groin pain in young, physically active adults, is increasingly recognized as an important precursor to early-onset hip OA. Participation in high-impact youth sports, particularly soccer, has been strongly associated with the development of cam morphology, a bony protrusion of the femoral head–neck junction, and subsequent symptomatic cam FAIS. However, the sport-specific hip kinematics and movement exposures thought to contribute to this condition remain poorly understood. While repetitive exposure to combined hip flexion, adduction, and internal rotation is thought to contribute to symptomatic cam FAIS, no validated tools currently exist to quantify the magnitude and frequency of exposure to these provocative hip positions during ecologically valid sport participation. This thesis contributed to addressing this gap through two complementary objectives. First, a wearable inertial measurement unit (IMU) system was validated against a gold-standard optical motion capture (OMC) system for quantifying 3D hip kinematics, encompassing sagittal, frontal, and transverse plane motion, during 35 soccer-specific movements performed by 20 elite adult soccer players (10 male, 10 female). Second, five supervised machine-learning classifiers were developed and evaluated to automatically identify a subset of 20 soccer-specific movements from IMU-derived signals. These movements were selected based on their kinematic relevance to cam FAIS and ecological relevance to soccer participation.

The IMU system demonstrated no significant differences between the right and left hip joint angles in sagittal (mean difference = -0.60˚ to -1.01˚, $p = 0.171$) or frontal (mean difference = -0.32˚ to +0.13˚, $p = 0.223$) plane range of motion, with very good-to-excellent waveform agreement with OMC, as indicated by the coefficient of multiple correlation (CMC2 = 0.964–0.967 and 0.853–0.876, respectively). Transverse plane internal/external rotation demonstrated a significant underestimation of ROM by the IMU (mean difference = -9.09˚ to -12.28˚, $p < 0.001$) and lower waveform agreement with OMC (CMC2 = 0.750–0.761) compared with the sagittal and frontal planes. Among the five ML classifiers evaluated, XGBoost achieved the highest overall classification performance, accurately distinguishing 20 soccer-specific movements with a macro-averaged F1-score of 0.905 and overall accuracy of 94.4%. When evaluated on continuous sliding-window data from unseen participants, classification accuracy decreased to 72.0% (F1-score = 0.759), although

misclassifications remained concentrated between kinematically similar technical actions rather than distinct movement categories.

Collectively, these findings demonstrate the feasibility of combining wearable IMUs with machine learning to provide estimates of sagittal and frontal plane hip joint angles and to distinguish a comprehensive range of soccer-specific movements associated with hip positions implicated in symptomatic cam FAIS. While further work is required to improve transverse plane measurement accuracy, develop classifiers using continuous movement data, and validate the framework in adolescent populations, this research establishes an important foundation for quantifying real-world exposure to sport-specific hip kinematics. This approach may extend beyond soccer to support movement exposure monitoring across a broader range of athletic populations at risk of cam FAIS, ultimately contributing not only to characterizing cam FAIS-related movement risk, but to the broader goal of reducing the burden of hip OA in physically active populations.

Acknowledgements

I would like to begin by expressing my sincere gratitude to all those who have supported me throughout the completion of this thesis. This work would not have been possible without the guidance, encouragement, and support of many individuals who have helped me along this challenging yet rewarding endeavour.

Please allow me to begin by thanking my supervisor, and friend, Dr. James Tung, for his invaluable mentorship, guidance, and the trust he has placed in me throughout my graduate studies. Having first crossed paths while coaching football five years ago, little did I know that we would meet again in a professional setting, let alone that he would become such an influential mentor in my academic career. Dr. Tung's commitment to my development as both an individual and a researcher has been instrumental throughout the past two years, while his encouragement, expertise, and belief in my abilities have motivated me to approach each new challenge with curiosity and determination. His compassion for and dedication to his students extend far beyond academic supervision, and I consider myself incredibly fortunate to have had the opportunity to learn from and work alongside him.

James – truly, thank you.

I would also like to thank Dr. Jordan Cannon, my co-supervisor, whose previous work and research contributions greatly influenced this thesis. Though our conversations were often few and far between, I am incredibly grateful for the wealth of knowledge, insight, and guidance that he provided at various stages of this work. Dr. Cannon ensured that I remained on track and encouraged me to consider perspectives that strengthened both my thesis and my approach to scientific inquiry. Not only did he provide invaluable academic support, but Dr. Cannon also brought a sense of familiarity to this thesis, both through our shared experiences with injury-related challenges and through his wonderful Scottish accent — a resounding reminder of home, albeit slightly further north! I thoroughly enjoyed every meeting spent laughing, reminiscing, and debating whose accent was harder to understand for Dr. Tung, and I am very thankful for the thoughtful advice he provided from start to finish.

All that I am, all that I will become, and everything that I have achieved is thanks to my family: my parents, Andy and Trixie, and my brother, George. To my parents, the selflessness that you have both embodied throughout mine and George's lives is a true testament to the remarkable people that you are. You have made countless sacrifices, from hours spent driving across the country for football, to supporting my decision to move to

Canada and enduring the distance that followed. You have always put us first, and without your unwavering love, support, and belief in me, I would not be half the person I am today. I can only hope to repay you by making the most of the incredible opportunities you have afforded me, and I promise that I will always do my best to make you as proud as you have made me.

To my closest friend, George, I am exceptionally lucky to be able to call you my brother. Your ambition, determination, and character have been constant reminders of why I have spent my life looking up to you and following closely in your footsteps. Despite our busy schedules meaning that we have not always been able to talk as much as we would have liked, I have always valued your opinion, trusted your advice, and appreciated the immense support you have provided from afar. I still recall the words you said to me when you first left to begin your adventure overseas, and I hope that I continue to live up to them as I begin this next chapter of my own.

While we may now be spread across continents, please know that you all hold an incredibly special place in my heart and thoughts. I am forever grateful for the love, support, and encouragement you continue to give me, and I hope that the distance between us closes before we know it so that we can once again share more moments together as a family.

And, to my best friend, my partner, and the love of my life, Sami. While this thesis may bear my name, this journey has never been mine alone. Every step of the way has been made easier simply because I had the privilege of walking it with you. From early mornings getting up for work, to late nights spent typing away together, and everything in between, you have shown me nothing but unconditional love, patience, and support. You have celebrated every success as if it were your own, and never once let me doubt myself when I needed you most. For that, I am forever grateful.

You are without a doubt the most empathetic, kind-hearted, and beautiful soul I have ever known, and your ability to care so deeply for the people you love is something I admire every day. Truthfully, there are no words that could ever come close to expressing the gratitude I feel for you, but I hope this serves as a small reminder of just how much you are loved, appreciated, and cherished. Thank you for believing in me, for teaching me to be a better person, and for growing alongside me. I cannot wait to see where our next adventure takes us.

I would also like to share a sincere thank you to those who have made Canada feel like home. You have all already filled my time here with countless moments that I will cherish, and I look forward to making many more memories together in the years to come.

Sandy, your endless warmth and willingness to help Sami and me whenever it was needed have meant a great deal during my time here. You made me feel welcome from the very beginning, always kept me well fed, and I am sincerely grateful to you for welcoming me into your amazing family with open arms. Your place has undoubtedly been a home away from home and your kindness knows no bounds.

Zev, thank you for your friendship and countless moments of fun that have made this journey far more enjoyable. Time spent together has always been a welcome break, filled with laughter, great conversation, and, of course, plenty of dogs. I am incredibly grateful to have gotten to know you over the past few years and am lucky to call you both a friend and family.

Ben, your generosity, support, and reassuring words, especially over the past two years, have meant more than you know and should not go unrecognized. I am deeply appreciative of your encouragement throughout this time, and I look forward to spending many more weekends pitch-side with you, cheering Sami on together.

Finally, no acknowledgement would be complete without a nod to our dog, Rooney! While you cannot read and sometimes act like you do not understand me and Sami for that matter, your companionship has made every day far brighter. Thank you for interrupting my work asking for head pats, the countless walks and welcome distractions during long days of writing, and for always reminding me that there is more to life than deadlines. You have been the best little helper we could have asked for.

Table of Contents

Author's Declaration ..... **ii**
Abstract ..... **iii**
Acknowledgements ..... **v**
List of Figures ..... **xi**
List of Tables ..... **xiv**
1 Introduction **1**
1.1 The Burden of Hip Osteoarthritis 1
1.2 Femoroacetabular Impingement Syndrome 1
1.3 Soccer as a High-Risk Sporting Environment 2
1.4 Movement-Monitoring Tools 3
1.5 Purpose and Hypotheses 4
2 Literature Review **6**
2.1 Femoroacetabular Impingement Syndrome Overview 6
2.1.1 Relevant Anatomy of the Hip 6
2.1.2 What is FAIS? 7
2.1.3 FAIS Diagnosis 11
2.1.4 Prevalence and Presentation of FAIS 15
2.2 FAIS Etiology 18
2.2.1 Genetic Predisposition 18
2.2.2 Paediatric Conditions 19
2.2.3 Proposed Mechanism: Sports Participation 21
2.3 Mechanisms of Sport-related Cam Development 28
2.3.1 Load-Induced Reactive Bone Remodelling 29
2.3.2 Developmental Alterations of the Proximal Femoral Physis 29
2.3.3 Mechanobiological Mechanisms 31
2.4 Soccer: A Model for Examining Repetitive Hip Joint Motion 33
2.4.1 Soccer Participation in Youth Athletes 33
2.4.2 Physical Demands 33
2.4.3 Technical and On-the-Ball Actions 35
2.4.4 The Role of the Training Environment 37
2.5 Quantifying Movement Exposure in Sport 38
2.5.1 Technologies for Capturing Athlete Movement 38

2.5.2 Field-based Athlete Monitoring 39
2.5.3 Laboratory-Based Motion Analysis 41
2.5.4 Wearable Inertial Measurement Units (IMUs) 43
3 Methods 49
3.1 IMU Validation 49
3.1.1 Participants and Setting 49
3.1.2 Experimental Set Up 49
3.1.3 Experimental Protocol 53
3.1.4 Data Processing 57
3.1.5 Data Analysis 60
3.2 Machine Learning Classifier 63
3.2.1 Movement Selection 64
3.2.2 Data Segmentation 65
3.2.3 Feature Extraction 68
3.2.4 Movement Classification 69
3.2.5 Classifier Evaluation 71
3.2.6 Model Generalizability to Unseen Movement Data 71
4 Results 73
4.1 Validation of IMU System 73
4.1.1 Range of Motion and Error Comparisons Between IMU and OMC Systems 73
4.1.2 Normalized RMS Error 76
4.1.3 Linear Mixed Model Analysis of RMS Error 77
4.1.4 Waveform Similarity 78
4.1.5 Bland-Altman Analysis 81
4.2 Machine-Learning Classifier 84
4.2.1 Classifier Evaluation 84
4.2.2 Best-performing Classifier Evaluation: XGBoost 85
4.3 XGBoost Classifier with a Sliding Window 89
4.3.1 Movement-Specific Classification Performance 89
4.3.2 Task vs. Other Classification 93
5 Discussion 94
5.1 Validity of IMU-derived Hip Kinematics 95
5.1.1 Sagittal and Frontal Plane Agreement 95

5.1.2 Transverse Plane (Internal/External Rotation) Limitations 96
5.1.3 Offset Correction and Waveform Agreement 98
5.2 ML Classification of Soccer-Specific Movements 99
5.2.1 Training Classification Performance Across 20 Movements 99
5.2.2 Sources of Misclassification 100
5.2.3 Participant-Level Variability 101
5.2.4 Model Generalizability 105
5.3 Limitations 106
5.4 Conclusions 111
References 113
Appendix A 130
Appendix B 131
Appendix C 136
Appendix D 137
Appendix E 140
Appendix F 149

List of Figures

Figure 1. A graphical representation of the normal anatomy of the articulating hip joint.....8

Figure 2. Pincer morphology of FAIS. The shaded region indicates excessive acetabular coverage of the femoral head.....9

Figure 3. Cam morphology of FAIS. The shaded region indicates asphericity of the femoral head and resultant flattening of the femoral head–neck junction caused by osseous protrusion.....10

Figure 4. Mixed morphology of FAIS. The shaded regions indicate the coexistence of both pincer and cam morphological changes.....10

Figure 5. Anteroposterior pelvic radiograph demonstrating cam morphology in a male pelvis. Small arrows indicate minor to moderate cam deformities at the femoral head–neck junction. The alpha angle (α) is approximated on the right femoral head, with the dotted line representing the expected spherical femoral head contour. Images are the personal medical images of the author.....13

Figure 6. Frog-leg lateral radiographs of the right and left proximal femur and acetabulum. Images are the personal medical images of the author. 13

Figure 7. Magnetic resonance imaging (MRI) of the hip joint demonstrating structural abnormalities associated with FAIS. (1) Radial view of the left hip showing the chondrolabral junction (circle). (2) Sagittal view of the right hip demonstrating focal cartilage defects (arrows). (3) Coronal view of the right hip showing cam morphology (arrow) and labral tear (circle). (4) Axial view of the pelvis demonstrating bilateral cam deformities. 15

Figure 8. Xsens MTw Awinda IMU used for 3D lower limb motion capture.....50

Figure 9. Front (left) and Back (right) view of the locations of the seven Xsens IMUs and sixteen Vicon retroreflective markers used for 3D lower-limb motion capture. 51

Figure 10. Overview of the methodological workflow used to develop and evaluate the IMU-based soccer movement ML classification models. 63

Figure 11. Example of the IMU-based repetition segmentation process using hip kinematic time-series data obtained from the OMC system during an Instep Pass (R) trial. Shaded regions indicate the ±0.25 s window surrounding each identified peak in hip flexion. Numbered annotations indicate the repetitions performed. *65*

Figure 12. Example of IMU-based repetition segmentation process using raw thigh angular velocity signals during an Instep Pass (L) trial. Positive angular velocity indicates rotation about the sensor's respective axis according to the positive direction defined by the sensor coordinate system (Top). *67*

Figure 13. Representative time-series comparison of IMU- and optical motion capture (OMC)-derived hip kinematics during selected movement tasks completed by P10, in order of appearance: Jump, Sprint to Side-step Cut to 90˚ (R), Instep Pass (R), and Dribble to Turn (R). The median repetition of each trial was selected for visualization. *76*

Figure 14. Box-and-whisker plots of pre-correction waveform similarity (CMC1) between IMU- and OMC-derived hip kinematics across movement planes for the right and left hips. Boxes represent the interquartile range, central lines indicate medians, and whiskers represent data variability. *79*

Figure 15. Box-and-whisker plots of pre-correction waveform similarity (CMC2) between IMU- and OMC-derived hip kinematics across movement planes for the right and left hips. Boxes represent the interquartile range, central lines indicate medians, and whiskers represent data variability. *81*

Figure 16. Bland–Altman plots demonstrating agreement between IMU- and OMC-derived hip kinematics across movement planes for the right and left hips. Red dashed lines represent mean bias, while black dotted lines indicate the 95% LOAs. *82*

Figure 17. Supplementary trial-level Bland-Altman plots demonstrating agreement between IMU- and OMC-derived hip kinematics across movement planes during select soccer-specific tasks. Right (black circles) and left (grey squares) are presented concurrently for visual comparison of side-specific differences. *84*

Figure 18. Subject-independent performance of the XGBoost classifier during LOSO evaluation. Classification accuracy is presented for each participant, with the overall mean per-fold accuracy indicated by the dashed red line. *87*

Figure 19. Confusion matrices illustrating task classification performance of the XGBoost classifier during model training LOSO evaluation, presented as (A) raw repetition counts and (B) row-normalized percentages (0–100%). Predicted and true class labels are shown on the x- and y-axes, respectively. Diagonal elements represent correctly classified movement repetitions, whereas off-diagonal elements indicate misclassifications between movement classes. 88

Figure 20. Confusion matrices illustrating task classification performance of the XGBoost classifier during sliding-window evaluation, presented as (A) raw window counts and (B) row-normalized percentages (0–100%). Predicted and true class labels are shown on the x- and y-axes, respectively. Diagonal elements represent correctly classified movement repetitions, whereas off-diagonal elements indicate misclassifications between movement classes. 92

Figure 21. Confusion matrix illustrating binary classification performance of the XGBoost classifier for distinguishing Task movements from the Other class during sliding-window evaluation. Predicted and true class labels are shown on the x- and y-axes, respectively, with cell values representing the number of classified windows. 93

Figure 22. Representative Vicon frames demonstrating differences in movement execution and post-task activity between P15 (top) and P06 (bottom) during an instep pass (right) repetition. P15 exhibited greater non-task movement following pass completion compared with the more discrete execution observed in P06. 102

Figure 23. Right and left hip flexion/extension kinematic time-normalized time-series traces derived from Vicon OMC (top) and Xsens IMU (red) systems during an Instep Pass (R) repetition for P15 (red) and P06 (blue). 104

List of Tables

Table 1. Anatomical locations and definitions of the sixteen retroreflective markers comprising the custom configuration based on the Vicon Plug-in Gait lower-body marker set. 52

Table 2. Summary of soccer-specific movement tasks performed by participants. Tasks are categorized as Range of Motion, Off-the-Ball, and On-the-Ball movements, with the required number of repetitions indicated. 55

Table 3. Comparison of hip joint ROM, mean differences, RMS error, and statistical comparisons of mean ROM (α = 0.05) between IMU- and optical motion capture (OMC)-derived kinematic measurements across movement planes. 74

Table 4. Comparison of hip joint motion error using mean nRMSE across movement planes. nRMSE was calculated relative to IMU- and OMC-derived ROM values to account for differences in movement magnitude. 77

Table 5. Bonferroni-adjusted pairwise comparisons of RMS error between hip joint motions following linear mixed model analysis for the right and left hips. 78

Table 6. Descriptive values of pre-correction waveform similarity (CMC1) between IMU- and OMC-derived hip kinematics across movement planes. The percentage of trials exceeding predefined good-to-excellent CMC thresholds are presented for each motion. 79

Table 7. Descriptive values of post-correction waveform similarity (CMC2) between IMU- and OMC-derived hip kinematics across movement planes. The percentage of trials exceeding predefined good-to-excellent CMC thresholds are presented for each motion. 80

Table 8. Bland–Altman analysis of agreement between IMU- and optical motion capture (OMC)-derived hip kinematics across movement planes. Mean bias, standard deviation of differences, and 95% limits of agreement are presented for the right and left hips. 81

Table 9. Performance comparison of ML classifiers for soccer-specific movement classification. Macro-averaged F1-score, precision, recall, and specificity are provided, along with overall accuracy and mean per-fold accuracy from LOSO evaluation. 85

Table 10. Class-specific performance of the XGBoost classifier for soccer-specific movement classification during model training using peak detection repetition segmentation. 86

Table 11. Class-specific performance of the XGBoost classifier for soccer-specific movement classification during sliding-window evaluation using a 4 s window and 1 s step size. Change in F1-score (ΔF1-score) relative to the primary peak detection-based repetition segmentation LOSO evaluation is presented. 90

1 Introduction

1.1 The Burden of Hip Osteoarthritis

Osteoarthritis (OA) is a prevalent and disabling condition affecting more than four million Canadians and accounting for 1% of total healthcare expenditures.[1] By 2031, the economic impact of OA is expected to reach $8.1 billion annually, with the number of affected Canadians projected to approach 10 million by 2041.[1] Hip OA represents a substantial component of this burden, affecting 47% of adults aged 50-64 and appearing particularly common among individuals exposed to high-impact sporting activities during adolescence.[1] Former elite athletes have been reported to exhibit up to an eightfold greater incidence of hip OA than non-athletic controls.[2–5] As no curative treatment exists, focus has shifted toward understanding the pathophysiological mechanisms behind hip OA and identifying modifiable risk factors that may delay or prevent disease onset. Recent research has primarily focused on the pre-arthritic hip as a means of improving early detection and prevention strategies.[2,6]

For many years, hip OA was frequently diagnosed as idiopathic because its underlying mechanisms were poorly understood.[4,6,7] However, advances in radiographic imaging have linked subtle developmental abnormalities of hip morphology arising before skeletal maturity to hip OA.[6] In a retrospective analysis, 79% of adult hip OA cases demonstrated conclusive radiographic evidence of an underlying morphological abnormality, suggesting a structural rather than idiopathic origin.[6] These observations led to the recognition of femoroacetabular impingement (FAI) as a mechanism by which abnormal hip morphology may contribute to OA development.[8]

1.2 Femoroacetabular Impingement Syndrome

Today, femoroacetabular impingement syndrome (FAIS) is widely recognized as a common cause of hip and groin pain in young, physically active individuals, with symptom onset reported as early as the second and third decades of life.[4,6,9] According to the 2016 Warwick Agreement, FAIS is "a motion-related clinical disorder of the hip," characterized by osseous deformities that results in symptomatic, premature contact between the proximal femur and the acetabulum during high degrees of hip flexion, adduction, and internal rotation.[10] Repetitive abutment between these osseous structures damage the articular cartilage and acetabular labrum, contributing to degenerative changes at the hip.[6,11,12] Two principal morphological variants have been identified: cam morphology, characterized by loss of

sphericity at the femoral head–neck junction, and pincer morphology, characterized by excessive acetabular coverage.[8,12,13] Although both variants may contribute to FAIS, cam morphology has received greater attention because of its stronger association with athletic participation and potential developmental origin during skeletal growth..[3,12] In the general population, approximately 20–30% of males and 0–10% of females exhibit cam morphology.[14–16]

Growing evidence implicates cam morphology as a significant contributor to the development of hip OA, especially among males who participated in high-impact sports childhood and adolescence,[2,3,17–20] with prospective studies linking its presence to increased long-term OA risk in former elite athletes.[4,21] These findings suggest that the high-impact youth sporting environments associated with cam morphology may represent an important window of opportunity for early intervention, before irreversible structural adaptation and/or joint tissue damage occurs. Understanding the specific exposure to movements involving potentially problematic hip positions experienced by young athletes is therefore essential to identifying movement patterns that may contribute to cam progression and informing effective, timely intervention strategies.

Confoundingly, not all individuals who exhibit osseous cam morphology progress to symptomatic FAIS. Many athletes present with radiographic evidence, yet remain entirely asymptomatic,[22,23] a disparity likely attributable to differences in the magnitude and frequency of exposure to at-risk activities, or to the absence of the altered hip kinematics observed in symptomatic individuals.[24–26] This suggests that bony morphology alone may be insufficient to generate symptomatic impingement; rather, repeated interaction between structural morphology and mechanical provocation is proposed to drive cyclical progression toward symptomatic disease and, ultimately, hip OA.[3,24] Determining how frequently youth athletes encounter specific hip motions that produce this mechanical conflict is a necessary first step toward developing targeted prevention methods or activity modification strategies in at-risk populations.

1.3 Soccer as a High-Risk Sporting Environment

Soccer is the most widely played sport globally, with the sport's global governing body, the Fédération Internationale de Football Association (FIFA), reporting approximately 21.5 million registered players under the age of 18,[27] while youth soccer participation in Canada now exceeds ice hockey and basketball.[28] This high participation base is accompanied by

increasing training and matchplay volumes, with many youth athletes competing more than four times per week across near year-round seasons.[29] Hip injuries account for 11-16% of all injuries in male professional and elite youth soccer players,[30] highlighting the clinical relevance of hip-related pathology in these athletes.

Soccer involves dynamic, multiplanar movements that repeatedly expose the hip to combinations of flexion, adduction, and internal rotation that create cam impingement during actions such as cutting, dribbling, and kicking.[29,31,32] Notably, these positions overlap with those used clinically to provoke symptoms in individuals with cam FAIS.[29,34] Despite this overlap, no practical method currently exists to quantify how frequently these potentially impinging positions occur during real-world soccer participation. This limits our ability to characterize injury risk associated with cam FAIS in youth soccer players.

1.4 Movement-Monitoring Tools

Common athlete-monitoring technologies used in soccer, including global/local positioning systems (GPS/LPS) and semi-automatic video tracking, provide valuable information regarding physical performance but offer little insight into the underlying joint kinematics that define technical actions.[31,32] Laboratory-based optical motion capture (OMC) remains the gold standard for quantifying hip joint angles with high precision and has been used to characterize both the altered hip kinematics in cam FAIS and the kinematic demands of basic soccer tasks.[26,33–38] However, OMC systems are expensive, restricted to laboratory environments, and involve extensive setup constraints that restrict their application to isolated tasks, which may not reflect the dynamic and unpredictable nature of soccer match play.[39,40] Consequently, despite strong evidence linking youth soccer participation to cam morphology development, it remains unclear how frequently, and in what specific joint positions, the hip is loaded in ecologically valid settings.

These limitations have prompted growing interest in wearable inertial measurement units (IMUs) as a practical alternative for capturing kinematics in real-world sporting environments. These compact sensors capture three-dimensional (3D) motion data, enabling estimation of lower-limb joint kinematics outside laboratory settings.[41,42] Validation studies comparing IMU-derived measures with OMC have generally demonstrated good-to-excellent agreement for hip motion in the sagittal and frontal planes during dynamic tasks such as running, cutting, jumping, and kicking, although accuracy is more variable in the transverse plane.[36,37,39,43,44] In soccer contexts, IMU-based approaches have been used primarily to

automatically detect and classify discrete actions such as passing, shooting, ball contacts, and changes of direction via velocity and orientation signals.[39,45,46] However, existing applications have largely focused on activity classification and physical load quantification (i.e., distance covered while running), rather than describing the hip joint positions occurring within these actions. Consequently, the extent to which players adopt hip positions associated with cam FAIS remains poorly understood. Given their portability and emerging validation evidence, IMUs may provide a feasible approach for quantifying in-field movement exposure and hip kinematics relevant to cam FAIS in youth soccer players.

While IMUs collect large volumes of rich movement data, extracting interpretable kinematic information from these signals requires additional processing and analysis. Machine-learning (ML) approaches provide an opportunity to automate the identification and classification of human movement patterns from IMU-derived data, and have been applied across a range of applications, including activities of daily living and individual/team sports.[47–49] In soccer, ML models have been used to classify basic technical skills, such as passing and shooting, achieving variable degrees of success.[45,50–52] However, the classification of diverse, soccer-specific actions remains challenging due to the broad range of complex motions performed during play, and existing approaches have generally been limited to a small number of isolated technical skills. Developing ML classifiers capable of identifying a comprehensive range of soccer-specific manoeuvres may therefore provide a means of quantifying how often movements associated with potentially provocative hip positions occur during sport participation.

1.5 Purpose and Hypotheses

Despite the established association between high-impact youth sport participation, cam morphology, and subsequent cam FAIS and hip OA, no practical tool currently exists to quantify exposure to potentially problematic hip kinematics during live soccer participation. This thesis therefore contributes to addressing this gap by (1) validating a wearable IMU system against a gold-standard OMC system for quantifying 3D hip kinematics during a comprehensive range of soccer-specific manoeuvres. It was hypothesized that IMU-derived hip kinematics would show good-to-excellent agreement with OMC across all motion planes. In addition, this thesis aimed to (2) develop custom ML algorithms that use IMU-derived signals to detect and classify soccer-specific movement techniques that may be associated with problematic hip joint positions potentially related to cam FAIS during both kicking and non-kicking actions. The second hypothesis was that the ML classifier trained on features

derived from IMU data would be able to distinguish between soccer-specific movement techniques with high accuracy (>90% accuracy).

This work represents an initial step toward enabling reliable field-based quantification of complex hip motion frequency during high-intensity sport participation in individuals at risk of developing cam FAIS. By establishing robust, data-driven methods for assessing hip joint exposure in ecologically valid environments, this research may improve understanding of movement-related risk profiles and inform the future development of targeted prevention and intervention strategies, like load management or activity modification, aimed at mitigating cam FAIS progression and its potential contribution to hip OA in young, physically active populations.

2 Literature Review

2.1 Femoroacetabular Impingement Syndrome Overview

2.1.1 Relevant Anatomy of the Hip

The hip joint represents a complex anatomical system adapted for weight-bearing, ambulation, and dynamic motion.[53] It is a large synovial ball-and-socket joint comprised of bony and soft tissue structures that balance stability with the capacity for multiplanar range of motion (ROM).[54] Articulation occurs between the acetabulum of the pelvis and the femoral head of the proximal femur.

The acetabulum is a cup-shaped depression located on the lateral aspect of the pelvis.[54] Its articular surface is lined with hyaline cartilage that is thickest towards the peripheries, facilitating smooth movement within the joint.[53] The outer surface, the acetabular rim, is surrounded by the acetabular labrum, a fibrocartilaginous structure that improves joint stability without restricting the end range of motion at the hip.[53,54] Further, the labrum provides a tight seal that protects the cartilage.[55] The transition zone (chondrolabral junction) between the hyaline cartilage and labrum is a region of structural weakness and is often implicated in pathological FAIS.[55]

The proximal femur consists of the femoral head and neck, which are particularly relevant in the context of FAIS. The spherical femoral head articulates within the acetabulum, while the narrower femoral neck creates a clearance zone between the femur and acetabular rim during physiological motion.[53,54] During weight-bearing, the femoral head is forced deeper within the acetabulum, and the head–neck offset permits substantial hip motion without bony contact.[53–55]However, abnormalities in femoral head–neck morphology may reduce this clearance, increasing the likelihood of premature abutment between the proximal femur and acetabulum during certain hip orientations.[10,24]

During skeletal development, the femoral head is separated from the femoral neck by the physis, a growth plate responsible for longitudinal bone growth. The epiphysis forms the end portion of the femoral head and contributes to the articulating joint surface.[56] These structures play key roles in shaping the proximal femur, and alterations in their development during growth have been implicated in the formation of deformities associated with FAIS.[3,5,56,57]

2.1.2 What is FAIS?

FAIS is defined as “a motion-related clinical disorder of the hip”, characterized by abnormal osseous deformities that result in symptomatic contact between the proximal femur and the acetabulum.[10] This repetitive mechanical abutment, arising from structural incongruity between bony surfaces, exposes the joint to irregular contact forces and subsequent microtrauma.[12,13,24] Over time, this recurrent microtrauma produces characteristic intra-articular damage, including acetabular labral tears and adjacent hyaline cartilage injury, often presenting as chondral delamination and progressive cartilage breakdown.[8,13,24] If left untreated, this cumulative damage may alter joint loading patterns and contribute to degenerative change within the hip.[8,9,13] Growing evidence detailed in longitudinal, imaging, and surgical studies increasingly implicates that such abnormal hip morphology associated with FAIS represents a potential precursor of early-onset hip OA, exacerbated by participation in high-impact, elite sports during adolescence.[3,6,8,9,12,20,58]However, opposing evidence also exists and the true progression of this condition remains undetermined.[24]

The original condition, termed femoroacetabular impingement (FAI), was first discussed clinically through surgical hip dislocation by Ganz et al.,[8] who proposed that in many cases of idiopathic OA, predisposing factors representative of FAI are present. This conceptual framework was expanded by the ‘five essential elements’ established by Sankar et al.,[58] that were deemed necessary and sufficient to diagnose FAI:

1. Abnormal morphology of the femur and/or acetabulum,
2. Abnormal contact between these two structures,
3. Especially vigorous supraphysiologic motion that results in such abnormal contact and collision,
4. Repetitive motion resulting in the continuous insult,
5. The presence of soft-tissue damage.

Collectively, these elements reinforce the premise that structural variations of the femur and/or acetabulum resulting in premature contact drive intra-articular injury and secondary degenerative changes.[8,58] Specifically, this mechanical conflict is exacerbated as the hip is exposed to excessive and repetitive motion that approaches, or exceeds, its physiological end range.[8,58] Crucially, upon clinical inspection, this most often presents as restricted internal rotation and adduction at 90˚ of hip flexion, reflecting the abutment between the bony surfaces.[6,8,58]

A formal consensus definition and diagnosis of FAIS was not established until 2016.[10] The Warwick Agreement concluded that, to accurately diagnose FAIS, patients must experience a triad consisting of: (1) motion- or position-related symptoms primarily in the hip or groin regions, including restricted ROM and clicking or locking of the joint (2) clinical signs such as pain reproduction in the back, buttock, or thigh during hip impingement testing; and (3) imaging findings of abnormal morphological characteristics from radiographic or cross-sectional imaging techniques.[10]

2.1.2.1 Morphological Variants of FAIS

The normal articulating hip joint consists of the spherical femoral head articulating within the acetabulum (*Figure 1*). FAIS can be broadly categorized into three morphological variants: pincer, cam, and mixed. Pincer FAIS is characterized by excessive acetabular coverage of the femoral head, which may arise from global over-coverage (e.g., coxa profunda or protrusio acetabuli) or focal over-coverage due to acetabular retroversion.[12,13,24] In this variant, the femoral head-neck junction typically retains normal morphology.[8] Mechanical conflict therefore occurs when the acetabular rim prematurely impacts the femoral head-neck junction.[6,10]

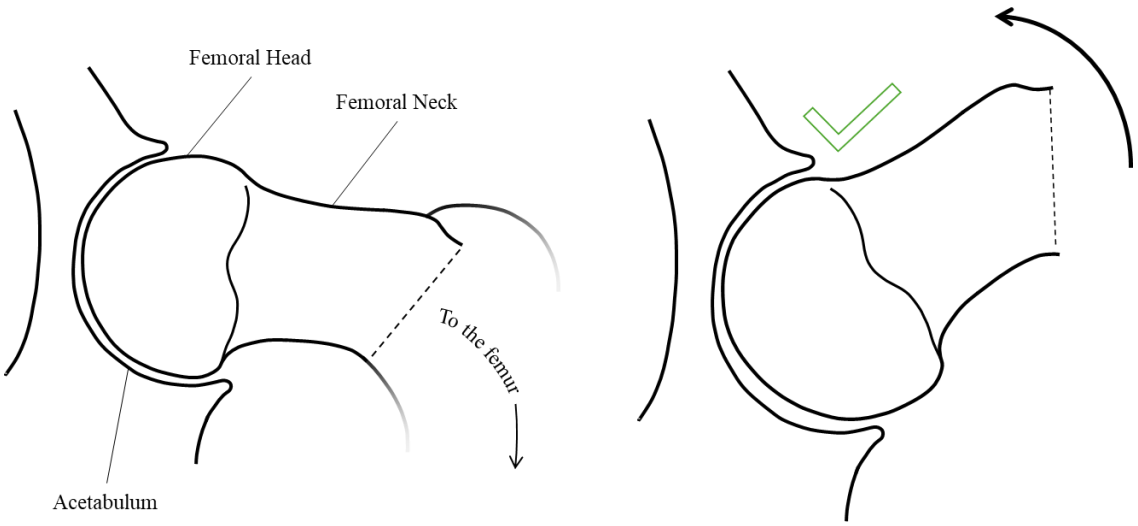


Figure 1. A graphical representation of the normal anatomy of the articulating hip joint.

In pincer morphology, the initial site of tissue failure is the anterior labrum (*Figure 2*). During hip flexion, the acetabular rim overgrowth compresses the labrum against the femoral neck.[6,12] Repetitive flexion subjects the labrum to progressive microtrauma, leading to labral thinning, tearing, and gradual separation from the acetabular cartilage.[6,12,24] Acetabular cartilage damage is observed secondary to this labral pathology through a “contrecoup”

mechanism.[11,12,24] As impingement persists, the femoral head undergoes posterior subluxation, or "levering out," within the socket.[11] This increases the pressure between the posteromedial aspect of the femoral head and posteroinferior acetabulum, causing cartilage degeneration in these regions.[11]

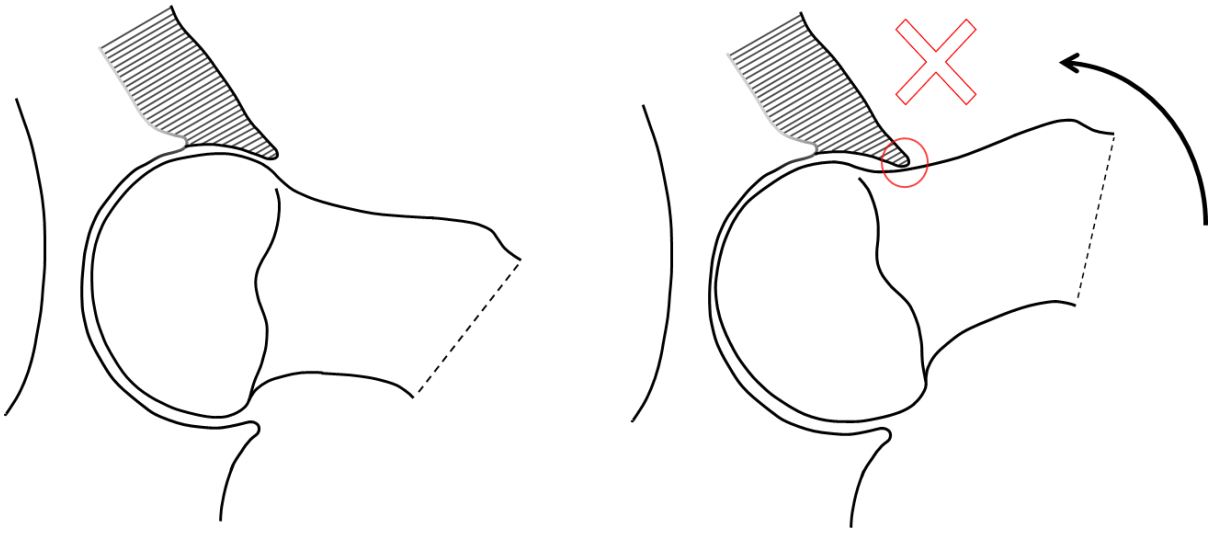


Figure 2. Pincer morphology of FAIS. The shaded region indicates excessive acetabular coverage of the femoral head.

In contrast, cam FAIS is defined by asphericity of the femoral head, commonly described radiographically as flattening of the femoral head–neck junction or the presence of an osseous prominence that reduces the normal head–neck offset (*Figure 3*).[12,24,59] This reduced offset decreases the clearance between the proximal femur and the anterior acetabular rim, shifting the regular contact location of the femoral head from the interior acetabulum to the anterosuperior acetabular rim.[8] Mechanical impingement therefore occurs when the abnormal prominence of the proximal femur is forced under the acetabular rim, particularly in positions of flexion.[8,59,60]

Unlike pincer FAIS, acetabular cartilage injury is the primary concern in cam morphology, while the labrum is often preserved in the early stages.[6,24] During hip flexion, the cam morphology rotates through the anterosuperior acetabulum, generating substantial compression and shear stresses at the chondrolabral junction.[11,12,24] These forces displace the labrum outwards while the cartilage translates centrally, resulting in progressive cartilage delamination.[11] Concomitant hip adduction and internal rotation exacerbate this loading, accelerating cartilage separation and ultimately leading to secondary labral tearing.[11,24]

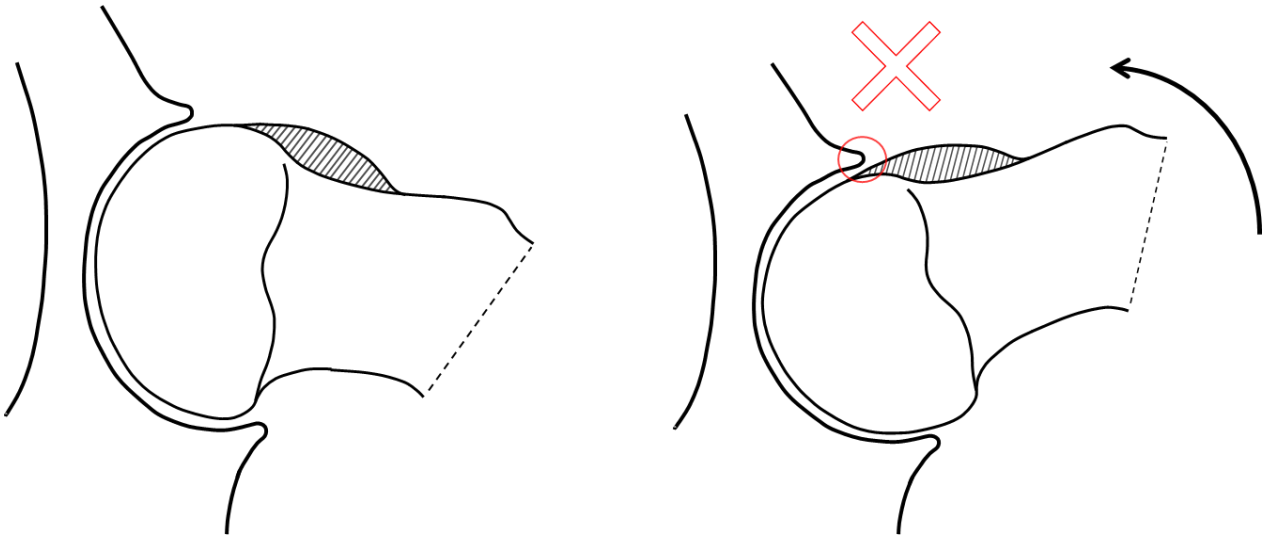


Figure 3. Cam morphology of FAIS. The shaded region indicates asphericity of the femoral head and resultant flattening of the femoral head–neck junction caused by osseous protrusion.

Mixed FAIS refers to the coexistence of both cam and pincer morphologies, to varying degrees, within the same hip (*Figure 4*).[9,13] The presence of both abnormal femoral morphology and acetabular over-coverage may amplify bony contact during hip motion.[13] Patients typically present with simultaneous acetabular cartilage and labral damage that is frequently more extensive as compared with isolated cam or pincer.[12,13]

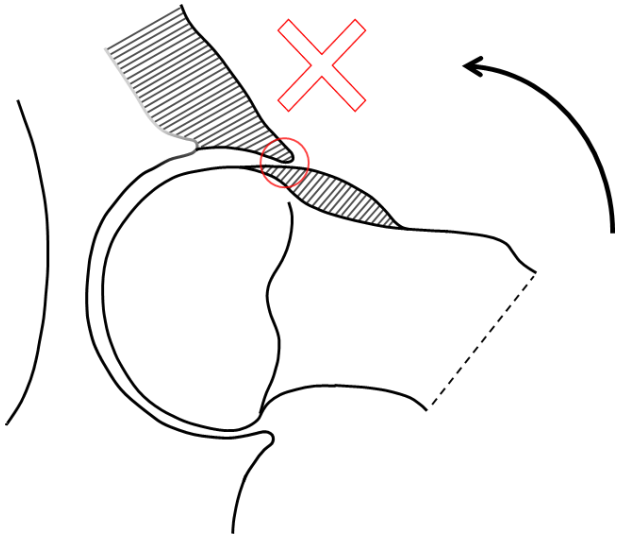


Figure 4. Mixed morphology of FAIS. The shaded regions indicate the coexistence of both pincer and cam morphological changes.

Despite structural differences in bony morphology, the pathological progression of FAIS is expected to be broadly similar across all variations, as both pincer and cam deformities generate anterior impingement.[24] However, the damage pattern induced by pincer FAIS is typically associated with a more gradual degenerative course and most commonly presents in middle-aged women between 30 and 40 years of age, likely due to sex-specific differences in pelvic anatomy.[6,12] Since the acetabular labrum is known to be innervated by nociceptive fibres responsible for signalling tissue damage, primary injury to this site often means that pain is experienced sooner by women with pincer FAIS than by men with cam FAIS.[6,59] In contrast, cam morphology is linked to more rapid, destructive, and severe joint degeneration and demonstrates an approximate 3:1 predilection for men, often presenting in athletic populations at least a decade earlier on average.[6,9,60] Patients with cam morphology may remain relatively asymptomatic until repetitive impingement leads to labral injury, after which symptoms typically persist for 12 to 36 months prior to surgical intervention.[61,62]

2.1.3 FAIS Diagnosis

With respect to the first component of the triad described in the Warwick International Agreement,[10] individuals with FAIS commonly report groin or hip pain during activities that place the hip in positions of rotation, during prolonged sitting, or during and after sport participation.[63]

The second component is typically assessed using physical examination procedures, most commonly the flexion, adduction, and internal rotation (FADIR) test and the flexion, abduction, and external rotation (FABER) test.[64] Of these, the FADIR test is more frequently used to assess anterior impingement between the femoral head–neck junction and acetabulum. To perform the test, the clinician passively moves the hip into approximately 90˚ of flexion, followed by 10˚ of adduction and 10˚ of internal rotation. Reproduction of the patient's usual sharp hip or groin pain is considered a positive test.[64] Hip ROM is often evaluated concurrently, as individuals with FAIS commonly demonstrate restricted motion, particularly during hip flexion and internal rotation.[63]

Despite its widespread clinical use, the diagnostic utility of the FADIR test remains uncertain due to large variability in reported sensitivity and specificity values, ranging from 0.08 to 0.96 and from 0.11 to 1.00, respectively.[64] Much of this variability reflects differences in how the test is performed and inconsistencies in the radiographic imaging threshold values used to confirm FAIS across studies.[64] Nevertheless, a positive impingement sign has been

reported in more than 90% of individuals with FAIS confirmed either radiographically or during surgery.[8] Moreover, a systematic review reported high sensitivity and high predictive value of the FADIR test for detecting labral pathology when confirmed by MRI, with values ranging from 0.95 to 1.00.[65] Given its simplicity, the FADIR test is most appropriately used as a low-risk screening and symptom-provocation tool prior to confirmation of FAIS via imaging.[64,65]

Imaging modalities are used both to identify structural abnormalities associated with FAIS and to exclude alternative conditions, such as OA or avascular necrosis.[63] Plain radiography is typically performed first to assess bony anatomy of the hip joint using combinations of the anteroposterior pelvis (*Figure 5*), frog leg lateral (*Figure 6*), and Dunn views.[63,66] All radiographs are obtained with the patient in a supine position. For the anteroposterior pelvis view, both hips are internally rotated by approximately 15˚. During the frog-leg lateral view, the contralateral hip and knee are flexed beyond 80˚ while the symptomatic limb remains internally rotated by 15˚. In the Dunn view, the symptomatic hip is positioned in 90˚ of flexion and 20˚ of abduction while held in neutral rotation.[66]

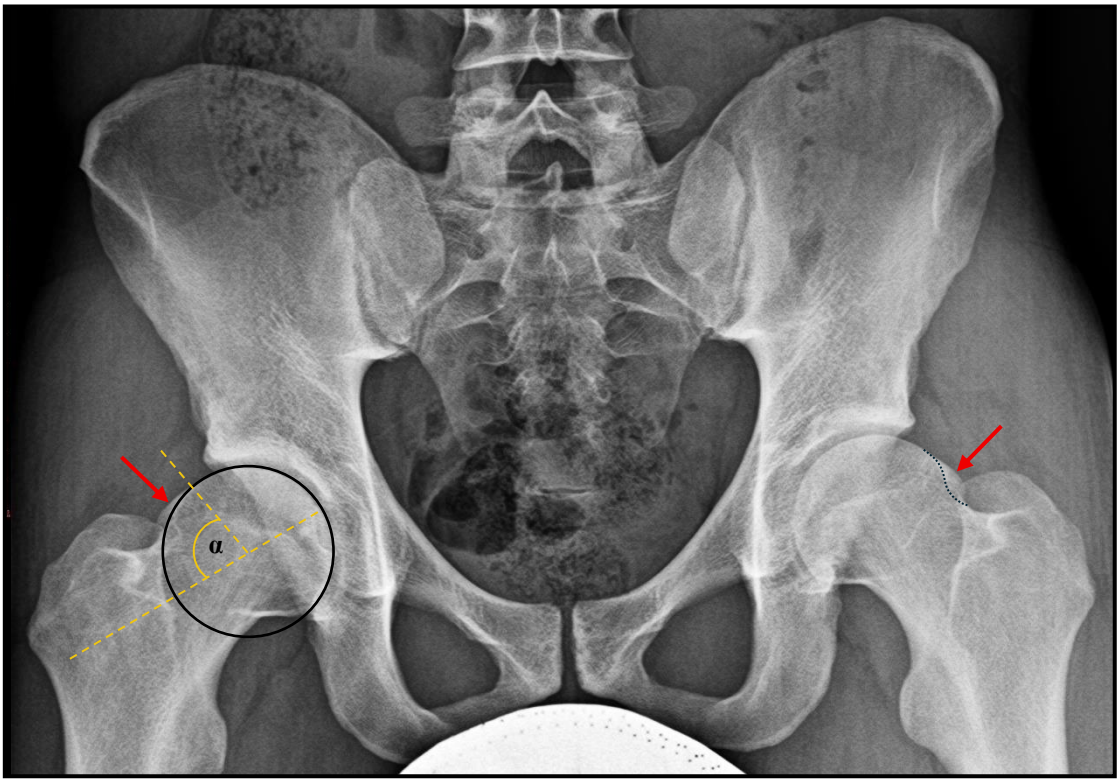


Figure 5. Anteroposterior pelvic radiograph demonstrating cam morphology in a male pelvis. Small arrows indicate minor to moderate cam deformities at the femoral head–neck junction. The alpha angle (α) is approximated on the right femoral head, with the dotted line representing the expected spherical femoral head contour. Images are the personal medical images of the author.

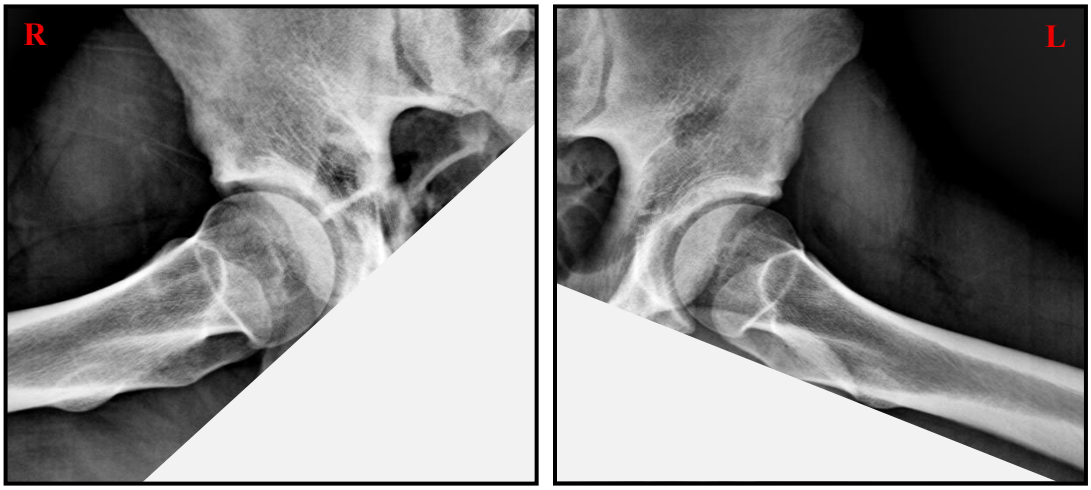


Figure 6. Frog-leg lateral radiographs of the right and left proximal femur and acetabulum. Images are the personal medical images of the author.

Magnetic resonance imaging (MRI) is commonly performed following radiology to provide a detailed view of the intra-articular structures, allowing the detection of associated chondral and labral damage when impingement is suspected (*Figure 7*).[63,66]

Abnormal morphology associated with FAIS is quantified using several radiographic measures, particularly the head–neck offset ratio and the alpha angle (*Figure 5*). The head–neck offset ratio describes the relationship between the anterior femoral neck offset and the diameter of the femoral head.[67] While this metric is still used clinically, the alpha angle remains the most widely adopted measure for assessing hip morphology.[68] First introduced by Nötzli et al.,[67] the alpha angle describes the angle between the axis of the femoral neck and a line extending from the centre of the femoral head to the point where the femoral head–neck junction loses sphericity. Larger alpha angles thereby reflect increasing asphericity of the femoral head–neck junction and greater prominence of osseous morphology.

An alpha angle threshold of 55˚ is often used to define a cam morphology,[67] although both lower and higher threshold values have been proposed in more recent investigations.[3,56,66] In fact, increasing the threshold to 60˚ has been shown to reduce the number of false-positive classifications of cam morphology identified using MRI.[69] The alpha angle demonstrates good diagnostic validity for identifying cam morphology, particularly when assessed using the Dunn radiographic view, with reported sensitivity, specificity, and accuracy values of 91%, 90%, and 90%, respectively, at a threshold of 50.5˚.[66]However, it has been suggested that reliance on a single alpha angle measurement is inadequate to accurately diagnose FAIS, and therefore assessment across multiple radiographic views is recommended to account for variation in the anatomical location and severity of morphology.[68]

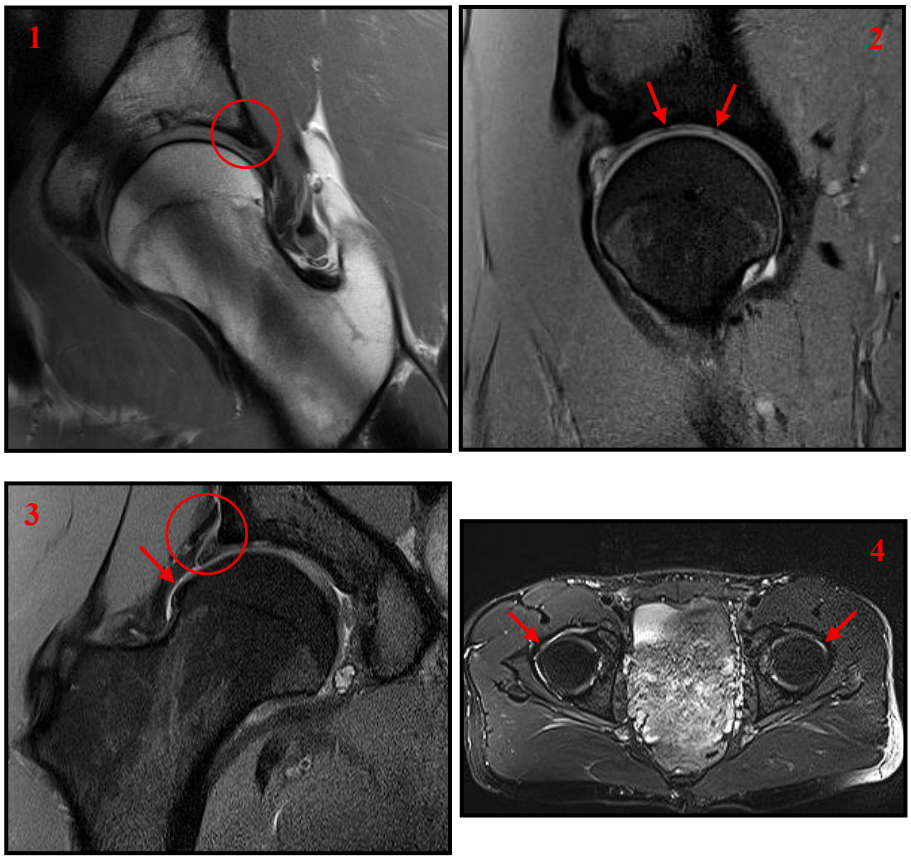


Figure 7. Magnetic resonance imaging (MRI) of the hip joint demonstrating structural abnormalities associated with FAIS. (1) Radial view of the left hip showing the chondrolabral junction (circle). (2) Sagittal view of the right hip demonstrating focal cartilage defects (arrows). (3) Coronal view of the right hip showing cam morphology (arrow) and labral tear (circle). (4) Axial view of the pelvis demonstrating bilateral cam deformities.

2.1.4 Prevalence and Presentation of FAIS

Among the general adult population, the estimated prevalence of clinically diagnosed FAIS ranges between 10% and 15%.[14] Epidemiological data further support the sex-based differences in morphological presentation described previously. Population-based studies report that approximately 20–30% of males, compared to 0–10% of females, present with cam morphology.[15,16] Conversely, pincer morphology appears to be more prevalent among women. In a large cohort of 3,620 individuals (1,332 men; 2,288 women), Gosvig et al.,[16] reported pincer impingement in 19.4% of women compared to 15.2% of men. In a smaller cohort of 1,130 hips (1,076 patients) undergoing operative treatment for symptomatic FAIS, 47.6% of hips were classified as cam-type, 44.5% as mixed morphology, and only 7.9% as isolated pincer-type FAIS.[62] Although not reported numerically in the text, the study's bar chart demonstrated that isolated pincer morphology was proportionally more common among female patients, whereas the prevalence among males was substantially lower.

The prevalence of radiographic findings suggestive of FAIS has also received considerable attention. In a cohort study of 2,081 healthy young adults (874 males; 1,207 females), Laborie et al.,[70] evaluated pelvic radiographs for features consistent with cam and pincer morphology. When considering the worse hip, 35% of males and 10.2% of females demonstrated at least one cam feature, while 34.3% of males and 16.6% of females exhibited one or more pincer features. Bilateral findings were consistently lower, with 24.7% of males and 6.3% of females displaying cam morphology in both hips, and 16.6% and 9.7%, respectively, showing bilateral pincer features.[70]

Similar trends have been observed in other radiographic investigations. Zhou et al.,[71] reported that 64.6% of male hips and 63.7% of female hips demonstrated at least one radiographic feature associated with FAIS; however, cam morphology was markedly more common in males (20.9% vs. 4.9%), whereas pincer morphology was more prevalent in females (24.4% vs. 4.5%). Mixed morphology was the most frequent presentation in both sexes (74.6% in males vs. 70.7% in females). Focusing specifically on cam morphology, Tsitskaris et al.,[72] found a higher prevalence in men than women, with 23.8% of men compared with 16.6% of women on the right side, and 19% of men compared with 16.6% of women on the left; however, the study was limited by a relatively small sample size (n = 45). Consistent with this trend, magnetic resonance imaging (MRI) of asymptomatic individuals revealed cam morphology in 24.7% of 89 men compared with only 5.4% of 111 women, further reinforcing the male predilection for cam deformities.[73] In contrast, a cohort of 100 patients with symptomatic FAIS (50 males; 50 females) showed more comparable distributions of isolated cam morphology between sexes (44% in males; 47% in females), with mixed presentations remaining highly prevalent (56% in males; 41% in females). Only 6% of females, and no males, presented with isolated pincer FAIS.[74]

Together, these studies highlight the crucial role of imaging in the diagnosis and characterization of morphological FAIS variants. However, routine use of radiographs for longitudinal monitoring or large-scale screening is limited by factors such as cost, or accessibility. These limitations emphasize the need for a non-invasive, inexpensive, and portable assessment strategy capable of identifying and tracking at-risk individuals over time. Moreover, an accurate diagnosis also requires consideration of clinical symptoms and functional movement- or position-related limitations, with pain being the primary presenting feature.[10]

From a clinical perspective, over 80% of individuals with FAIS report moderate to severe pain at presentation, typically described as both aching and sharp in nature and worsens with activity.[75,76] Symptom onset is typically insidious, occurring gradually without a distinct event in the majority cases (65%- 92%),[75,76]whereas substantially fewer patients attribute their symptoms to an acute or major traumatic injury. This pattern is further supported by epidemiological data from a North American cohort of 1,076 patients (1,130 hips), in which 89% of hips were classified as idiopathic FAI in individuals with a mean age of 28.4 years, characterized by atraumatic hip pain persisting for more than one year.[62]

Pain is most frequently localized to the groin, with clinical studies reporting that between 72% and 94% of patients primarily experience groin discomfort, although associated pain is often reported in adjacent regions including the low back, thigh, and buttock.[74–77] Beyond its characteristic location, FAIS-related pain substantially impairs quality of life and everyday functional capacity. In cohorts with mean ages of 35 years and 34.9 years, respectively,[75,77] a large proportion of patients report discomfort during running (69% and 87%, respectively) and participation in other athletic activities (71% and 77%). Functional limitations are not confined to sport; many individuals also report difficulty with routine daily activities such as walking, stair climbing, and prolonged sitting. These impairments often result in compensatory movement strategies, including mild limping or altered weight-bearing patterns adopted to reduce hip joint loading and mitigate pain.[75–77]

Notably, FAIS disproportionately affects a relatively young and otherwise active population, with mean ages close to 30 years across multiple cohorts. The combination of early functional limitation and primarily insidious, idiopathic symptom onset suggests that the development and progression of FAIS are multifactorial rather than attributable to a single mechanism. These concerns are heightened by the proposed association between FAIS and early-onset hip OA.[3,6,8,9,12] Recognition of FAIS as a pre-arthritic condition, and early intervention before advanced joint degeneration, may meaningfully alter the natural history of the disease and delay progression to end-stage OA in this young patient demographic.[8] As such, a clearer understanding of the underlying etiology of FAIS is essential to facilitate early detection and inform preventative strategies in at-risk individuals.

2.2 FAIS Etiology

Since many cases of symptomatic FAIS are classified as idiopathic,[62] research has increasingly focused on identifying factors that may predispose individuals to the development of the condition. Despite its frequent idiopathic presentation, FAIS is widely recognized as a common cause of hip and groin pain not only in the general population, but also in young, physically active adults, with symptom onset reported as early as the second and third decades of life.[9,10,12,24] Although FAIS can result from both cam and pincer morphologies, the majority of research in this field has focused on cam deformities, as these are more strongly associated with progression to symptomatic disease and subsequent hip OA.[3,78]

For example, Agricola et al.,[3] evaluated radiographs from 1002 middle-aged patients with early symptomatic OA of the knee or hip at baseline, 2-year, and 5-year follow-up. Although 76% of hips demonstrated no radiographic signs of OA at baseline, 2.76% progressed to end-stage OA within 5 years. When adjusted for either a moderate alpha angle (>60˚) or severe alpha angle (>83˚), the odds of developing end-stage OA increased to 3.67 and 9.66, respectively, with corresponding positive predictive values of 10.9% and 25.0%. Furthermore, patients presenting with both a severe alpha angle and restricted hip internal rotation (≤20˚) at baseline demonstrated an odds ratio of 25.21 and a positive predictive value of 52.6% for progression to end-stage OA. Consequently, the following discussion focuses primarily on factors implicated in the development of cam morphology.

Despite advances in understanding, largely informed by direct observation of hip pathomechanics through surgical dislocation and by improved radiographic imaging and interpretation [79] the precise etiology of FAIS remains unclear. While recent reviews addressing the epidemiology, surgical intervention, and imaging practices surrounding FAIS have expanded current knowledge, controversies persist regarding the condition's origin, natural history, and the factors that determine symptomatic presentation, highlighting the need for further investigation.[9,22,24,62]

2.2.1 Genetic Predisposition

Genetic factors that affect hip development have been suggested to increase the risk of developing FAIS, in addition to the mechanical conflict caused by abnormal bony morphology of the proximal femur and/or acetabulum. However, the role of genetics in the etiology of FAIS is inconclusive.[80] Some researchers have therefore investigated whether the

abnormal joint morphology associated with FAIS may represent an underlying genetic predisposition to hip OA, given the established influence of genetic factors in the development of hip OA.[81]

Genetic involvement was explored by Pollard et al.,[82] who compared patients treated for FAIS to their siblings (n = 96) and a spouse control group (n = 77). Siblings were significantly more likely to present with clinical signs of impingement and to exhibit similar radiographic cam (relative risk = 2.8) and pincer deformities (relative risk = 2.0) compared with controls. Relative risk was calculated by dividing the incidence in siblings by that in controls; values greater than one therefore indicate a potential genetic predisposition. Furthermore, when evaluating the parents of participants, 13 of 64 parents of patients with FAIS had hip OA or had undergone hip replacement, compared with only 6 cases among the 77 control families. Despite these findings, the methodology has been criticized for its inability to isolate genetic factors, as this epidemiological approach cannot distinguish genetic influences from common environmental or social factors shared within families, such as participation in athletic activity.[80,81]

Subsequent investigations have explored potential genetic associations through the analysis of single nucleotide polymorphisms (SNPs). However, robust evidence remains limited, with few studies demonstrating associations between specific SNPs, proximal femoral morphology, and an increased risk of hip OA.[81,83] The SNPs examined were primarily selected due to their known associations with hip OA. As such, no causal relationship with FAIS has been established; rather, current evidence suggests that certain SNPs may influence hip morphology, either by influencing the shape of the proximal femur or by increasing the vulnerability of cartilage to abnormal bony morphology, which may then contribute to the development of hip OA.[81]

2.2.2 Paediatric Conditions

Childhood and adolescent pathologies that alter normal hip anatomy may also increase the risk of developing cam FAIS. Two paediatric conditions frequently discussed in this context are slipped capital femoral epiphysis (SCFE) and Legg–Calvé–Perthes disease (LCPD).[12] A third condition, developmental dysplasia of the hip (DDH), is characterized by irregular acetabular development, resulting in under-coverage of the femoral head.[13] However, the morphological changes to the acetabulum associated with DDH are more closely related to

pincer impingement and therefore fall outside the primary focus of cam-related mechanisms discussed here.

2.2.2.1 Slipped Capital Femoral Epiphysis, SCFE

SCFE is a common adolescent hip disorder that has been proposed as a precursor to cam morphology, as it produces morphological changes of the proximal femur that resemble those observed in cam-type FAIS, including reduced femoral head–neck offset and a prominent head–neck junction.[80,84] Retrospective follow-up studies of patients treated for SCFE have reported positive impingement signs on clinical examination, as well as anterosuperior labral degeneration, chondrolabral damage, and femoral head asphericity consistent with patterns observed in cam-type FAIS.[80,84] These findings suggest that residual deformity following surgical correction of SCFE may lead to femoroacetabular impingement and contribute to the development of cam morphology.[80,83,84]

However, the interpretation of these findings is limited by the retrospective nature of these studies, which often lack information regarding patients' lifestyle and activity levels between the time of treatment and follow-up evaluation. As a result, it is difficult to determine whether the observed changes are solely attributable to SCFE-related deformity or whether other factors also contribute to the development of cam FAIS.

Furthermore, evidence suggests that cam-type deformities occurring in the absence of prior hip pathology display distinctly different morphological characteristics compared with those resulting from residual SCFE.[85] When viewed on lateral radiographs, the centre of the femoral head typically migrates posteriorly in hips with a history of SCFE, while the same displacement is rarely observed in idiopathic cam deformities.[81,85] In addition, the femoral shaft–physeal angle, which describes the orientation of the proximal femoral growth plate (physis) relative to the femoral shaft, differs significantly between these conditions. In idiopathic cam deformities, the proximal femoral physis is oriented more horizontally, typically ranging between 60˚ and 77˚, whereas in hips with residual SCFE it remains relatively more vertical (<55˚).[85] Based on these observations, it has been suggested that most cam deformities are, in fact, unlikely to represent a sequela of SCFE.

2.2.2.2 Legg–Calvé–Perthes Disease, LCPD

LCPD occurs in young children when disruption of the blood supply to the femoral head results in osteonecrosis and subsequent collapse of the epiphysis, leading to deformities of the proximal femur and, secondarily, the.[12,86,87] During growth, the femoral head undergoes

healing and remodeling, often becoming enlarged, flattened, or aspherical, which disrupts normal hip articulation.[12,86] As a result of these structural changes, hips affected by LCPD may develop symptomatic bony impingement; consequently, the condition has been considered by some authors to represent a complex form of FAIS.[80,87]

However, the pattern of impingement observed in LCPD differs substantially from the classic intra-articular mechanisms associated with the subtypes of FAIS.[80] In a retrospective analysis, Tannast et al.,[87] used computed tomography–based virtual motion analysis to compare 13 hips with LCPD to 27 normal hips and 22 hips with FAIS. They reported that both intra-articular and extra-articular impingement occurred more frequently in LCPD hips than in either comparison group. Specifically, intra-articular impingement was identified in 79% of LCPD hips, compared with 15% of normal hips and 36% of FAIS hips, while extra-articular impingement was present in 86% of LCPD hips, compared with 15% and 14%, respectively. Moreover, extra-articular impingement in LCPD was both more prevalent and more widely distributed across femoral and acetabular regions, in contrast to FAIS, where impingement is predominantly intra-articular and more localized to the femoral head, femoral head–neck junction, and acetabular rim.[87]

While these findings support that impingement is a prominent feature of LCPD, neither its location nor its underlying mechanism mirror that of FAIS. Therefore, although LCPD may result in symptomatic bony impingement, its contribution to the development of FAIS remains unclear.[80]

2.2.3 Proposed Mechanism: Sports Participation

A growing body of evidence suggests a relationship between sport participation and the development of hip OA. A systematic review of retrospective studies reported moderate evidence for a positive association between hip OA and sports participation,[17] with the activities assessed being predominantly high-impact, including running, soccer, athletics, ballet, and combined sporting activities. This is supported by findings that male athletes involved in similar running, cutting, and jumping sports demonstrate both an earlier onset and a greater risk of hip OA, while former elite athletes exhibit a relative risk of approximately 2.0 compared with non-athletic controls.[20,21,88] Furthermore, high-impact athletes have been shown to be at greater risk of developing hip OA than those participating in lower-impact activities.[20] Beyond relative risk, the incidence of hip OA is estimated to be 3 to 8.5 times

higher in athletes than non-athletes, depending on activity intensity and the extent of physical hip loading.[19]

Given the established relationship between sport participation and hip OA, and the predominance of cam FAIS in young, physically active individuals, the role of athletic activity in the development of cam morphology has become a major focus of investigation.[3,5,12,18] Accordingly, repetitive participation in high-impact physical activity, particularly during skeletal development, is now considered a key factor in the development of cam FAIS.[18,24,89,90] For example, evidence from early childhood and adolescent cohorts has consistently linked participation in elite-level ice hockey, basketball, and soccer, to the development of cam morphology.[3,18,19,56,57,90–93] Consistent with this, athletes competing in these sports have also been shown to be at increased risk of hip OA compared with both non-impact athletes and the general population, with reported risk increases of up to 2.5-fold in ice hockey players and 75% in soccer players. [20,88]

To further investigate the risk of developing cam morphology prior to skeletal maturity, Westermann et al.,[18] compared dual X-ray absorptiometry scans of the left hip in the anteroposterior view among power sport athletes (basketball, cheerleading, football, gymnastics, soccer, and volleyball), non-power sport athletes (wrestling, baseball, track and field, and tennis), and non-athletic controls. By early adulthood (23 years old), power sport athletes demonstrated higher odds of cam morphology compared with non-athletic controls based on both the head-neck offset ratio and alpha angle, whereas no such differences were observed in non-power sport athletes. Moreover, higher levels of physical activity, as assessed by questionnaire, were associated with morphological changes consistent with cam morphology.

These findings reinforce that both a greater volume of physical activity and participation in high-impact sports characterized by higher peak strain and ground reaction forces are associated with an increased likelihood of developing cam morphology prior to skeletal maturation.[18] Other studies corroborate these findings using sport-specific approaches, consistently reporting a greater prevalence of cam morphology in youth and adolescent athletes compared with their non-athletic peers, further supporting the role of repetitive hip loading during sports participation in the development of abnormal bony morphology.[24,56,93]

Before discussing sport-specific evidence, it is important to recognize that the presence of cam morphology does not necessarily result in symptomatic FAIS. Although cam morphology has been reported in up to 90% of athletic populations,[94] with athletes estimated to be between 1.9 and 8 times more likely to develop cam morphology than non-athletes,[7] a large proportion of athletic individuals remain entirely asymptomatic despite displaying the characteristic irregular osseous morphology associated with cam FAIS.[22,24] A review of 26 studies comprising 2,114 asymptomatic hips found that the prevalence of asymptomatic cam morphology in the general population was 37%, with 54.8% of these deformities observed in athletes compared with 23.1% in non-athletes.[22] One study included in this review similarly assessed the hips of 244 asymptomatic young men and reported cam deformities in 24% of participants.[23]

The existence of individuals with confirmed radiographic evidence of cam morphology, but without symptoms, indicates that abnormal bony morphology alone may be insufficient to produce symptomatic impingement. Rather, anterior hip and groin pain in cam FAIS patients is suggested to occur only after damage to intra-articular structures is sustained, notably the acetabular labrum and adjacent cartilage.[24] It is therefore probable that asymptomatic individuals either do not participate in high-risk activities frequently or vigorously enough, and so are not exposed to sufficient magnitudes of repetitive hip loading thought to initiate symptomatic FAIS.[24]

2.2.3.1 Ice Hockey

With an incidence rate of approximately 20 hip and groin injuries per 100 elite-level ice hockey players, and over 600,000 registered participants in Canada during the 2024–2025 season, hip and groin overuse or non-contact injuries are highly prevalent within the sport.[28,91,95] Given the similarity in clinical presentation, it is likely that cam FAIS remains underreported in ice hockey athletes due to misdiagnosis as more general hip or groin injury.[92] Considering results from a study involving players between 10 and 13 years of age, it is now generally accepted that the skating motion itself, characterized primarily by repetitive hip flexion and internal rotation under load, can expose developing hips to “at-risk” mechanics like those previously identified in adult populations.[95] During the push-off phase of the skating stride, the stance (push) limb is positioned in hip extension with abduction and external rotation, while the contralateral limb simultaneously moves into hip flexion and internal rotation. As the stride progresses, the lead limb is carried through increasing degrees

of hip flexion and internal rotation under dynamic load, repeatedly placing the hip in positions associated with increased contact between the femoral neck and acetabular rim.[95]

In comparisons between elite-level ice hockey players and non-athletic control populations, several studies have reported that elite hockey athletes are approximately 2.5 to 3 times more likely to demonstrate cam morphology than their control counterparts.[91,93] Lerebours et al.,[91] investigated the prevalence of radiographic hip deformities using X-ray imaging in National Hockey League and American Hockey League players, reporting cam morphology in 180 of 260 hips (69.4%) based on an alpha angle greater than 55˚. Similarly, Ayeni et al.,[93] used MRI-based assessment alongside clinical examination to evaluate whether repetitive mechanical loading in elite hockey athletes led to morphological changes consistent with cam FAIS. Significant between-group differences were observed only for MRI-derived alpha angle measurements, with elite hockey athletes demonstrating substantially greater alpha angles than non-athletic controls (athletes: 54.2˚; non-athletes: 43.2˚). Importantly, participants in both studies were asymptomatic and younger than 30 years of age, despite a high prevalence of radiographic cam morphology, implying that bony changes may arise long before symptom onset.

In a subsequent investigation, Philippon et al.,[96] also assessed alpha angle measurements obtained through clinical examination and MRI in 61 asymptomatic male youth ice hockey players and 27 male youth skiers who served as an athletic control group. Based on previous reports, cam morphology was again defined as an alpha angle greater than or equal to 55˚.[67] Ice hockey players demonstrated significantly higher alpha angles than skiers, with 75% of hockey players exceeding the threshold for cam morphology compared with 42% of skiers. Furthermore, alpha angle increased significantly with age only in the ice hockey cohort, whereas no comparable relationship was observed in the skiing control group, suggesting a sport-specific association between hockey participation and progressive development of cam morphology during adolescence. Additionally, 93% of ice hockey players within the oldest age category (16–19 years) demonstrated labral tears associated with cam FAIS despite remaining asymptomatic. This finding, together with the high prevalence of asymptomatic cam morphology reported in young athletes in previous studies, reinforces the presence of early intra-articular changes in youth hockey athletes and raises important questions regarding the timing at which repetitive sport-specific loading begins to initiate structural damage during skeletal development.

Some investigations have specifically aimed to identify the timing of cam morphology development in elite youth ice hockey athletes.[97,98] Using MRI, Siebenrock et al.,[97] quantified alpha angle and physeal status (open versus closed) in 77 hips of elite male ice hockey players with a mean age of 16.5 years (range 9–36 years). Alpha angles were significantly greater in athletes with closed physes compared with those with open physes (59˚ versus 50˚, respectively). Furthermore, 56% of hips with closed physes demonstrated an elevated alpha angle greater than 55˚, whereas only 6% of hips with open physes exceeded this threshold. These findings suggest that substantial cam morphology development occurs during the period surrounding physeal closure.

Interestingly, when hips were stratified according to symptomatic status, determined using self-reported hip pain and a positive anterior impingement test involving 90° hip and knee flexion coupled with internal rotation, symptomatic athletes demonstrated significantly greater alpha angles and reduced hip internal rotation compared with asymptomatic athletes (17˚ versus 23˚). This finding supports the association between increasing cam morphology, restricted hip motion, and symptomatic impingement.

Similar conclusions were reported by Hanke et al.,[98] who suggested that cam morphology develops predominantly between 13 and 16 years of age in elite youth ice hockey athletes. In this longitudinal study, 25 players were assessed at baseline, 1.5-year follow-up, and 3-year follow-up using MRI. Cam morphology, defined as an alpha angle greater than 60˚ at any measured location, was absent at baseline but became evident in 10 of 25 participants by the 1.5-year follow-up, and in 12 of 25 by the final assessment. Across the study period, reductions in hip internal rotation below 20˚ and decreases in hip flexion were also observed in 6 of 22 hips (3 lost to final follow-up), consistent with progressively restricted hip mobility concomitant with the development of cam morphology.

Collectively, findings from ice hockey suggest that structural changes associated with cam FAIS likely develop during adolescence, particularly around physeal maturation, in response to repetitive, sport-specific loading. In many cases, these changes appear to precede symptom onset while progressively contributing to limited hip motion, which may result in symptomatic impingement. The apparent relationship between these factors highlights the importance of identifying high-risk movement patterns and loading exposures in youth athletes prior to physeal closure.

2.2.3.2 Basketball

While comparatively underexplored, basketball is another high-impact sport frequently considered an "at-risk" activity for the development of cam FAIS.[18,19] In a retrospective study, the hips of 72 elite male basketball players with mean age 17.6 years were compared with 76 asymptomatic hips in an age-matched, non-athletic control group.[19] Like findings in elite ice hockey athletes, basketball players exhibited elevated alpha angles that increased to abnormal values during or after physeal closure, particularly within the anterosuperior region of the femoral head–neck junction, the location most often associated with cam morphology. By this developmental stage, 89% of athlete hips displayed an alpha angle greater than 55˚ compared with only 9% of hips in the non-athletic control group. The same association between athletic activity and progressively restricted hip mobility was also observed. Internal rotation during hip flexion was markedly decreased in basketball athletes across all age groups compared to the controls, declining from a mean of 34.2˚ at ages 9–12 years to just 12.4˚ by 22–26 years.

Further evidence from the same cohort of basketball players suggests that alterations about the proximal femoral physis during growth may occur before the development of a cam morphology in this population.[5] This finding is explored further within proposed mechanistic models of cam-type morphology (*1.3.4: Mechanisms of Sport-related Cam Development*).

2.2.3.3 Soccer

Soccer is also considered a particularly "at-risk" sport for cam FAIS due to the highly repetitive and dynamic nature of movements performed during training and competition. For example, the primary offensive action used to strike a ball, the instep kicking motion, is characterized by multiplanar segmental and joint rotations.[99] To execute a kick, the hip is first moved through extension and external rotation during the backswing phase. At the point of ball contact, the hip is positioned in flexion, external rotation, and abduction. Finally, the follow-through phase requires further hip flexion while simultaneously bringing the hip into internal rotation and adduction — the same combined maneuver commonly used clinically to reproduce pain and assess femoroacetabular impingement.[29,99] Repeated exposure to these positions, in addition to the many other multidirectional movements performed during soccer participation, may help to explain the high prevalence of cam morphology observed in youth and adolescent soccer athletes.

In fact, pre-professional male soccer athletes as young as 12 to 14 years have been shown to exhibit radiographic cam deformities that increase in size throughout adolescence until closure of the proximal femoral physis.[3,56,57] In the same cohort of 89 soccer players, the prevalence of cam morphology in hips with an open growth plate increased significantly over a two-year period, rising from 2.1% at baseline to 17.7% at 2-year follow-up among the 63 players reassessed. In contrast, once the proximal femoral physis had closed, both the prevalence and severity of the morphology remained relatively stable.[3] Unlike many previous investigations that used a threshold of 55˚, cam morphology was defined using a more conservative alpha angle threshold exceeding 60˚, thereby reducing the likelihood of overestimating pathological morphology in athletic populations. Furthermore, 58% of hips exceeding this threshold demonstrated bilateral morphology, suggesting that morphology development may occur independently of limb dominance.

In a subsequent study, the baseline radiographs of the same 89 elite soccer players were compared with 92 male controls within the same age range (12-19 years).[56] The soccer athletes trained approximately 8 hours per week and had participated in the sport for an average of 9 years, whereas controls were excluded if regular sports participation was documented within their medical records. Cam morphology, defined by an alpha angle exceeding 60˚, was more prevalent in soccer players than controls (26% vs 17%, respectively), while visual flattening of the head–neck junction, indicative of femoral head asphericity, was also considerably more common in athletes (53% vs 19%, respectively).

In contrast, Johnson et al.,[29] reported no significant difference in radiographic signs of cam FAIS between 25 male individuals who participated in high-level soccer while skeletally immature and 25 controls, all aged between 18 and 30 years. Evidence of cam morphology was identified in 15 participants from the soccer cohort and 14 controls, with predominantly bilateral presentation in both groups. Despite using the more permissive alpha angle threshold of 55˚ to define cam morphology, mean alpha angles differed only marginally between groups, averaging 57.5˚ and 55.1˚ in the right and left hips of the soccer cohort, compared with 55.4˚ and 54.4˚ in controls.

One possible explanation for the absence of significant between-group differences relates to the reported level of sport participation during adolescence. Participation history was determined retrospectively through self-report, in some cases up to 18 years after the period of athletic involvement. Furthermore, youth soccer participation was defined as a minimum of three on-field sessions per week for at least 36 weeks per year between 10 and

14 years of age. When contrasted with the much greater training exposure reported in pre-professional soccer cohorts,[56] it is plausible that the loading magnitude and frequency experienced by these athletes was insufficient to bring about the structural adaptations often associated with cam morphology development. This interpretation is further supported by Tak et al.,[100] who reported that professional soccer players who began participating in soccer at least four times per week before the age of 12 years were more likely to develop cam morphology than those who reached this training frequency later during adolescence.

Much like in ice hockey, the true prevalence of cam morphology in high-risk and (pre)professional soccer players may remain underrecognized, not least because many athletes continuing to participate while symptomatic.[101,102] In support of this, a final radiographic analysis of 75 elite male soccer players reported considerably high prevalence rates of cam morphology and elevated alpha angles.[101] Although a normal alpha angle is generally considered to be less than 55˚, the mean alpha angle in this cohort was 65.6˚, while cam-positive athletes averaged even higher, reaching 70.7˚. Cam morphology was identified in 68% of players, with 76.5% demonstrating bilateral involvement.

Radiographic investigations serve to reinforce the association between elite soccer participation during childhood and adolescence and the gradual development of cam morphology. However, because most current evidence is derived from retrospective imaging studies performed only after structural changes have already begun to take place, opportunities for early intervention and preventative strategies may already be limited at the point of detection. As such, there remains a need for specific and accessible methods capable of identifying high-risk movement and loading patterns earlier in athletic development, before problematic morphological adaptations become radiographically evident.

2.3 Mechanisms of Sport-related Cam Development

Although the association between high-impact sport participation in “at-risk” activities and cam morphology is now well established, the exact mechanism underlying sport-related cam development remains incompletely understood. Current evidence suggests that cam morphology may develop as a normal physiological response to repetitive mechanical loading imposed on the proximal femur during growth while the physis remains open, or due to abnormal developmental of the proximal femoral physis.[19,89,91,103,104]

2.3.1 Load-Induced Reactive Bone Remodelling

Immature skeletal tissue is particularly sensitive to mechanical stress, which influences both the structural and material properties of bone, due to increased tissue elasticity and heightened remodelling during growth.[104,105] In youth athletes exposed to high-magnitude, abnormal loading via participation in high-impact sports, these forces may trigger bone growth at the femoral head–neck junction and ultimately contribute to irregular hip morphology.[19,21,89]

Bony abutment between the femoral neck and anterosuperior acetabulum generally requires approximately 90˚ of hip flexion.[8,24] However, the degree of hip flexion required to produce impingement is likely influenced by simultaneous motion in the frontal and transverse planes, namely internal rotation and adduction, which may contribute to earlier femoroacetabular contact during movement.[24] This concept is supported by finite element analyses demonstrating that peak shear stresses and contact pressures at the anterosuperior acetabulum occur primarily during combined deep hip flexion and internal rotation.[106,107]

Accordingly, the repetitive performance of athletic movements that demand large magnitudes of hip flexion, internal rotation, and adduction may elicit structural changes of the developing hip joint in athletes participating in "at-risk" sports.[24,80] Many of these activities require supraphysiological hip motion under load, increasing stress across the proximal femoral physis, which may cause the joint to remodel in response.[80] A similar bone remodelling response to repetitive activity has been observed in the shoulders of youth baseball pitchers,[108,109] supporting the concept that movements such as skating, running, cutting, and kicking may induce comparable adaptive changes.[29]

One confounding factor is the existence of the large asymptomatic athletic population that exhibit morphological adaptations consistent with cam FAIS yet remain symptom-free. As previously discussed, this likely reflects insufficient exposure of these individuals to high-risk loading conditions or hip positions required to progress from structural adaptation to symptomatic disease.[24,29]

2.3.2 Developmental Alterations of the Proximal Femoral Physis

There is conflicting evidence regarding whether cam formation results from a developmental abnormality rather than a reactive bone formation process. This concept was first described by Siebenrock et al.,[110] in 15 symptomatic cam FAIS patients with aspherical femoral heads, where decreased femoral head–neck offset was observed alongside increased epiphyseal

extension toward the femoral neck. Specifically, epiphyseal extension refers to abnormal growth of the femoral head physis toward the femoral neck, which may contribute to reduced head–neck concavity and loss of sphericity.[5] These alterations were most prominent within the anterosuperior region of the femoral head-neck junction, the location most commonly linked to cam morphology, suggesting that abnormal physeal growth may contribute to the development of cam morphology.[110] It has therefore been proposed that this growth may occur as a structural adaptation of the epiphysis, much like bone remodelling, to resist the higher shear stresses applied to the proximal femur during sport-specific movements.[56]

To further investigate this theory, Siebenrock et al.,[5] later examined the same cohort of elite youth basketball players, speculating that sports participation modifies the shape and growth of the physis, as quantified by abnormal epiphyseal extension. Greater epiphyseal extension was observed predominantly in younger athletes (9.3–16.2 years) with open physes, even before the development of cam morphology, when compared with their non-athletic peers, supporting the possibility that this mechanism interferes with normal skeletal development. Furthermore, increased epiphyseal extension correlated with greater alpha angles only within the anterosuperior region highlighted in the previous study.[110] While altered physeal shape was identified and may even precede and contribute to the development of cam morphology in this population, the authors noted that whether these anatomical changes ultimately progress to symptomatic impingement remains inconclusive.

Similar conclusions were drawn from a cohort of 103 male soccer players aged 9 to 18 years, recruited from the Southampton Football Club Academy, a pre-professional youth environment in the United Kingdom.[111] Given that soft tissue structures also impact FAIS, this study compared cartilage alpha angles obtained via MRI in soccer athletes with an age-matched inactive control group (52 males and 53 females). By the age of 10, soccer athletes demonstrated evidence of increased cartilage alpha angles at the femoral head-neck junction, which may represent soft tissue hypertrophy preceding epiphyseal extension and subsequent osseous morphological changes. Between 12 and 14 years of age, both cartilage alpha angle and epiphyseal extension increased most markedly, particularly within the anterosuperior region, before plateauing as athletes neared physeal closure. Importantly, approximately 50% of the variability in cartilage alpha angle in males was explained by epiphyseal extension, supporting a potential role for epiphyseal extension as a determinant of cam development. However, due to the cross-sectional design, it remained unclear whether these hips would ultimately progress to symptomatic cam morphology.

This study also found a dose-response relationship between soccer activity levels, cartilage alpha angles, and epiphyseal extension.[111] Progressive increases in both cartilage alpha angles and epiphyseal extension were observed across groups, from non-participants, to recreational players, and finally to athletes competing at national or international level. A similar pattern has been reported in other soccer cohorts, validating that the frequency of soccer participation during skeletal growth is associated with the development of a cam morphology.[56,100]

To examine whether radiographic features could predict the formation of cam morphology, a separate study assessed epiphyseal extension at the anterosuperior head–neck junction via radiograph in 126 hips of elite pre-professional soccer players aged 12 to 19 years.[56] Over a 2-year period, cam deformity developed progressively during skeletal maturation, such that only 43.2% of players retained a normal head–neck junction appearance at follow-up compared with 84.1% of players aged 12 or 13 years at baseline. The authors also tracked epiphyseal extension throughout this period, again reporting a strong positive correlation between epiphyseal extension and alpha angle in hips with cam morphology. However, despite this strong association, epiphyseal extension was not found to predict later cam development. Instead, the findings suggested that this abnormal growth occurs concurrently with the gradual formation of cam morphology, rather than prior to it.

2.3.3 Mechanobiological Mechanisms

Despite these theories, the deterministic hip loading patterns and corresponding magnitudes that stimulate the formation of a cam morphology remain underrepresented in the literature. To address this, Roels et al.,[105] investigated the influence of specific physical activities on the development of cam-type morphology using finite element analysis of a growing hip model. The authors simulated musculoskeletal loading patterns applied to the proximal femur during four representative movement tasks experienced by athletes practicing high-impact sports: gait, hip internal rotation, hip external rotation, and hip flexion. These loading conditions were examined in combination with varying degrees of epiphyseal extension.

The osteogenic index (OI), a measure often used to estimate the mechanical loading of tissues, was used to quantify the stimulus required for bone growth, with higher OI values indicating greater osteogenic stimulus.[112] Compared with gait and internal rotation, greater OI values were observed during hip flexion and external rotation, suggesting that these movements generate greater mechanical stimuli for bone formation at the proximal femur.

Importantly, these findings should be distinguished from the mechanism of impingement involved in symptomatic cam FAIS. Movements combining hip flexion and external rotation, potentially with hip abduction, may generate sufficient strain to contribute to cam morphology development during skeletal maturation,[114] whereas hip flexion, adduction, and internal rotation are primarily implicated in the subsequent impingement of an already-developed cam morphology.[6] As such, the comparatively low OI observed during internal rotation reported by Roels et al.,[114] may indicate that its relevance to cam FAIS is more closely related to the impingement mechanism than to the osteogenic stimulus underlying cam morphology development.[24] In contrast, gait requires approximately 30% of the total hip flexion ROM, and so does not regularly place the hip in positions associated with femoroacetabular abutment.[24]

As epiphyseal extension increased, so did the likelihood of cam morphology formation.[105] This was attributed to asymmetric growth of the proximal femoral physis caused by inhibitory and stimulatory stresses acting on opposing sides of the growth plate, reflected by progressively greater differences in OI values between these regions. Critically, during hip external rotation and flexion loading cases, the greatest imbalance between OI values across the growth plate occurred within the anterosuperior region where cam deformities usually form. While limitations exist due to modelling assumptions, this study integrated both mechanical stress exposure and osseous adaptation, providing a unifying framework for sport-related cam development. Given the dynamic, impact-like forces in sports, the authors concluded that that young elite athletes participating in activities requiring repetitive weight-bearing during hip flexion and external rotation are likely at increased risk for cam morphology development.[105]

Consequently, although the precise etiology of cam morphology remains unclear, understanding has advanced through retrospective, longitudinal, and modelling studies examining skeletal maturation and high-impact sport participation, particularly in soccer, indicating that youth athletes in these sports are at increased risk. It has further been proposed that the initial consequences of cam FAIS (i.e., abnormal joint mechanics) may accelerate progression of the condition through a cyclical process of repetitive impingement and continued intra-articular degeneration, ultimately contributing to symptomatic disease and potentially early-onset hip OA (Cannon et al.).[24] To mitigate longer-term injury risk and reduce the potential progression toward hip OA associated with cam FAIS, this warrants the identification and implementation of preventive strategies aimed at limiting harmful exposure

during skeletal development. However, to effectively inform such strategies, a clearer understanding of the specific movement exposures experienced during sport participation is still required.

2.4 Soccer: A Model for Examining Repetitive Hip Joint Motion

2.4.1 Soccer Participation in Youth Athletes

Association soccer is one of, if not the most popular sport worldwide, being played and watched by more people than any other sport.[113,114] Recent official reports published by soccer's global governing body, Fédération Internationale de Football Association (FIFA), estimate approximately 130,000 registered professional players across nearly 4000 official clubs, and, most importantly in the context of FAIS, a further 21.5 million registrants under the age of 18.[27] These figures do not include unregistered players, which make up the remaining estimated 242.9 million players.[27] Of the registered under-18 cohort worldwide, an estimated 18.7 million are male, representing the demographic most discussed in association with cam deformities in the literature.

Soccer participation among youth athletes also trends towards significant increases each year.[115] Alongside this growth is a concomitant rise in training and matches. In the United States, many children competing in organized soccer participate in training or matchplay more than four times per week, in addition to multi-game weekend tournaments, for up to 48 weeks annually.[29] In Canada, soccer is now the most played youth sport across both general physical activity participation (50%) and organized sport participation (39%), surpassing the likes of ice hockey and basketball.[28] Hip injuries already account for approximately 11–16% of all injuries sustained by male professional and elite youth soccer players.[30] Consequently, not only are increasing numbers of children participating in soccer during skeletal maturation, but many are also being exposed to progressively greater training volumes and movement demands that may contribute to the development of cam morphology and subsequent cam FAIS.

2.4.2 Physical Demands

Whether during training or matchplay, soccer is characterized by its highly dynamic nature, whereby multiplanar physical actions are integrated with a multitude of technical skills.[116] In terms of physical demand, analyses of in-game running performance across the top three tiers of English soccer demonstrate that elite players usually cover between 10 and 13 km per match depending on their position, with approximately 10% completed at high-intensity, both

in and out of ball possession.[31,116,117] In these studies, high-intensity running was quantified as the combined distance covered by players performed at speeds ≥ 19.8 km/hr. Over a seven-season period (2006-07 to 2012-13), high-intensity running and sprint distances in the English Premier League, widely regarded as the highest standard of professional soccer globally, were estimated to increased by approximately 30-50%.[116]

In addition to the sheer distances covered by soccer players each match, running is frequently interrupted by intermittent bouts of unpredictable, change-of-direction movement.[118] Approximately 1000 to 1500 discrete movement changes are performed every match.[118] Time-motion analysis of the purposeful activity (i.e., competing for the ball, evading or tracking opponents) of 55 male English Premier League players found an average of 726 directional changes per match, with 609 involving 0–90˚ turns to either side.[118] Additionally, approximately 30.7% of purposeful movement is non-linear, including backward, lateral, diagonal, or curvilinear motion. These movements demand rapid and reactive deceleration and re-acceleration under unanticipated conditions, requiring multiplanar hip motion rather than isolated, sagittal plane movement.[118,119] Moreover, sharper changes of direction (>90˚) are thought to require greater force generation due to increased whole-body momentum redirection, necessitating increased muscle activity to produce higher braking and propulsive forces.[119] From a cam FAIS perspective, this likely elevates hip joint loading during weight-bearing, increasing exposure to troublesome combinations of hip motion associated with cam morphology development and symptomatic femoroacetabular contact.

Kinematic analysis highlights that these change-of-direction tasks place the hip joint in alignments that may predispose soccer players to cam FAIS injury mechanisms. A stepwise increase in the magnitude of combined hip flexion, internal rotation, and abduction was observed in the plant leg of 26 male semi-professional soccer players performing maximal-effort change-of-direction tasks of increasing sharpness.[120] The protocol consisted of a 5 m approach and 5 m exit separated by a single directional change of 45˚, 90˚, 135˚, or 180˚. As change-of-direction angle increased, peak hip flexion increased progressively from 47.6˚ during 45˚ cuts to 75.2˚ during 180˚ turns, while hip abduction increased from 11.8˚ to 23.5˚, and hip internal rotation from 7.2˚ to 15.7˚. While most change-of-direction actions performed during matchplay occur between 0–90˚,[118] the larger directional changes placed the hip in positions approaching those commonly used clinically to assess cam FAIS, namely hip flexion approaching 90˚ combined with approximately 20˚ of internal rotation.[3,6,58]

Jumping and landing also represent relevant high-impact movements during soccer match play. Analysis of professional English Premier League players during the 2003-2004 season demonstrated that jumping, and subsequently landing, among other non-running activities occur regularly during match play.[120] These movements involve rapid generation and absorption of whole-body forces and require substantial lower-limb motion, particularly hip flexion, during take-off and landing to compete against opponents to win the ball. They are even used to assess performance levels when profiling young players.[40] As such, their frequency and high-impact nature may contribute to the overall mechanical loading experienced by a developing hip, while the hip positions adopted during take-off and landing may also be relevant to symptomatic impingement in athletes with pre-existing cam morphology.

2.4.3 Technical and On-the-Ball Actions

These manoeuvres extend beyond running-based directional changes, or jump-land tasks, and into technical soccer actions performed under more complex match or training conditions. For example, dribbling - the skill of advancing the ball with repeated touches to beat an opponent, maintain possession, or create space - requires repeated acceleration, deceleration, cutting, and turning while simultaneously maintaining ball control and responding to defensive pressure. Resultantly, on-ball techniques may expose athletes to similar hip joint positions and multiplanar loading strategies as off-ball movement tasks, while the additional technical demands of kicking and controlling the ball may further increase mechanical demand across the hip joint.

In addition to directional running and dribbling tasks, soccer players perform a substantial volume of other demanding on-ball actions. When assessing positional demands in the English Premier League, professional players performed an average of 111 on-the-ball activities per match regardless of playing position.[121] Although the techniques considered were not exhaustive, and excluded several common actions such as shooting, or passing with the non-dominant limb, the analysis still included frequent technical skills such as passing, ball reception, and dribbling. Consequently, the true volume of technically demanding hip movements performed during matchplay is likely far greater.

Further analyses of elite match performance demonstrate that professional players attempt approximately 39.8 passes per match, receive the ball up to 40.3 times, and average 2.9 touches per possession.[121–123] Importantly, passing is widely regarded as the fundamental

technical action underpinning successful soccer performance,[99,124] accounting for approximately 69% of all on-ball actions during matchplay. The total number of passes completed per match is suggested to have increased by approximately 40% over recent seasons, with teams often completing upwards of 500 passes per game.[116,124] Although players may legally use any body segment except the upper limbs to pass the ball, the foot is the preferred method for passing actions, with the instep kick representing the most used kicking technique in soccer. Given the frequency with which this skill is performed, several studies have conducted biomechanical assessments of the instep pass to characterize hip joint positions and movement patterns, which may provide indirect insight into mechanisms relevant to cam FAIS in youth soccer players.[125]

2.4.3.1 Kicking Biomechanics

One of the early three-dimensional analyses of the instep kick used cinematographic data to characterize lower-limb motion and mechanics during the instep kick.[125] In relation to cam FAIS, hip joint kinematics were examined across the kicking cycle, from initial foot-off to ball contact. Prior to the backswing phase, the hip was near neutral in the sagittal plane but already positioned in approximately 12˚ of abduction and 10˚ of external rotation. During the backswing, the hip moved into extension, reaching ~19˚, while abduction increased to ~29˚. In preparation for ball contact, the hip then transitioned into flexion, reaching ~31˚ at impact, while maintaining abduction and external rotation throughout. These kinematic characteristics are particularly relevant to the development of cam morphology proposed by Roels et al.,[107] as the combination of hip flexion, external rotation, and abduction observed during the instep kick overlaps with loading patterns previously associated with greater osteogenic stimulus at the proximal femur.

A subsequent study by Shan and Westerhoff,[33] compared hip range of motion during instep kicking between novice and elite players using a nine-camera motion capture system. Across both the run-up and kicking steps, elite players demonstrated greater hip excursion in all planes, with significant differences observed for flexion–extension. During the run-up, hip flexion–extension range reached approximately 93˚ and 92˚ in the kicking and non-kicking limbs, respectively, compared with 60˚ and 58˚ in novices. Differences were more pronounced during the kicking phase, where elite players demonstrated approximately 130˚ of hip flexion–extension in the kicking limb and 113˚ in the support limb, compared with 72˚ and 66˚ in novices. Elite players also exhibited greater abduction–adduction (22˚ vs 14˚) and rotational range (17˚ vs 12˚) compared with novices. Notably, peak flexion values in elite

players approach or exceed clinical thresholds commonly used in the assessment of cam-related impingement (>90˚), particularly when combined with concurrent motion in the frontal and transverse planes.

These findings should be interpreted with methodological considerations. Both analyses capture the kinematics of a single ball-striking surface (the inside of the foot), whereas players frequently use alternative surfaces, including the outside of the foot or laces, to pass, shoot, or receive the ball, which would likely require different hip joint positions to execute successfully. In addition, neither study accounts for the follow-through phase after ball contact, during which the hip moves into flexion, adduction, and internal rotation—mimicking the combined position used clinically to reproduce symptoms of cam FAIS.[29] Despite this, these observations suggest that repetitive performance of both off-the-ball and on-the-ball actions such as cutting, passing, dribbling, and receiving may expose players to frequent multiplanar hip positions consistent with those implicated in cam FAIS development and symptom provocation.

2.4.4 The Role of the Training Environment

While much of the existing literature has focused on matchplay demands, this represents only part of the overall exposure profile. The training environment contributes substantially to cumulative hip joint exposure during skeletal development, as technical skills and movement patterns are often performed repeatedly within specialized activities, allowing athletes to accumulate considerably more repetitions of specific actions than would occur during matchplay. However, relatively little research has examined soccer training sessions designed to isolate specific technical elements, such as structured passing drills, although recent work has begun to focus on small-sided games.[126,127]

The high repetition potential of training activities is particularly relevant given that, during a 90-minute match, players are in possession of the ball for only approximately 2% of total game duration.[127] Small-sided games are therefore widely used in coaching practice across all age groups due to the increased levels of player interaction and facilitate technical engagement through reduced pitch dimensions and smaller team sizes compared with full 11-a-side matchplay.[126] Typical formats range from 3v3 to 9v9. FIFA resources suggest that these formats drastically increase technical repetition, with players in 4v4 environments performing approximately five times more ball touches and ~50% more touches in 7v7 formats compared with full-sided play.[128]

In youth age groups (U9, under 9 years old; and U14, under 14 years old), which broadly align with the developmental period during which radiographic features of cam morphology begin to emerge, 20-minute small-sided games (5v5, 7v7, and 9v9) have been shown to elicit significantly higher ball involvement, with average touches per outfield player decreasing significantly as team size increases.[126] Similarly, both the number of dribbles and attempted passes were consistently higher in smaller formats. Comparable findings have been reported in a cohort of 34 trained 13-year-old players, where 3v3 formats produced significantly greater numbers of short passes ad dribbles than 6v6 formats, alongside elevated physical demand, reflected by mean heart rates of approximately 87.6% of maximum.[127] While targeted training exercises are critical for technical skill acquisition and player development in youth soccer, these findings raise concern that the repetitive volume and intensity of such drills may simultaneously increase exposure to the patterns and triggers associated with the development of cam morphology.

Despite the global popularity and increasing technical and physical demands of youth soccer, objective monitoring approaches capable of identifying and quantifying high-risk hip joint movements remain limited, particularly within training environments where most technical repetition is accumulated. To mitigate the risk and reduce the burden of cam FAIS in this population, greater emphasis should be placed on the development of accessible monitoring and early identification strategies during skeletal growth, when participation volume and intensity may still be modified prior to the development of structural adaptation and symptomatic cam FAIS.

2.5 Quantifying Movement Exposure in Sport

2.5.1 Technologies for Capturing Athlete Movement

Coaches, athletes, and clinicians continually seek to optimize athletic performance while minimizing injury risk.[129] Central to both goals is the ability to objectively quantify how athletes move within their sporting environment.[129] As demand for real-time feedback in sport continues to grow, advances in technology have facilitated increasingly sophisticated analysis of performance indicators and biomechanical variables, reducing reliance on subjective observation alone, which may be influenced by a coach's experience and bias.[129,130] Consequently, researchers have developed technologies capable of quantifying physical demands, movement patterns, and joint kinematics, providing valuable information

for performance enhancement, injury prevention, rehabilitation, and return-to-play decision-making.[130]

A variety of athlete-monitoring technologies are now available, including global positioning systems (GPS), local positioning systems (LPS), semi-automatic video tracking systems, and OMC systems.[32,130,131] For detailed kinematic assessment of movement technique and joint kinematics, OMC is widely regarded as the gold-standard approach due to its high spatial resolution, precision, and measurement accuracy.[40,41] However, among other limitations, OMC systems are generally restricted to laboratory environments, restricting their ability to provide real-time feedback during training or competition.[41,130]

Recently, growing attention has been directed toward wearable sensing technologies as an alternative means of kinematic monitoring. Wearable sensors, most commonly inertial measurement units (IMUs), offer the potential to capture movement data in real sporting environments while providing more accessible and immediate feedback to athletes and practitioners.[41,129,130] Following validation for their intended application, IMUs have demonstrated sufficient accuracy for quantifying joint kinematics and movement characteristics across a variety of sporting contexts,[129] making them a promising tool for monitoring movement exposure outside of the laboratory.

The following sections will review current approaches used to quantify athlete movement in addition to emerging technologies for automated movement detection and classification. This literature provides the foundation for the development of practical monitoring strategies capable of quantifying sport-specific movement exposure in real-world environments, which is essential for improving understanding of the soccer-specific movement patterns potentially associated with the development of cam FAIS.

2.5.2 Field-based Athlete Monitoring

Common modalities used to acquire positional information during sports performance include GPS, LPS, and semi-automatic video tracking systems. GPS technology has become integral to the quantification of physical demands in field-based sports, particularly soccer.[31] Worn by individual athletes, typically on the upper back, GPS units use satellite signals to estimate position, velocity, distance covered, and acceleration throughout training and competition. Modern systems may additionally record physiological measures, such as heart rate, and provide information relating to collision frequency and intensity with impressive detection accuracy.[31,130] To allow comparison against OMC systems, GPS devices are often validated

using predefined, sport-specific courses that approximate real movement demands within the capture volume of the OMC setup, rather than through assessment during actual training or competition.[131]

Similar information can be obtained using local positioning systems (LPS) and semi-automatic video tracking systems. Unlike GPS, LPS relies on a network of locally positioned transmitters and receivers surrounding the playing area rather than satellite signals.[132] Athletes continue to wear a receiver, but positional information is determined relative to the local antenna network.[132] Compared with GPS, LPS systems generally provide higher sampling frequencies and are not dependent on satellite reception, making them suitable for indoor environments and large stadiums where signal quality may be compromised.[132] Furthermore, LPS has been shown to outperform GPS when estimating distances covered during linear and multidirectional walking, jogging, and sprinting activities.[32]

Semi-automatic video tracking systems use multiple synchronized cameras positioned around the playing area to record player movement, often operating only within the environment in which they are permanently installed.[129] Although capable of tracking multiple athletes simultaneously, these systems typically require extensive post-processing and manual event labelling, limiting their suitability for real-time analysis. In team sports, tracking accuracy may also be affected by player occlusion or visual similarities between athletes or their uniforms.[32] Additional limitations include privacy concerns and substantial infrastructure requirements, as stadiums often require modifications to optimize camera placement and lighting conditions.[32,131]

Despite their widespread adoption, including use by professional organizations, these technologies primarily quantify where, how far, and how fast an athlete moves rather than how they move. Metrics such as heart rate, total distance covered, velocity, acceleration, and collision frequency provide valuable information regarding work rate and fatigue management, thereby informing training or playing load and tactical in-game decision-making. However, they offer limited insight into joint kinematics during specific techniques and the movement patterns potentially associated with injury mechanisms. While GPS, LPS, and video-based systems are valuable tools for athlete monitoring to an extent, they are less suited to investigating the movement exposures hypothesized to contribute to the development of conditions such as cam FAIS. For this purpose, more detailed kinematic motion analysis approaches are required.

2.5.3 Laboratory-Based Motion Analysis

Traditionally, research has relied on laboratory-based motion analysis systems to obtain detailed information regarding human movement and performance. Joint angle estimation is particularly important in the assessment and management of several musculoskeletal conditions, including hip OA and FAIS.[24,34,133] OMC systems are the widely accepted standard for the estimation of joint angles.[41,133] Within a controlled laboratory environment, multiple infrared cameras track retroreflective markers attached to anatomical landmarks attached to a person's body, enabling 3D reconstruction of body segment motion and subsequent estimation of joint angles relative to adjacent segments.[133]

The main advantage of these systems is their excellent accuracy and precision, with validation studies frequently reporting sub-millimeter positional accuracy for individual markers.[134] Commercial systems, such as Vicon (Oxford Metrics Group Ltd., Oxford, UK), have demonstrated static and dynamic mean absolute errors of ≤ 0.15 mm and 2 mm, respectively.[38,131] The ability to quantify movement in three dimensions has made OMC an indispensable tool in clinical gait analysis, while also enabling the capture of rapid and complex movements present in sporting activities.[134] Resultantly, the capability of OMC to estimate joint kinematics has allowed researchers to identify movement adaptations associated with pathology and to characterize sport-specific movement demands.

For example, an OMC assessment of 27 individuals with mild-to-moderate hip OA demonstrated a 41% reduction in sagittal-plane hip range of motion during walking compared with healthy age-matched controls, characterized primarily by reductions in hip flexion, extension, and adduction during stance.[34] Regarding FAIS, studies have reported altered pelvis mechanics during dynamic tasks, such as gait, stair climbing, or deep squatting.[24] In individuals with symptomatic unilateral cam FAIS, patients displayed increased hip flexion during walking (+4.9˚) and stair ascent (7.8˚) compared to healthy subjects. Consistent with the findings in the hip OA group in Constantinou et al.,[34]a systematic review showed moderate evidence for reduced peak hip extension angle during stance in patients with FAIS compared to controls, as determined by 3D motion capture models.[94] In motion capture analyses of deep squat tasks, patients with cam FAIS consistently display greater anterior pelvic tilt under maximum hip flexion, decreased posterior pelvic tilt, and decreased hip internal rotation.[24,25] Additionally, when performing constrained squats (i.e., narrow foot width, neutral foot position, limited trunk lean), 15 patients with cam or combined FAIS demonstrated equivalent squat depth but with greater hip adduction maintained throughout

the movement compared to controls, all of which may reflect compensatory movement strategies adopted to avoid painful impingement as the hip approaches end-ranges of flexion.[26] These findings demonstrate the capacity of OMC systems to identify even subtle changes in movement mechanics associated with hip pathology that may not be detectable through clinical observation alone.

Similar approaches have been applied to characterize hip kinematics during soccer-specific tasks, although their relevance to cam FAIS and movement exposure has received comparatively little attention. The instep kick has been the focus of most 3D biomechanical analyses, largely due to its importance as a fundamental technical skill.[33,99] Other studies have extended this approach to examine multiplanar lower limb joint angles during physical soccer tasks such as accelerations, decelerations, changes of direction, and single- and double-leg jump-landing manoeuvres.[35–38] In most cases, however, these kinematic measures have been collected to identify determinants of successful performance or inform training programmes designed to improve athletic execution,[40] rather than to investigate movement-related mechanisms specific to cam FAIS or monitor cumulative exposure to potentially provocative hip positions. [37]

This focus represents a notable limitation within the literature. Soccer is characterized by a diverse combination of complex physical and technical actions, many of which occur simultaneously while under highly variable environmental and competitive constraints.[33] The kinematic demands of other on-the-ball actions, including passing with different surfaces of the foot, receiving, or dribbling, remain comparatively underexplored despite their frequent occurrence during play.[117,121,123] From a cam FAIS perspective, this significantly limits the current understanding of the movement exposures experienced by players throughout normal participation.

The relative lack of kinematic analyses investigating other game-representative actions likely reflects some of the inherent challenges of studying these skills in laboratory settings using OMC systems, which may explain why only a few studies have assessed soccer kinematics outside of the lab environment.[33,39] Despite their accuracy, OMC systems are expensive, complex to set up, confined to a relatively small, calibrated capture volume, require trained personnel to operate effectively, and, perhaps most importantly, possess limited portability.[36,38–40] As a result, athletes are often required to perform simplified representations of sport-specific tasks that may not sufficiently replicate normal movement behaviour.

The importance of ecological validity has recently been highlighted in anterior cruciate ligament injury research, where high-risk movement patterns identified in the laboratory only partially reflected those observed during on-field participation in female soccer players.[135] Although the mechanisms underlying cam morphology development are less clearly defined than those associated with anterior cruciate ligament injuries, these findings emphasize the importance of assessing movement within the environments in which athletes naturally train and compete.[36,135] In this context, relying on laboratory-derived motion profiles alone may potentially limit understanding of the soccer-specific movement patterns associated with cam FAIS development in youth athletes. Considering this, researchers and practitioners have increasingly explored wearable sensing technologies, particularly IMUs, as a portable and cost-effective alternative for obtaining movement data, including joint kinematics, in field-based settings while better preserving the athlete–environment interaction.

2.5.4 Wearable Inertial Measurement Units (IMUs)

Body-worn IMUs are small, portable, self-contained devices capable of unobtrusive human motion tracking outside of laboratory environments.[41,42] A single IMU houses a tri-axial gyroscope, accelerometer, and magnetometer, which measure 3D angular velocity, linear acceleration, and magnetic field, respectively.[136] Through the integration of gyroscope and accelerometer signals using sensor fusion algorithms, commonly based on Kalman filtering techniques, the 3D orientation of each sensor can be determined relative to a local reference frame.[42] When multiple IMUs are attached to connected body segments, these orientation data can be combined to reconstruct whole-body motion and derive segment and joint kinematics.[136,137] Prior to data collection, however, a dedicated calibration procedure is required to estimate subject-specific body dimensions and establish the alignment between each sensor and its corresponding anatomical segment.[137] A systematic review of inertial sensors for human motion analysis concluded that IMUs can provide both accurate and reliable measures; however, their performance is task-specific.[48] Therefore, to monitor exposure to potentially high-risk soccer movements in real-world environments, confidence in the ability of these sensors to accurately quantify lower-limb kinematics must first be established for the specific sporting tasks in which they are intended to be applied.

2.5.4.1 Validity and Reliability of IMUs Compared to OMC Systems

To assess the validity and reliability of IMUs, numerous studies have compared IMU-derived kinematics directly against those obtained using OMC systems. Overall, the validity of IMUs for lower-limb motion analysis appears promising, particularly for sagittal and frontal plane movements, although performance is generally reduced for transverse plane motions.[43,138,139] During dynamic tasks, various IMU configurations have demonstrated good-to-excellent agreement with OMC systems in the sagittal and frontal planes, as evidenced by favourable root mean squared error (RMSE), coefficient of multiple correlation (CMC), cross-correlation, and range-of-motion comparisons.[37,41,43] Accurate and accessible kinematic assessment of the hip joint in more dynamic tasks is of particular interest given the established associations between altered hip ROM and pelvis mechanics, FAIS, and hip OA.[24,140]

Using seven research-grade Xsens MTw Awinda (Xsens Technologies B.V., Enschede, The Netherlands) sensors during a six-minute walking trial, Teufl et al.,[41] reported relatively low RMSE values for hip kinematics relative to a 13-camera OMC system. For the left hip, RMSE values averaged 3.61˚, 2.65˚, and 5.50˚ for flexion-extension, adduction-abduction, and internal-external rotation, respectively, while corresponding values for the right hip were 3.68˚, 2.61˚, and 5.00˚. Although these absolute errors appear relatively small, their magnitude should be considered in relation to the amount of motion occurring within each plane. However, corresponding ROM values were not reported, and so direct comparison of error relative to the total ROM is not possible. Waveform agreement was good-to-excellent in the sagittal plane (CMC = 0.89–1.00), moderate-to-good in the frontal plane, and substantially lower in the transverse plane (CMC = 0.53–0.67), indicating reduced agreement for rotational movements. Similar findings were reported during walking and stair negotiation tasks by Zhang et al.,[138] who observed excellent waveform similarity for sagittal plane hip kinematics (all tasks: CMC > 0.96) but notably poorer agreement for frontal and transverse plane measures (CMC = 0.50–85).

Several authors have proposed that the reduced correlation observed in the frontal and transverse planes is partly attributable to differences in the anatomical reference frames and zero-joint positions used by IMU and OMC systems.[37,38,138,139] Previously, correcting for these alignment offsets has been shown to improve waveform similarity, and so corrections are recommended when IMU- and OMC-derived lower limb kinematics are compared or used interchangeably.[37,138,139] When interpreting agreement between systems, a recent review

by Cuesta-Vargas et al.,[48] concluded that between-system errors of ≤2˚ are generally acceptable, whereas errors exceeding 5˚ should be interpreted with caution.

With these error thresholds in mind, IMUs have demonstrated good-to-excellent agreement with OMC systems during certain soccer-related movements, particularly in the sagittal plane, as measured by cross correlation (XCORR). During a series of change-of-direction and jumping tasks, including single-leg deceleration-to-push-off, 45˚ sidestep cutting, single-leg hop-and-land, and double-leg jump-and-land with lateral shuffle, participants wearing a full-body seventeen-sensor Xsens IMU system demonstrated high agreement with OMC-derived hip angles in the sagittal (XCORR = 0.98) and frontal (XCORR = 0.89) planes.[36] The only exception occurred during the single-leg hop-and land task, where frontal plane agreement was lower (XCORR = 0.69). Across all tasks, transverse-plane hip kinematics demonstrated only fair agreement (XCORR = 0.66), reinforcing previous findings that IMUs have greater difficulty accurately quantifying finer rotational motion about the longitudinal axis.[36,43]

Using the same set of tasks, Heuvelmans et al.,[37] evaluated the Noraxon MyoMotion system, comprising nine IMUs. Following correction for alignment offsets, similarly strong agreement was observed for sagittal-plane hip kinematics (all tasks: XCORR > 0.88). However, considerably larger variability was observed in frontal and transverse plane kinematics. The greater variability observed outside the sagittal plane may reflect differences in sensor hardware and the number of sensors worn, sensor fusion algorithms, or biomechanical modelling approaches, emphasizing that validation findings should not be generalized across IMU systems and are likely device- and task-specific.[48]

Similar results have been reported during other dynamic movements relevant to sport participation. Al-Amri et al.,[38] observed excellent waveform similarity between a lower-body Xsens IMU configuration and a Vicon OMC system during both vertical jump and squat tasks, with sagittal plane hip kinematics demonstrating the strongest agreement (CMC > 0.90) and frontal and transverse plane measures showing acceptable agreement following offset correction. Taken together, these studies indicate that IMUs can quantify hip motion during a range of dynamic sporting movements, although caution remains warranted when interpreting rotational kinematics.

Most relevant to soccer-specific technical skills, Blair et al.,[39] concurrently validated in-field kicking biomechanics obtained from a seventeen-sensor Xsens system against an

OMC setup in thirty athletes participating in kicking sports, including ten soccer players. Participants performed 12 m, 20 m, and maximal instep kicks. Although comprehensive hip kinematics were not reported, the mean difference in peak hip extension between systems was only 1.7˚, while differences in velocity-related measures, including foot speed and pelvis velocity, were similarly trivial. Interestingly, measurement error increased with kicking velocity in both systems, suggesting that highly explosive movements may present greater challenges for accurate assessment irrespective of the measurement method.

These studies suggest that IMUs can provide valid estimates of hip kinematics during a range of soccer-relevant movements, particularly in the sagittal plane. However, validation evidence has yet to be extended to many of the highly dynamic, multiplanar actions that characterize soccer participation and may be most relevant to cam FAIS development. Nevertheless, the growing body of validation research represents an important step toward conducting movement exposure monitoring in ecologically valid sporting environments, rather than relying solely on laboratory-based assessment.

2.5.4.2 IMU-Based Movement Classification and Emerging Hip Kinematic Applications in Soccer

The agreement reported between IMU-based and OMC-derived motion analysis has facilitated the development of numerous wearable systems for soccer performance analysis. While research-grade systems such as Xsens have been the primary focus of validation studies,[43] advances in sensor technology and automated signal processing have enabled the development of wearable devices capable of detecting, classifying, and quantifying soccer-specific movements in training and competition. These systems have the potential to measure sport-specific movement exposure outside the laboratory.

One of the most prominent examples is the foot-mounted PlayerMaker IMU (Playermaker, Tel Aviv, Israel), which combines gait analysis with proprietary event-detection algorithms to quantify both physical and technical soccer skills. Through identification of gait events, ball contacts, and foot orientation, the system provides metrics including turns performed on and off the ball, ball contacts, time in possession, distance covered, and the surface of the foot used during ball release.[141] Through foot-mounted sensing and soccer-specific event-detection algorithms, these devices identify limb orientation, translational movement, and discrete technical actions, enabling bilateral performance profiling of individual players.[141]

When compared against an OMC system, PlayerMaker demonstrated good agreement for velocity estimation (mean difference = 0.048 m/s) during the soccer-specific aerobic field test 90 (SAFT90), an off-the-ball multidirectional intermittent movement protocol, which included jogging, sprinting, sidestepping, and cutting.[141] However, agreement decreased at higher movement speeds, with PlayerMaker underestimating velocity during actions exceeding 6.26 m/s, reinforcing that accuracy may be reduced under more explosive conditions.[39,141]

Regarding technical parameters, Lewis et al.,[46] compared the number of ball releases detected by the PlayerMaker system with those obtained from a high-speed camera setup in 21 professional soccer players. The first phase assessed the system's ability to detect kicks across a range of velocities, with strong correlations observed between systems across low, moderate, and high-intensity conditions. In the second phase, the IMUs were used to quantify the frequency and speed of ball releases from both feet; however, these outputs were not directly validated against manually labelled high-speed camera event data. Although the system shows strong validity for detecting ball release events, the lack of comparison to a reference system limits confidence in its ability to accurately quantify true movement exposure.

A similar automated classification approach was employed to differentiate between passes and shots in training and competitive matchplay using custom-made shoe-mounted IMUs.[45] The dataset comprised 884 passes and 181 shots from 11 male players during training sessions, and 336 passes and 18 shots from 17 male players during a 60-minute 11 vs 11 match. Using an algorithm incorporating peak detection of accelerometer signals, repetition segmentation, event leg identification, and action classification, the system achieved classification accuracies of 81.7% for passes and 86.7% for shots.[45] These findings indicate the feasibility of IMU-based classification of soccer-specific technical actions, but do not extend to the characterization of joint movement patterns potentially associated with injury mechanisms.

In contrast, a smaller body of research has used IMU systems to estimate hip joint angles during dynamic soccer activities. Representative results from five soccer players performing a maximal 30 m linear sprint test demonstrated the potential for IMUs to capture hip kinematics throughout high-intensity running tasks.[44] Maximal hip flexion and extension angles were observed across acceleration, maximal velocity, and deceleration phases; however, these measures were not validated against OMC. The authors also noted that

conventional sensor attachment directly to the skin may be unsuitable for high-intensity soccer actions due to the risk of sensor detachment.[44] This limitation prompted the development of a garment solution using smart tights with integrated IMUs to enable unobtrusive monitoring of lower-limb kinematics during soccer participation.[142]

In this system, IMUs were embedded into the tights at the shanks, lateral thighs, and waistband.[142] To validate the sensors, 5 recreational male soccer players performed soccer-specific tasks in a controlled laboratory, including acceleration, cutting, 180˚ turning, kicking, and jumping, while simultaneously being recorded using an OMC system. Although only sagittal plane hip kinematics were reported, the IMU-derived measures demonstrated good to excellent agreement with OMC for both limbs (CMC = 0.830 and 0.968 for right and left hips, respectively), indicating that IMU systems can provide valid estimates of sagittal hip joint angles during soccer-specific movements.[142]

While these approaches are promising in terms of monitoring participation demands, they remain largely non-specific to detailed joint-level movement exposure, focusing instead on activity counts or physical metrics to inform load-management strategies. As a result, they provide limited insight into repeated exposure to potentially harmful hip joint positions implicated in the development and provocation of conditions such as cam FAIS. Given the portability and accessibility of IMUs, there is a clear need for further exploration of hip joint kinematics relevant to FAIS and the frequency of movements associated with potentially high-risk hip positions during soccer participation. Such work may help to better contextualise the mechanical demands placed on the developing hip, particularly in youth male soccer players, who demonstrate some of the highest reported prevalences of cam morphology among athletes participating in high-impact sports. Beyond soccer, establishing practical approaches capable of automatically detecting and quantifying both movement exposure and associated hip kinematics may have broader applicability across sporting populations, providing a foundation for early identification of at-risk athletes and informing intervention strategies aimed at mitigating the development and long-term burden of cam FAIS.

3 Methods

3.1 IMU Validation

3.1.1 Participants and Setting

To address the first objective of this study, which was to compare lower-limb joint kinematics measured using a wearable IMU system with those measured using a gold-standard OMC system during 35 soccer-specific movements, 20 elite adult soccer players were recruited. Participants were recruited through direct communication with members of local varsity soccer teams (University of Waterloo, Conestoga College, Cambridge United, Guelph United), with permission from the respective head coaches. Eligibility was confirmed using a screening questionnaire administered prior to obtaining consent. Inclusion criteria required participants to be at least 18 years of age and to have elite-level soccer experience, defined as current participation on a varsity team or equivalent competitive league and extensive formal training over several years. Exclusion criteria included any musculoskeletal injury or surgical procedure to the lower limbs within the past six months that limited mobility, strength, balance, or limb use; and concussion or traumatic brain injury reported within the past six months.

The study was conducted in the Neural and Rehabilitation Engineering Laboratory (Room E7-6349) at the University of Waterloo. A convenience sample of ten young male adults (ages: 20.4 ± 1.6 years, mass: 76.0 ± 5.4 kg, height: 180.7 ± 5.8 cm) and ten young female adults (ages: 22.1 ± 4.1 years, mass: 63.7 ± 2.9 kg, height: 167.1 ± 4.7 cm) provided written informed consent to participate in the study, which was approved by a University of Waterloo Research Ethics Board (REB #47610). The sample size was estimated based on prior experience with movement data collection in the laboratory.

3.1.2 Experimental Set Up

Each participant completed a single controlled movement analysis session during one laboratory visit, lasting approximately 1.5-2 hours. At the beginning of the session, participant demographics and anthropometric measurements were recorded, including sex, height (cm), body mass (kg), leg length (right/left; cm), knee width (right/left; cm), ankle width (right/left; cm), and foot length (dominant foot, cm). Participants also reported their foot dominance (i.e., preferred kicking limb) and primary soccer position. Participants were

instructed to wear tight-fitting sportswear to minimize movement artefacts and soccer cleats to replicate their typical performance environment.

To compare IMU-derived lower-limb 3D kinematic data with those obtained from OMC, both systems were used simultaneously during data collection. Lower-body movement patterns were captured using seven Xsens MTw Awinda inertial measurement units (IMUs; 47 × 30 × 13 mm, 16 g), each integrating a tri-axial gyroscope, accelerometer, and magnetometer, with data recorded at a sampling frequency of 100 Hz (*Figure 8*).[42]



Figure 8. Xsens MTw Awinda IMU used for 3D lower limb motion capture.

IMUs were fitted to the participant's body segments in line with manufacturer guidelines using elasticated Velcro straps and reinforced with medical-grade adhesive tape (*Figure 9*).[136] Sensors were placed proximal to the dorsum of each foot (secured above the soccer cleat at the distal shank), the lower legs (proximal medial surface of the tibia), and the upper thighs (centrally on the lateral thigh, midway between the greater trochanter and lateral femoral epicondyle), with an additional sensor positioned on the posterior pelvis at the level of the anterior superior iliac spine (ASIS), midway between the left and right posterior superior iliac spine (PSIS) landmarks.[136]

Concurrent validity was assessed by comparing IMU-derived kinematic data with measurements obtained from a 200 Hz, 20-camera Vicon (Oxford Metrics Group Ltd., Oxford, UK) OMC system. Lower-body motion was tracked during dynamic trials via sixteen retroreflective kinematic markers (*Figure 9*) positioned bilaterally at anatomical landmarks (*Table 1*). The custom marker set was developed based on the Vicon Plug-in Gait (PiG) lower-body model,[143] with minor modifications implemented to prevent interference with kicking actions. This model was selected due to its well-documented test–retest repeatability and measurement accuracy, particularly for sagittal plane kinematics.[36] Markers were affixed directly to the skin where possible or over clothing using double-sided adhesive discs and

were further secured with medical-grade tape. Three retroreflective markers were also attached to each IMU in a non-collinear configuration (top left, bottom left, and bottom right corners) to allow the IMU to be tracked as a rigid body by the OMC system.

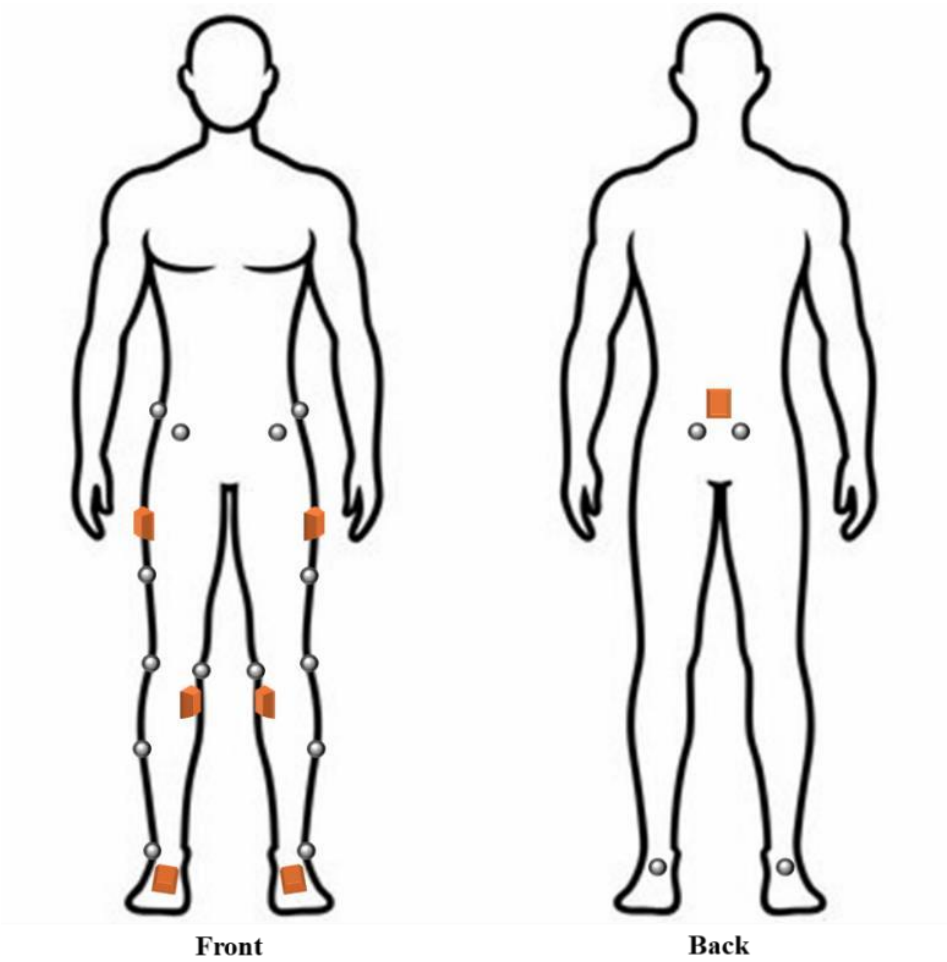


Figure 9. Front (left) and Back (right) view of the locations of the seven Xsens IMUs and sixteen Vicon retroreflective markers used for 3D lower-limb motion capture.

Table 1. Anatomical locations and definitions of the sixteen retroreflective markers comprising the custom configuration based on the Vicon Plug-in Gait lower-body marker set.[143]

Marker Label	Definition	Position on Participant
LASI	Left ASIS	Left/Right anterior superior iliac spine.
RASI	Right ASIS	
LPSI	Left PSIS	Left/Right posterior superior iliac spine, below the sacroiliac joints.
RPSI	Right PSIS	
LTHI	Left thigh	Over the lateral surface of the respective thigh, midway between the corresponding -ASI and -KNE markers.
RTHI	Right thigh	
LKNE	Left knee	On the flexion-extension axis of the respective knee about the lateral epicondyle of the femur.
RKNE	Right knee	
LFME	Left medial knee	On the flexion-extension axis of the respective knee about the medial epicondyle of the femur.
RFME	Right medial knee	
LTIB	Left tibia	Over the lateral surface of the respective shank, positioned towards the distal third of the tibia.
RTIB	Right tibia	
LANK	Left ankle	On the lateral malleolus of the respective ankle.
RANK	Right ankle	
LHEE	Left heel	At the calcaneus of the respective heel, at the same height as that of the metatarsophalangeal joints.
RHEE	Right heel	

To generate and scale biomechanical models, participant-specific anthropometric data were entered into the respective data acquisition software. For the IMU system, height and foot length were specified in Xsens MVN Analyze Pro (v2021.0.1, Xsens Technologies B.V., Enschede, The Netherlands). For the OMC system, height, body mass, leg length, knee width, and ankle width were entered into Vicon Nexus (v2.17).

Independent calibration procedures were subsequently performed for each system in accordance with manufacturer recommendations. For the IMU system, participants completed an N-pose followed by a walk calibration, consisting of standing quietly in a neutral posture with arms by the sides, walking a short distance forward and returning to the start position, and then resuming the N-pose until instructed otherwise. For the OMC system, camera calibration was first performed using the manufacturer's Active Wand, and the global

coordinate system was defined by setting the volume origin. A range-of-motion subject calibration was then completed to generate a subject-specific labelling skeleton (.vsk) file. Participants adopted a T-pose, with their feet positioned approximately hip-width apart and their arms abducted to 90˚ with the elbows flexed and palms facing downward, at the centre of the capture volume and performed a series of trunk, hip, knee, and ankle flexion and extension movements representative of those performed during the experimental protocol.

Once calibration procedures were completed, the investigator confirmed "Good" calibration quality in the Xsens software and verified correct marker identification within the Vicon system. Participants then completed a self-directed 5-minute warm-up within the calibrated capture volume of the OMC setup (6 m × 3 m). This warm-up period allowed participants to familiarize themselves with the testing environment and with movement while wearing the IMUs and kinematic markers, and to reduce the risk of musculoskeletal injury during subsequent physical activity testing.

In each trial, the Xsens and Vicon systems were synchronized using a hardware-based signal. The Xsens IMU system was configured as the leader device, such that initiation of recording in this software triggered the OMC system to begin data collection, operating as the follower. Synchronization settings were initialized according to Xsens recommendations. The trigger output was set to the Out 1 "Start Recording" signal with a rising-edge polarity, a pulse width of 5 ms, and no skipped pulses (skip factor = 0; skip first = 0).

3.1.3 Experimental Protocol

All trials were performed on an artificial turf surface (approximately 6 m × 2 m) positioned within the calibrated capture volume of the Vicon system. The turf was secured using double-sided carpet tape, with the corners further stabilized using weight plates to prevent movement during dynamic tasks. Prior to each trial, the task was demonstrated by the investigator. Participants were encouraged to take rest periods between trials to minimize the effects of fatigue on movement execution, and additional rest was provided upon request at any point during the session. Each trial began with participants standing quietly in a neutral position for 2-3 s to enable automatic marker labelling in Vicon Nexus (v2.17).

Participants performed a total of 35 movements comprising 19 unique soccer-specific tasks, of which 16 were performed bilaterally. The tasks were broadly categorized into three groups: (1) Range of Motion (Trials 1–9), (2) Off-the-Ball (Trials 10–17), and (3) On-the-Ball tasks (Trials 18–35). The movements and techniques were selected to reflect common

soccer-specific actions that are relevant to the study objectives. Participants completed a minimum of five successful trials per movement, using both limbs when applicable, with a maximum of ten repetitions performed for any single task. Trial order was standardized and identical for all participants to ensure consistency across sessions; however, this approach did not eliminate potential effects of task sequencing, such as participant fatigue, learning over the session, or IMU signal drift over the course of the testing session. A detailed summary of all tasks and required repetitions is provided in *Table 2*.

All activities were performed at a self-selected speed. However, participants were encouraged to perform On-the-Ball tasks as close to competition intensity as possible while maintaining full control within the confines of the calibrated capture volume. Although previous validation studies have reported mixed findings regarding the influence of kicking and movement velocity on measurement accuracy using IMUs and OMC systems,[42,49,141] this approach was intended to elicit movement patterns representative of competitive soccer during On-the-Ball tasks. That said, movement velocity was not directly quantified; therefore, the extent to which differences in velocity influenced IMU or OMC measurement accuracy cannot be determined. For running, cutting, and dribbling tasks (Trials 11–35), participants were instructed to perform at a submaximal intensity (approximately 70–80% of perceived maximum speed) and were verbally reminded if deviations from this range were observed. For tasks involving movement between a start and end position (Trials 12–17; 30–35), participants were instructed to decelerate to a complete stop at the designated endpoint and pause momentarily before walking back to the starting position. This pause ensured clear separation between repetitions for segmentation during post-processing. During Range of Motion trials, participants used a cane adjusted to hip height for balance support, without interfering with lower-limb movement. Trials were assessed by the investigator and discarded and repeated immediately if task execution was unsuccessful or if technical issues occurred, including improper synchronization between the Xsens and Vicon systems or IMU/marker detachment during movement.

Table 2. Summary of soccer-specific movement tasks performed by participants. Tasks are categorized as Range of Motion, Off-the-Ball, and On-the-Ball movements, with the required number of repetitions indicated.

Movement Category	Trial Name and Number	Description	Repetitions
(1) Range of Motion	1. Squat	A repeated bodyweight exercise involving lowering the hips into a deep squat position toward the ground, followed by returning to an upright standing position.	10
	2. Flexion/Extension Swing (R)	Forward and backward swinging of one leg while standing on the other	10
	3. Flexion/Extension Swing (L)		10
	4. Adduction/Abduction Swing (R)	Side-to-side swinging of one leg across the front of and away from the body's midline	10
	5. Adduction/Abduction Swing (L)		10
	6. Hip Flexion (R)	Lifting one leg toward the chest with knee bent at 90˚ then lowering it back to the floor	10
	7. Hip Flexion (L)		10
	8. Transverse Plane Hip Internal/External Rotation (R)	Rotating the thigh inward and outward while the hip and knee are bent and held at 90˚	10
	9. Transverse Plane Hip Internal/External Rotation (L)		10
(2) Off-the-Ball	10. Jump	A vertical leap from two feet, landing in place	10
	11. Lateral Shuffle	A continuous, side-to-side movement with rapid steps	10
	12. Submaximal Sprint to Turn (R)	Sprint forward, then perform a sharp, 180˚ turn around a cone before sprinting to another cone marking the endpoint. Walk back to the starting position	5
	13. Submaximal Sprint to Turn (L)		5
	14. Sprint to Side-step Cut to 45˚ (R)	Sprint forward at 70–80% of maximum effort to a cone, then perform a side-step change of	5

	15. Sprint to Side-step Cut to 45˚ (L)	direction at 45˚ and run straight to another cone marking the endpoint. Walk back to the starting position	5
	16. Sprint to Side-step Cut to 90˚ (R)	Sprint forward at 70–80% of maximum effort to a cone, then perform a side-step change of direction at 90˚ and run straight to another cone marking the endpoint. Walk back to the starting position	5
	17. Sprint to Side-step Cut to 90˚ (L)		5
(3) On-the-Ball	18. Instep Pass (R)	Pass the ball to the investigator using the inside of the foot	10
	19. Instep Pass (L)		10
	20. Instep Receive (R)	Receive the ball from the investigator, controlling it with the inside of the foot, then pass the ball back to the investigator using the inside of the foot	10
	21. Instep Receive (L)		10
	22. Outstep Receive (R)	Receive the ball from the investigator, controlling it with the outside of the foot, then pass the ball back to the investigator using the inside of the foot	10
	23. Outstep Receive (L)		10
	24. Instep Volley (R)	Strike the ball mid-air using the inside of the foot	10
	25. Instep Volley (L)		10
	26. Laces Volley (R)	Strike the ball mid-air using the top of the foot	10
	27. Laces Volley (L)		10
	28. Aerial Control (R)	Control a falling ball using the thigh, then trap it on the floor using the sole of the foot	10
	29. Aerial Control (L)		10
	30. Dribble to 45˚ Cut (R)	Dribble forward to a cone and cut diagonally at 45˚ to another cone, then continue to dribble straight to another cone marking the endpoint	5
	31. Dribble to 45˚ Cut (L)		5

	32. Dribble to 90˚ Cut (R)	Dribble forward to a cone and cut diagonally at 90˚ to another cone, then continue to dribble straight to another cone marking the endpoint	5
	33. Dribble to 90˚ Cut (L)		5
	34. Dribble to Turn (R)	Dribble forward to a cone, perform a 180˚ turn around the cone using the outside of the foot, and dribble back to another cone marking the endpoint	5
	35. Dribble to Turn (L)		5

3.1.4 Data Processing

Raw motion data collected from the IMUs were processed using Xsens MVN Analyze software (v2021.0.1, Xsens Technologies B.V., Enschede, The Netherlands). For each trial, data were reprocessed offline using the High-Definition (HD) reprocessing mode with the default Single Level processing scenario. In this scenario, all contact points are assumed to interact with a zero-level floor.[42]

During reprocessing, the Xsens biomechanical model was also used to estimate segment orientations and subsequently extract 3D joint kinematics for all joints included in the lower-limb model. Segment orientations were determined by the proprietary Xsens Kalman Filter for human motion tracking (XKF3-hm), which fuses data from each sensor's tri-axial gyroscope, accelerometer, and magnetometer to provide drift-free, highly accurate, and absolute 3D orientation. [42]

Xsens defines joints based on the International Society of Biomechanics' guidelines for the standard reporting of lower-limb kinematics.[136] For the present study, only hip joint kinematics were processed, and so hip joint angles were calculated internally by the Xsens software by estimating the relative orientation between adjacent body segments using quaternion-based representations.[136] Unlike Euler-angle representations, which describe orientation as a sequence of rotations about specified axes and may be susceptible to singularities such as gimbal lock, quaternions provide a continuous representation of three-dimensional orientation without such singularities.[45] This mathematical advantage makes quaternion representations preferable when analyzing 3D segment orientations. For easier interpretation of joint kinematics, quaternions can subsequently be converted to Euler angles, as described below.[45]

Reprocessed trials were manually checked to confirm the absence of obvious processing artifacts. Data from all trials were then batch exported from Xsens MVN Analyze (v2021.0.1, Xsens Technologies B.V., Enschede, The Netherlands) and converted into Microsoft Excel worksheets for subsequent data handling.

Vicon Nexus software (v2.17) was used to process data acquired from the OMC system. Marker trajectory reconstruction and automatic labelling were first performed to create a 3D lower-limb model. All trials were then visually inspected, and any unlabelled trajectories, marker swaps, or gaps were identified and manually corrected.

Marker trajectory gaps were addressed using a hierarchical gap-filling approach based on gap duration and segment rigidity. For markers attached to the pelvis segment, gaps of up to 350 frames were filled using the Vicon Nexus *Rigid Body Fill* pipeline, with all pelvis markers, including those attached to the IMU positioned at the posterior pelvis (e.g., LASI, RASI, LPSI, RPSI, Sacr_IMU1, Sacr_IMU2, Sacr_IMU3), used to reconstruct missing trajectories under the assumption of rigid segment motion.[144] For markers on other segments, *Rigid Body Fill* was first attempted using manually selected donor trajectories that exhibited rigid or semi-rigid relationships with the marker being reconstructed. Any remaining gaps that could not be resolved in this manner were filled using interpolation methods. Specifically, cubic spline interpolation was applied for non-cyclic movements of up to 100 frames, while *Cyclic Fill* was used in tasks that involved repetitive motion patterns (e.g., sprinting, dribbling, lateral shuffling).

Following this, the *Plug-in Gait dynamic* pipeline was executed to compute lower-limb joint kinematics. The resulting kinematic outputs were exported as comma-separated value (CSV) files for comparison with IMU-derived data. The IMU and OMC data were further processed using custom-written Python scripts (Python v3.13.5) executed in Jupyter Notebook to isolate and compare hip joint kinematics across the duration of each trial.[145]

Segment orientation data exported from Xsens MVN Analyze (v2021.0.1, Xsens Technologies B.V., Enschede, The Netherlands) were provided as quaternions and extracted in the *xyzw* format for the pelvis and bilateral thigh segments, as only these segments were required to calculate hip joint orientations. Hip joint orientations were calculated as the relative orientation of the thigh segment with respect to the pelvis segment. Specifically, the pelvis orientation quaternion was inverted and multiplied by the corresponding thigh

quaternion. The resulting relative quaternion described the orientation of the thigh segment expressed in the coordinate system of the pelvis.

To enable direct comparison between systems, joint angle conventions from the Xsens IMU system were matched with those of the OMC system. Vicon's PiG model computes hip joint angles using a Y–X–Z Euler rotation sequence, with positive directions defined as flexion, adduction, and internal rotation, respectively.[143] Accordingly, relative hip joint quaternions derived from Xsens were converted to Euler angles in degrees by rotation matrix using the same Y–X–Z rotation order. Sign conventions were adjusted where necessary to match the PiG outputs, accounting for differences in left-right coordinate system definitions between the two systems.

Joint angle time series from both systems were subsequently low-pass filtered using a zero-lag, fourth-order Butterworth filter with a cutoff frequency of 6 Hz to reduce high-frequency noise. A fourth-order, 6-Hz low-pass Butterworth filter was selected based on its established and widespread use for filtering human motion data and its demonstrated effectiveness in reducing high-frequency noise while preserving relevant movement characteristics.[146]

To account for differences in sampling frequency between systems (IMU: 100 Hz; OMC: 200 Hz), Vicon joint angle data were resampled to match the IMU time base. The IMU data were retained at their native sampling frequency to avoid artificially adding temporal information through interpolation, while resampling the higher-frequency Vicon data enabled direct comparison between systems. Following filtering and resampling, both signals were trimmed to a consistent analysis window. The first 0.25 s of each trial was removed to exclude any non-representative initial motion. The signals were assumed to be sufficiently synchronized via the hardware-based trigger, so no additional temporal alignment was applied.

For each trial, a constant offset equal to the mean difference between the signals over the entire analysis window was removed separately for each hip joint kinematic plane (flexion/extension, adduction/abduction, and internal/external rotation) to correct for systematic baseline differences between the IMU and OMC systems. Such offsets typically arise from differences in joint zero definitions between systems during calibration, biomechanical model differences, or minor marker placement variability, rather than technical errors, and are therefore routinely removed when comparing IMU and OMC data.[36–

[38] However, systematic differences may also reflect measurement error in either system, and removing them may reduce apparent absolute error. Therefore, between-system agreement was assessed both before and after offset removal to evaluate the influence of systematic baseline differences on the comparison, as described below.

3.1.5 Data Analysis

Data analysis was performed across the entire duration of each synchronized trial using custom-written Python scripts (Python v3.13.5) executed in Jupyter Notebook.[145] Sagittal (flexion/extension), frontal (abduction/adduction), and transverse (internal/external rotation) hip joint kinematics were determined bilaterally. Two trials from (Hip Flexion R/L) from the same participant were excluded from the analysis due to incomplete right and left ASIS kinematic marker data; the participant's remaining trials were retained. In addition, hardware-based synchronization failed to start both measurement systems simultaneously in six on-the-ball trials from one participant (Instep Pass R/L, Instep Receive R/L, and Outstep Receive R/L). For these cases, temporal alignment between IMU and Vicon signals was achieved post hoc using a manual time-shift correction implemented in Python, based on waveform onset matching of hip flexion/extension signals. These trials were subsequently retained for analysis, resulting in a final dataset comprising 698 participant–trial combinations.

Descriptive comparisons between the IMU (Xsens) and OMC (Vicon) systems included differences in maximum angle, minimum angle, and range of motion (ROM), with ROM calculated as the difference between the maximum and minimum joint angle values observed across the full trial for each system. Trial-level ROM values were averaged within each participant, movement, and hip side to obtain participant-level mean ROM values. Six paired-samples *t*-tests were performed in JASP statistical software (v0.97; JASP Team, Amsterdam, The Netherlands) to compare Xsens- and Vicon-derived participant-level mean ROM values for each of the three hip motions (flexion/extension, abduction/adduction, and internal/external rotation) separately for the right and left hips. All tests were conducted separately for the right and left hip to account for potential side-specific differences in measurement agreement. Statistical significance was assessed at $\alpha = 0.05$. Effect sizes were calculated using Cohen's *d* and are reported with 95% confidence intervals.

The root mean squared error (RMSE, °), calculated as the square root of the mean squared difference between synchronized Xsens and Vicon (Xsens – Vicon) joint angle time series across the full trial duration, was used to evaluate the IMU system. For each

participant, RMSE values were averaged across all soccer-specific movement tasks within each hip joint motion (flexion/extension, adduction/abduction, and internal/external rotation). To determine whether RMSE differed among hip joint motions, linear mixed-effects models (LMMs) were fitted separately for the right and left hip. Hip joint motion was included as a fixed effect, with participant included as a random effect to account for repeated measures within individuals. Post-hoc pairwise comparisons with Bonferroni correction were used to identify specific differences between motions.

Additionally, to assess the relative magnitude of error in relation to the range of motion (ROM) measured by each system, normalized RMSE (nRMSE, %) was calculated by dividing the RMSE by the corresponding ROM of either the Vicon or Xsens system and expressing the result as a percentage. Thus, Vicon-normalized and Xsens-normalized RMSE values were calculated separately:

$$nRMSE_{Vicon}(\%) = \frac{RMSE}{ROM_{Vicon}} \times 100$$

$$nRMSE_{IMU}(\%) = \frac{RMSE}{ROM_{IMU}} \times 100$$

Since nRMSE accounts for the ROM of the reference system, differences in normalized error magnitude provide context for interpreting absolute RMSE relative to the magnitude of joint motion.

Waveform similarity was assessed using the coefficient of multiple correlation (CMC), which compares overall similarity between kinematic waveforms obtained from synchronized measurement systems, accounting for differences in offset, correlation, and gain.[147] In accordance with Ferrari et al.,[147] CMC was calculated before (CMC1) and after (CMC2) offset removal to assess the influence of systematic baseline differences.[38] Interpretation thresholds were adopted from prior kinematic validation studies, whereby values of 0.75–0.84 were considered good, 0.85–0.94 very good, and ≥ 0.95 excellent.[138,139] Box-and-whisker plots were used to visualize the median, interquartile range, and spread of trial-level CMC values across participants and tasks for each hip motion. CMC was calculated over the complete duration of each trial; therefore, each observation represented a single trial-level CMC value.

Bland–Altman analyses were performed to assess agreement between IMU-derived and Vicon-derived ROM values.[148] For each observation, the mean ROM was calculated as the average of the IMU- and Vicon-derived ROM values, and the difference was calculated as the IMU-derived ROM minus the corresponding Vicon-derived ROM value (Xsens – Vicon). The mean difference (bias) was calculated for each movement task and hip motion plane, representing the systematic difference between measurement systems. Positive values indicated that the IMU overestimated ROM relative to Vicon, whereas negative values indicated underestimation. The standard deviation (SD) of the differences was calculated, and the 95% limits of agreement (LOA) were defined as[148]:

$$95\%\ LoA = Bias\ \pm 1.96\ \times SD$$

Complementary to the analysis based on pooled data across motion categories, Bland–Altman plots were generated separately for each movement task and hip motion. Hip joint data from all participants were pooled within each movement task. Mean ROM values were plotted against the corresponding IMU–Vicon differences. Right and left hip measurements were displayed to allow visual assessment of agreement between systems.

3.2 Machine Learning Classifier

To address the second objective, five supervised machine-learning classifiers were developed and evaluated to classify 20 soccer-specific movements using IMU-derived signals. An overview of the methodological workflow used for classifier development and model evaluation is provided in *Figure 10.*

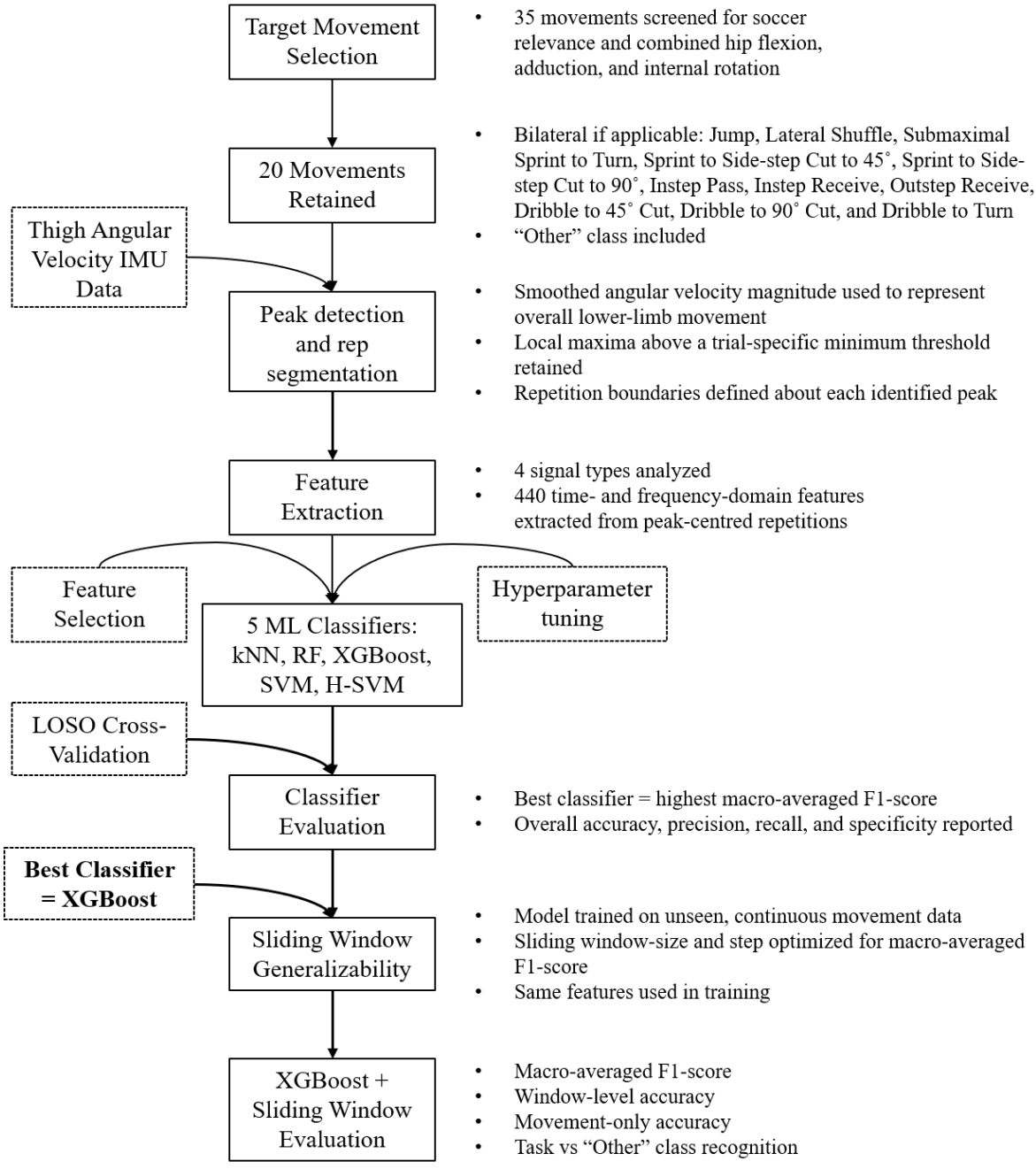


Figure 10. Overview of the methodological workflow used to develop and evaluate the IMU-based soccer movement ML classification models.

3.2.1 Movement Selection

Prior to model development, all 35 trials were qualitatively screened to identify movements that both reproduced the combined hip position of flexion, adduction, and internal rotation associated with cam FAIS provocation and reflected actions commonly performed during soccer.

For each trial, hip motion time-series for both limbs, obtained from the OMC system, were overlaid and visually inspected. The timing of peak hip flexion for each limb and each repetition was detected, and a ±0.25 s window surrounding each peak was examined to determine whether peaks in hip adduction and internal rotation occurred concurrently. The literature does not provide an optimal window for evaluating the coincidence of these three hip motions during dynamic tasks. Accordingly, the ±0.25 s window was selected to capture close temporal proximity between the peak in hip flexion and the corresponding peaks in adduction and internal rotation, consistent with the expectation that a clinically relevant provocative hip position involves the approximately simultaneous occurrence of these three motions. Tasks in which the timing of peak hip flexion consistently coincided with elevated hip adduction and internal rotation were considered representative of the combined movement pattern associated with symptomatic cam FAIS and were retained for classification.[3,58] Here, consistency referred to the repeated observation of concurrent peaks across the repetitions manually inspected for each trial. This assessment was based on visual inspection of the overlaid hip joint angle waveforms, with a task retained when the three motion peaks were repeatedly observed within the ±0.25 s window across a trial's repetitions. Tasks in which these motions occurred at different phases of the movement cycle were excluded. A representative example of this process for a single trial is shown in *Figure 11*.

In addition to kinematic screening, task selection considered the relevance and frequency of each movement during soccer participation, with preference given to movements that occur commonly during match play or training.[117,120,121,123,125] Based on these criteria, 20 movement classes were retained for subsequent classifier development: Jump, Lateral Shuffle, Submaximal Sprint to Turn, Sprint to Side-step Cut to 45˚, Sprint to Side-step Cut to 90˚, Instep Pass, Instep Receive, Outstep Receive, Dribble to 45˚ Cut, Dribble to 90˚ Cut, and Dribble to Turn. Bilateral movements were retained for both the right and left limbs where applicable. To more closely reflect the conditions under which this system

would operate in a real-time soccer context, a twenty-first class labelled “Other” was also incorporated into the framework to represent non-task movement periods.



Figure 11. Example of the IMU-based repetition segmentation process using hip kinematic time-series data obtained from the OMC system during an Instep Pass (R) trial. Shaded regions indicate the ±0.25 s window surrounding each identified peak in hip flexion. Numbered annotations indicate the repetitions performed.

3.2.2 Data Segmentation

Continuous IMU data for all retained tasks was divided into individual repetitions by identifying peaks in the right and left thigh angular velocity signals (*Figure 12*). Angular velocity magnitude was calculated from the three orthogonal gyroscope axes (x, y, and z) using the following equation:

$$Angular\ Velocity\ Magnitude = \sqrt{x^2 + y^2 + z^2}.$$

The larger angular velocity between the right and left thighs was used to identify the limb exhibiting the greater movement during each repetition and to create a single signal representing the overall lower-limb movement. The resultant signal was smoothed using a moving average filter with a 175 ms window to reduce high-frequency fluctuations. The use of a moving average filter was informed by previous studies,[50,51] although these studies did not specify the filter window duration; therefore, the 175-ms window was selected for the present analysis.

Candidate repetitions were initially identified by detecting local maxima (peaks) in the smoothed signal that exceeded a trial-specific adaptive threshold. The threshold was calculated as the median of the smoothed signal plus a predefined multiple of its median absolute deviation, with the multiplier adjusted for specific trials when necessary. Following initial detection, further processing was applied to ensure that each repetition was represented by a single peak. Peaks were only retained when their amplitude exceeded the minimum threshold and were separated from neighbouring peaks by a trial-specific temporal interval. This interval was adjusted separately for each trial to accommodate differences in signal characteristics and repetition frequency/duration across movement tasks. When multiple peaks occurred within the same movement event, peak amplitudes were compared and only the dominant peak was retained to represent that repetition. This process prevented additional peaks occurring within the same movement cycle from being incorrectly classified as separate repetitions. The final number of detected peaks was compared with the expected number of repetitions performed in each trial to confirm that each trial was appropriately segmented.

Repetition boundaries were then determined relative to each retained peak. For most movement classes, the start and end of each repetition were isolated by searching outward from each peak until the angular velocity signal decreased toward its baseline level. For more discrete passing and receiving tasks, where the signal decayed rapidly following the primary movement peak, a fixed 2.5 s window centred on each detected peak (±1.25 s) was applied to ensure consistent capture of the complete repetition. The 2.5 s window was selected based on visual inspection of the angular velocity profiles across these tasks and was sufficiently long to capture the full movement while minimizing inclusion of adjacent repetitions. All segmented repetitions across all movement classes were manually checked to confirm that the identified movement cycles accurately represented the performed tasks and that segmentation boundaries did not overlap between consecutive repetitions. For each participant, the 15 trials excluded from the primary movement selection were used as the source of Other class data. A sliding window of 2.5 s was advanced across each excluded trial in 0.25 s increments, and 10 equally spaced windows were selected per trial to ensure a consistent contribution from each excluded trial. These windows were assigned the Other label and appended to the participant datasets, enabling the classifiers to differentiate between structured task executions and non-target movement patterns.

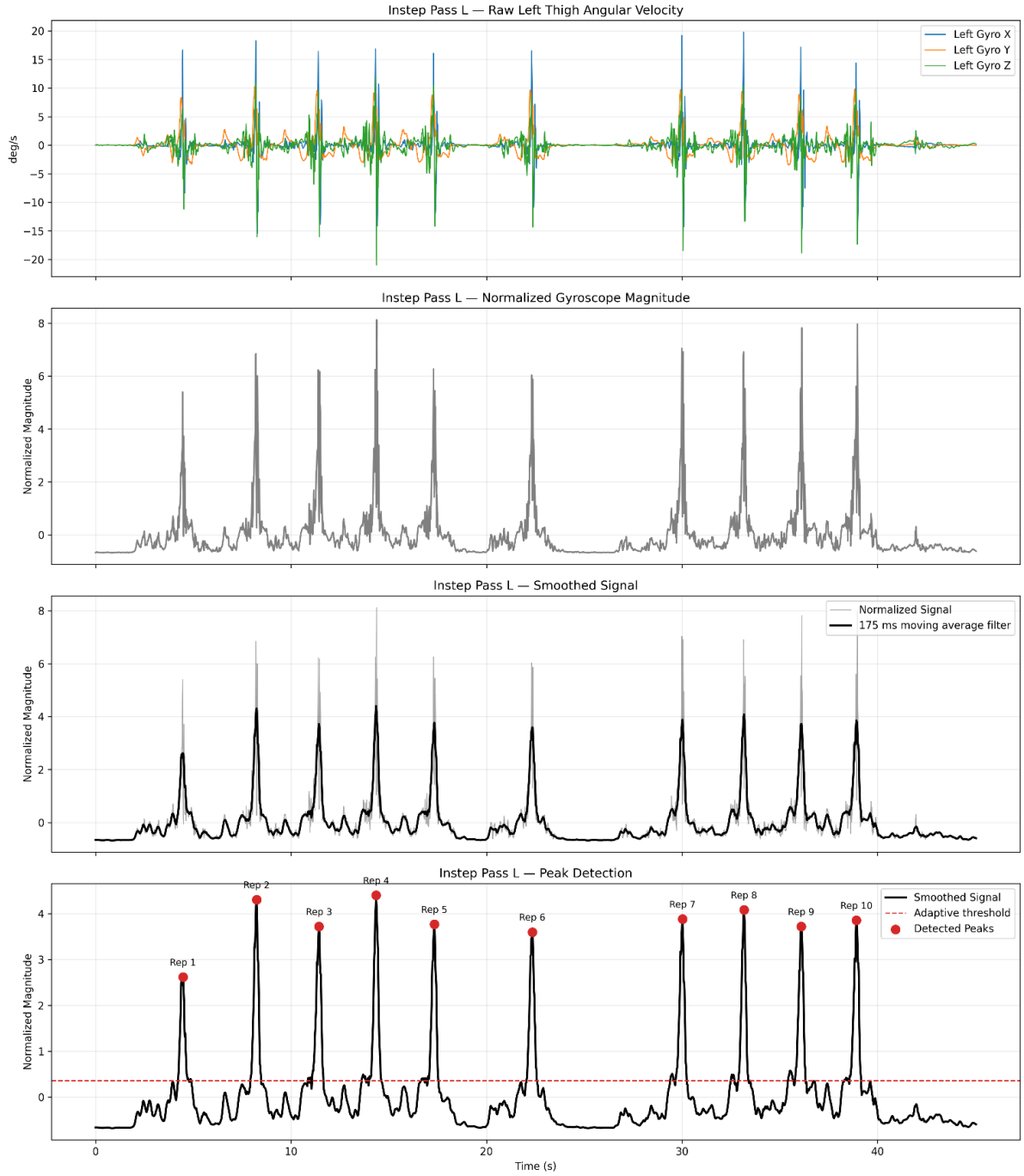


Figure 12. Example of IMU-based repetition segmentation process using raw thigh angular velocity signals during an Instep Pass (L) trial. Positive angular velocity indicates rotation about the sensor's respective axis according to the positive direction defined by the sensor coordinate system (Top).

3.2.3 Feature Extraction

Features corresponding to the right and left thigh segments were extracted from the segmented repetitions across all 20 movement tasks and the "Other" class for classifier development. Four signal types were analyzed: linear acceleration, angular velocity, angular acceleration, and segment orientation. These signals were selected based on their established use in previous IMU-based analyses of a wide range of sporting applications reviewed by Poitras et al.,[46] including the instep soccer kick. Although angular acceleration is derived from angular velocity, it characterizes the rate of change in rotational velocity and may therefore provide additional temporal information that may improve discrimination between technically similar soccer-specific movements. For each signal, features were calculated independently for each axis (*x, y,* and *z*), and separately for the right and left thighs to preserve limb-specific movement characteristics. A combination of time-domain and frequency-domain features was extracted based on features commonly used in IMU-based human activity recognition and basic soccer-specific task classification.[45,47,50] Time-domain features included mean, standard deviation, peak absolute amplitude, root mean square, energy, skewness, kurtosis, and zero-crossing rate while frequency-domain features included spectral entropy and band power. Detailed descriptions and calculations for each extracted feature are provided in *Appendix A*.

To provide a direction-independent representation of overall movement intensity, resultant magnitude features were also calculated for acceleration, angular velocity, and angular acceleration using the vector magnitude of the three orthogonal axes.

To quantify inter-limb differences within each repetition, and to account for the unilateral nature of many of the trials selected for classification, a Symmetry Index, adapted from commonly used symmetry measures in gait analysis,[149,150] was calculated for matching right and left limb features:

$$Symmetry\ Index = \frac{Right - Left}{|\ Right\ | + |\ Left\ |}$$

Values approaching zero indicated greater similarity between limbs, whereas positive and negative values indicated larger right- and left-sided feature values, respectively. The feature extraction process resulted in a total of 440 features per segmented repetition.

3.2.4 Movement Classification

Following feature extraction, five supervised ML classification models were evaluated using Python (Python v3.13.5): k-Nearest Neighbors (kNN), Random Forest (RF), Extreme Gradient Boosting (XGBoost), Support Vector Machine (SVM), Hierarchical SVM (H-SVM). The kNN, RF, SVM, and H-SVM models were implemented using the scikit-learn library (v1.7.2), while XGBoost was implemented using the XGBoost Python package (v3.3.0). Scikit-learn was also used for data preprocessing, hyperparameter tuning, cross-validation, and calculation of classification performance metrics. In the H-SVM model, a coarse SVM classifier was first trained to classify movements into one of three broader categories: Off-the-Ball, On-the-Ball, or Dribbling movements. At the second level, category-specific expert SVM models were trained to further distinguish between individual movements within each coarse category. These models were selected based on their established application in human activity recognition and previous approaches for soccer-specific task classification.[45,49,50] Each repetition was labelled according to the known task performed during the trial, with each unique movement representing a target class. These target classes represented the outcomes that the supervised ML models were then trained to predict.

Each classifier was evaluated using leave-one-subject-out (LOSO) cross-validation. During each LOSO iteration, data from 19 participants were used for model training and the remaining participant was used for testing. Given the high-dimensional nature of the extracted feature space, within each LOSO iteration, Random Forest-based feature selection was implemented using only the training participants for kNN, SVM, and H-SVM classification to reduce dimensionality. Feature selection is commonly used in supervised machine learning when a large number of candidate features may contain irrelevant or redundant information, as retaining only the most informative features can reduce model complexity and improve generalizability.[151] Accordingly, Random Forest feature importance was used to rank the candidate features according to their contribution to classification, and only the highest-ranked features were retained for subsequent classifier training. Importantly, feature selection was performed independently within each LOSO training fold to prevent information from the held-out participant from influencing feature selection.

3.2.4.1 Model Hyperparameter Tuning

Hyperparameters for each classifier were optimized using randomized search (RandomizedSearchCV, scikit-learn), which samples a fixed number of parameter combinations rather than exhaustively evaluating all combinations as in grid search (GridSearchCV, scikit-learn) to maintain computational efficiency. For each model, 30 parameter combinations were evaluated using five-fold cross-validation. For kNN, SVM, and H-SVM, hyperparameter tuning was conducted first using a 40-feature configuration as a representative feature-retention level to identify a stable set of classifier parameters before evaluating the feature-retention levels described below. For RF and XGBoost, hyperparameter tuning was performed using the full feature space. To prevent subject-level data leakage during tuning, a single subject-wise 80/20 split (GroupShuffleSplit, scikit-learn) was used in all models to separate the tuning training and held-out tuning validation sets. The selected hyperparameters were then evaluated on the held-out tuning participants as a check of performance on unseen subjects before being fixed for the subsequent LOSO evaluation.

3.2.4.2 Feature Selection and Feature-Count Optimization

After hyperparameter tuning, multiple feature retention levels were then assessed to determine the optimal number of features for classifier training, with macro-averaged F1-score as the optimization criterion. For kNN, SVM, and expert H-SVM models, feature counts of 20, 40, 60, 80, and 100 were compared, with the feature count yielding the highest macro-averaged F1-score selected for final model training. Within the H-SVM model, a separate feature count with 10, 20, and 30 features was also evaluated for the coarse classifier. Macro F1-score was selected as the optimization criterion because it provides equal weighting across all movement classes. In contrast, the full feature space was retained for RF and XGBoost models, since tree-based ensemble classifiers perform feature selection implicitly through their tree-splitting procedures to retain the most informative predictors during model training.[151]

Following feature-count optimization, each classifier was trained using the selected feature set and optimized hyperparameters and then applied to the held-out participant. Predictions were compared with known movement labels, and this process was repeated until each participant had served as the independent test set once.

3.2.5 Classifier Evaluation

Model performance was first evaluated using overall accuracy and macro-averaged performance metrics, including precision, recall (sensitivity), F1-score, and specificity.[151] Accuracy reflects the overall proportion of movement repetitions that were correctly classified across all 20 movement categories. Precision describes how often the model was correct when it predicted a particular movement. The F1-score, used to quantify overall performance, provides a combined measure of precision and recall, demonstrating the model's ability to correctly identify movements while minimizing incorrect classifications. Finally, specificity reflects the model's ability to correctly reject non-target movements and avoid false-positive predictions. These metrics all have values ranging from 0 to 1, with higher values representing better performance.[152]

Macro-averaging was used first to provide equal weighting across all movement classes and enable comparison between models independent of differences in class-specific performance. Following optimization, the model achieving the highest macro F1-score was selected as the best-performing classifier. Confusion matrices were generated for all classifiers to examine class-specific classification performance and identify movement categories associated with increased misclassification.

3.2.6 Model Generalizability to Unseen Movement Data

A sliding-window approach was used to assess the generalizability of the best-performing classifier beyond segmented repetition-level classification. This evaluated whether a classifier trained on clean, repetition-based movement examples could generalize to continuous, temporally unsegmented movement data from previously unseen participants. The best-performing classifier was trained using the same segmented movement feature dataset used for the primary LOSO analysis, where features were extracted from peak-centred movement repetitions from 19 participants.

Raw Xsens signals from the held-out participant were converted into overlapping sliding windows of variable duration and step size between consecutive windows. Window durations of 2, 3, 4, and 5 s were evaluated in combination with step sizes of 0.5 and 1.0 s. The window configuration producing the highest macro-averaged F1-score for task movement classification was selected for the final analysis. Previous research has also reported high classification accuracy (84%) using a sliding window of comparable duration for the recognition of basic soccer actions, although using different machine learning models

and movement sets.[51] The same features used for model training were extracted from each sliding window. Windows corresponding to labelled movement tasks were assigned their respective movement class, whereas windows from trials excluded from the primary 20-movement selection were labelled as Other to evaluate non-target activity rejection.

The trained classifier was subsequently evaluated on continuous trials from the withheld participant. For each LOSO fold, the XGBoost classifier was trained on segmented repetitions from the remaining 19 participants and tested on all available sliding windows from the withheld participant. Prediction probabilities were generated for each window, and windows with a maximum class probability below 0.50 were assigned to the Other class to reduce low-confidence false detections. Performance was assessed using macro-averaged F1-score, overall window-level accuracy, movement-only accuracy, and Task versus Other class recognition.

4 Results

4.1 Validation of IMU System

4.1.1 Range of Motion and Error Comparisons Between IMU and OMC Systems

A task-specific breakdown of hip ROM and RMS error between IMU- and OMC-derived kinematics is presented in *Appendix B*. Mean Vicon and IMU ROM values were comparable for flexion/extension and adduction/abduction motions at both the right and left hip, suggesting that the IMU provides similar estimates of ROM to the OMC system for these joint angles, irrespective of the movement task (*Table 3*). In the sagittal plane, mean differences were -1.01˚ and -0.60˚ for the right and left hip, respectively, while in the frontal plane, differences equalled 0.13˚ to -0.32˚. In contrast, larger discrepancies were evident in the transverse plane, with internal/external rotation ROM consistently underestimated by the IMU relative to Vicon (right hip: -9.09˚; left hip: -12.28˚). Time-series data from a single median repetition of select trials are presented in *Figure 13.*

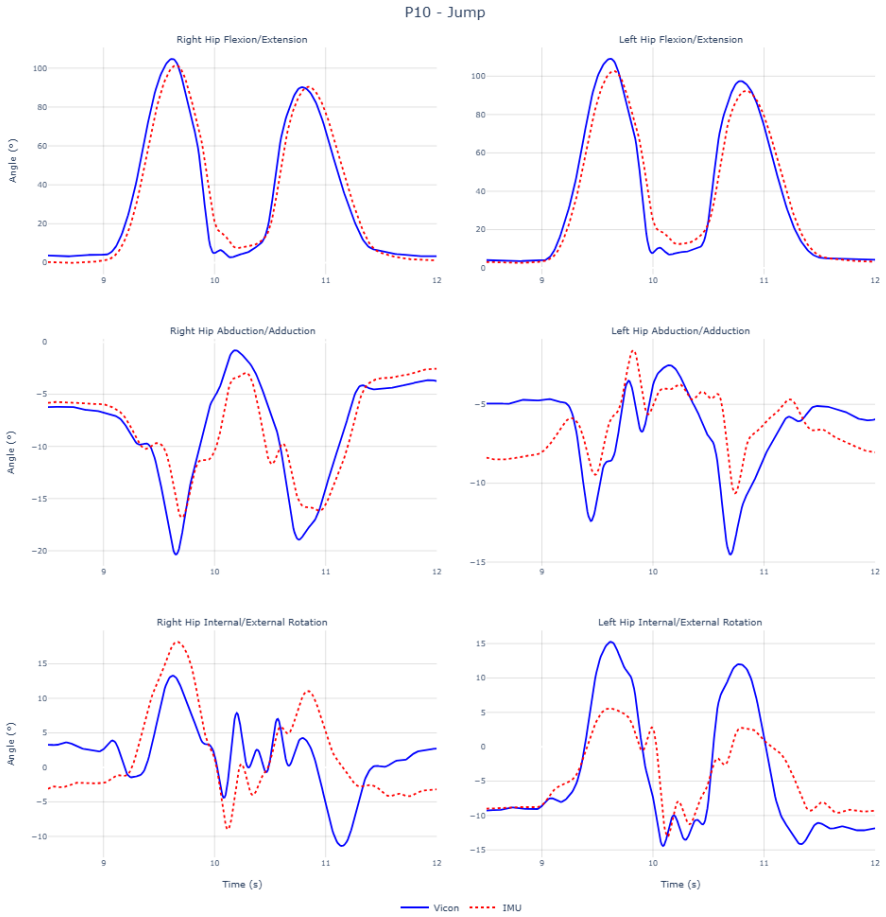
Paired-samples t-tests confirmed no significant differences between IMU and Vicon ROM values for flexion/extension (right hip: p = 0.171, d = -0.318; left hip: p = 0.496, d = -0.155*)* and adduction/abduction (right hip: p = 0.579, d = 0.126; left hip: p = 0.223, d = -0.282) at either hip ($p > 0.05$). However, significant differences were observed for internal/external rotation at both the right (d = -1.253) and left hips (d = -1.817) ($p < 0.001$).

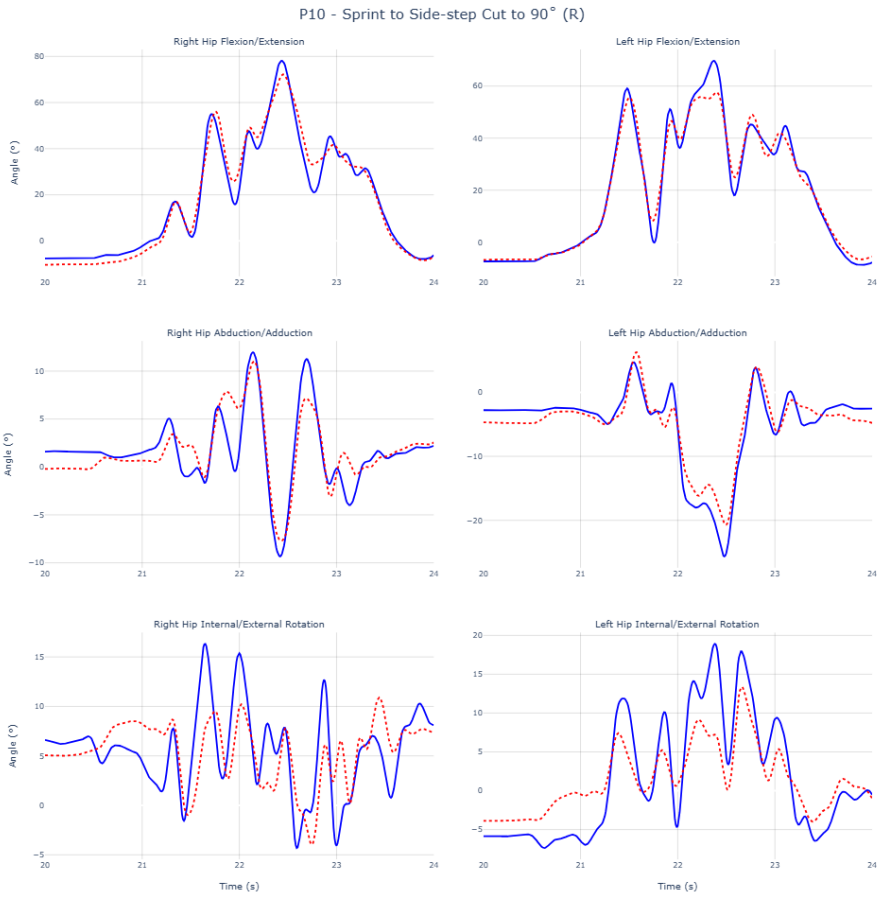
RMS error values followed a similar pattern across motion planes. Sagittal and frontal plane motions demonstrated lower absolute error values, ranging from 2.45˚ to 3.58˚, whereas transverse plane motions showed higher error magnitudes of 5.97˚ and 6.67˚ for internal/external rotation at the right and left hip, respectively.

Table 3. Comparison of hip joint ROM, mean differences, RMS error, and statistical comparisons of mean ROM (α = 0.05) between IMU- and OMC-derived kinematic measurements across movement planes.

Side	Motion	Mean Vicon ROM ± SD (°)	Mean IMU ROM ± SD (°)	IMU-Vicon Mean Difference (°)	Mean RMS Error ± SD (°)	*p*-value
Right Hip	Flex/Ext	75.34 ± 6.20	74.33 ± 5.99	-1.01	3.45 ± 0.64	0.171
	Add/Abd	28.16 ± 3.00	28.29 ± 3.04	+0.13	2.69 ± 0.59	0.579
	Int/Ext	37.68 ± 8.14	28.59 ± 2.56	-9.09	5.97 ± 1.89	< 0.001
Left Hip	Flex/Ext	75.02 ± 5.76	74.42 ± 6.21	-0.60	3.58 ± 0.62	0.496
	Add/Abd	28.48 ± 2.80	28.16 ± 2.98	-0.32	2.45 ± 0.46	0.223
	Int/Ext	41.16 ± 8.14	28.88 ± 3.13	-12.28	6.67 ± 2.06	< 0.001

Flex/Ext = Flexion/Extension. Add/Abd = Adduction/Abduction. Int/Ext = Internal/External Rotation. ROM = range of motion. RMS Error = root mean squared error.




P10 - Sprint to Side-step Cut to 90° (R)
Right Hip Flexion/Extension
Left Hip Flexion/Extension
Right Hip Abduction/Adduction
Left Hip Abduction/Adduction
Right Hip Internal/External Rotation
Left Hip Internal/External Rotation
Angle (°)
Time (s)


P10 - Instep Pass (R)
Right Hip Flexion/Extension
Left Hip Flexion/Extension
Right Hip Abduction/Adduction
Left Hip Abduction/Adduction
Right Hip Internal/External Rotation
Left Hip Internal/External Rotation
Angle (°)
Time (s)
Vicon
IMU

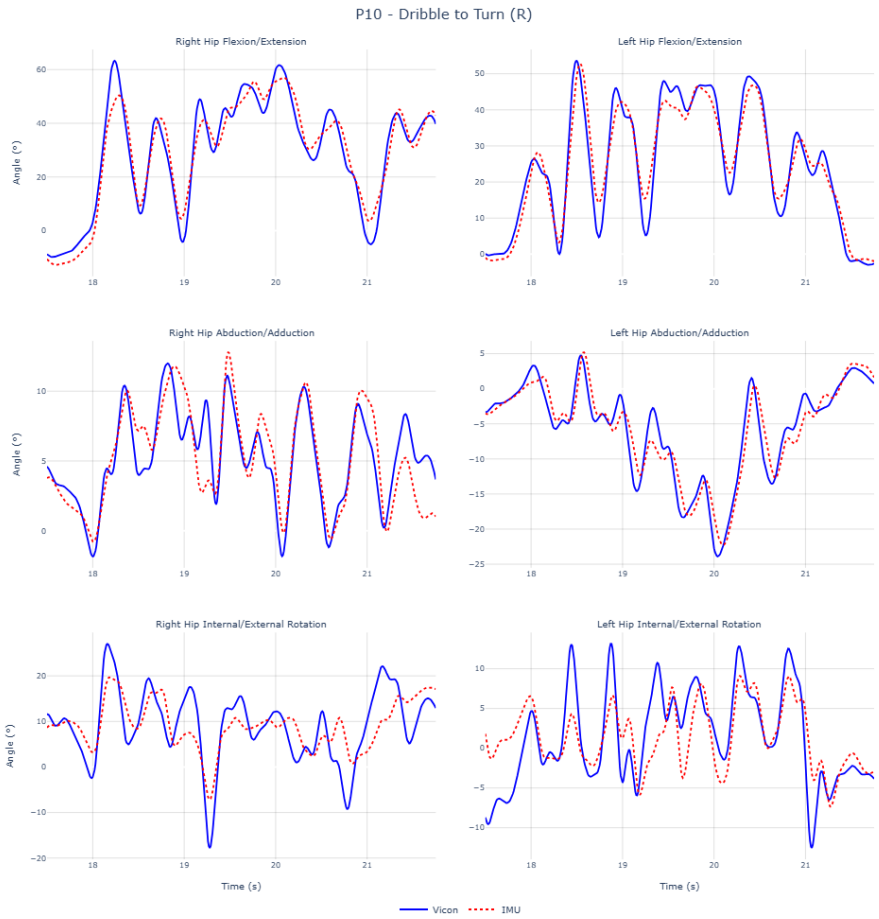


Figure 13. Representative time-series comparison of IMU- and optical motion capture (OMC)-derived hip kinematics during selected movement tasks completed by P10, in order of appearance: Jump, Sprint to Side-step Cut to 90˚ (R), Instep Pass (R), and Dribble to Turn (R). The median repetition of each trial was selected for visualization.

4.1.2 Normalized RMS Error

nRMSE values are presented in *Table 4*. Flexion/extension exhibited the lowest relative error across both hips, with comparable mean nRMSE values regardless of system (4.58% Vicon and 4.63% IMU for the right hip; 4.77% Vicon and 4.79% IMU for the left hip). This was followed by adduction/abduction, which ranged from 8.58–9.60%, while internal/external rotation demonstrated the highest relative error across both normalization approaches (15.76-15.99% Vicon; 20.81-22.92% IMU), reflecting reduced IMU ROM recorded in the transverse plane compared to Vicon.

Table 4. Comparison of hip joint motion error using mean nRMSE across movement planes. nRMSE was calculated relative to IMU- and OMC-derived ROM values to account for differences in movement magnitude.

Side	Motion	Mean RMS Error (˚)	Mean nRMSE ± SD (% Vicon ROM)	Mean nRMSE ± SD (% IMU ROM)
Right Hip	Flex/Ext	3.45	4.58 ± 0.86	4.63 ± 0.71
	Add/Abd	2.69	9.60 ± 2.15	9.54 ± 1.97
	Int/Ext	5.97	15.76 ± 2.44	20.81 ± 5.94
Left Hip	Flex/Ext	3.58	4.77 ± 0.81	4.79 ± 0.63
	Add/Abd	2.45	8.58 ± 1.24	8.67 ± 1.17
	Int/Ext	6.67	15.99 ± 2.62	22.92 ± 6.15

Flex/Ext = Flexion/Extension. Add/Abd = Adduction/Abduction. Int/Ext = Internal/External Rotation. RMS Error = root mean squared error. nRMSE = normalized root mean squared error.

4.1.3 Linear Mixed Model Analysis of RMS Error

Table 5 summarizes the results of the separate linear mixed models used to examine whether RMS error differed significantly across motions for the right and left hips. The model demonstrated a significant effect of motion on right-side RMS error ($F(2, 38) = 56.92$, $p < 0.001$) and left-side RMS error ($F(2, 38) = 77.55$, $p < 0.001$). For the right hip, Bonferroni-adjusted post-hoc pairwise comparisons indicated that RMS error during internal/external rotation was significantly greater than during both flexion/extension ($p < 0.001$) and adduction/abduction ($p < 0.001$), whereas RMS error did not differ significantly between flexion/extension and adduction/abduction ($p = 0.056$). All pairwise comparisons were significant for the left hip, with RMS error during internal/external rotation differing significantly from both flexion/extension and adduction/abduction ($p < 0.001$), while RMS error also differed significantly between flexion/extension and adduction/abduction ($p = 0.004$). The corresponding estimated marginal means data are shown in *Appendix C*.

Table 5. Bonferroni-adjusted pairwise comparisons of RMS error between hip joint motions following linear mixed model analysis for the right and left hips.

Side	Pairwise Post-hoc Comparison	Estimate (°)	SE	95% Cl		z	*p*-value
				Lower	Upper		
Right Hip	Flex/Ext vs. Add/Abd	0.76	0.322	0.13	1.39	2.35	0.056
	Flex/Ext vs. Int/Ext	-2.52	0.322	-3.16	-1.89	-7.84	< 0.001
	Add/Abd vs. Int/Ext	-3.28	0.322	-3.91	-2.65	-10.19	< 0.001
Left Hip	Flex/Ext vs. Add/Abd	1.13	0.351	0.44	1.82	3.22	0.004
	Flex/Ext vs. Int/Ext	-3.09	0.351	-3.78	-2.40	-8.81	< 0.001
	Add/Abd vs. Int/Ext	-4.22	0.351	-4.91	-3.53	-12.03	< 0.001

Flex/Ext = Flexion/Extension. Add/Abd = Adduction/Abduction. Int/Ext = Internal/External Rotation. SE = standard error.

4.1.4 Waveform Similarity

The similarity before and after offset correction between IMU- and OMC-derived hip joint angle waveforms across all trials are mapped in the box-and-whisker plots in *Figure 14* and *Figure 15*, respectively.

4.1.4.1 Pre-Correction Waveform Similarity (CMC1)

Prior to offset correction, CMC1 values were generally lower and more variable across motions, indicating modest waveform similarity between systems overall (*Table 6*). The lowest CMC1 values were observed at the hip joint in the transverse plane for internal/external rotation, with mean values of 0.318 at the right hip and 0.398 at the left. Frontal plane adduction/abduction demonstrated somewhat greater similarity, with mean CMC1 values of 0.640 and 0.612 for the right and left hip, respectively; however, only 4.1% and 4.4% of trials exceeded the excellent threshold (CMC > 0.95) for this motion, respectively. Flexion/extension exhibited good pre-correction waveform similarity, with mean CMC1 values of 0.839 at the right hip and 0.806 at the left. Consistent with this, 37.8% of right hip trials and 31.8% of left hip trials achieved excellent similarity prior to offset correction.

Table 6. Descriptive values of pre-correction waveform similarity (CMC1) between IMU- and OMC-derived hip kinematics across movement planes. The percentage of trials exceeding predefined good-to-excellent CMC thresholds are presented for each motion.

Side	Motion	CMC1 Mean ± SD	CMC1 Median (+ IQR)	CMC1 > (%)		
				0.75	0.85	0.95
Right Hip	Flex/Ext	0.839 ± 0.197	0.926 (0.788–0.965)	78.11	67.95	37.77
	Add/Abd	0.640 ± 0.212	0.677 (0.490–0.806)	38.63	18.03	4.15
	Int/Ext	0.318 ± 0.164	0.283 (0.207–0.396)	2.00	0.14	0
Left Hip	Flex/Ext	0.806 ± 0.207	0.885 (0.726–0.963)	71.39	55.65	31.76
	Add/Abd	0.612 ± 0.229	0.609 (0.452–0.827)	32.47	21.17	4.43
	Int/Ext	0.398 ± 0.188	0.355 (0.277–0.494)	6.87	0.86	0

CMC = Coefficient of multiple correlation.

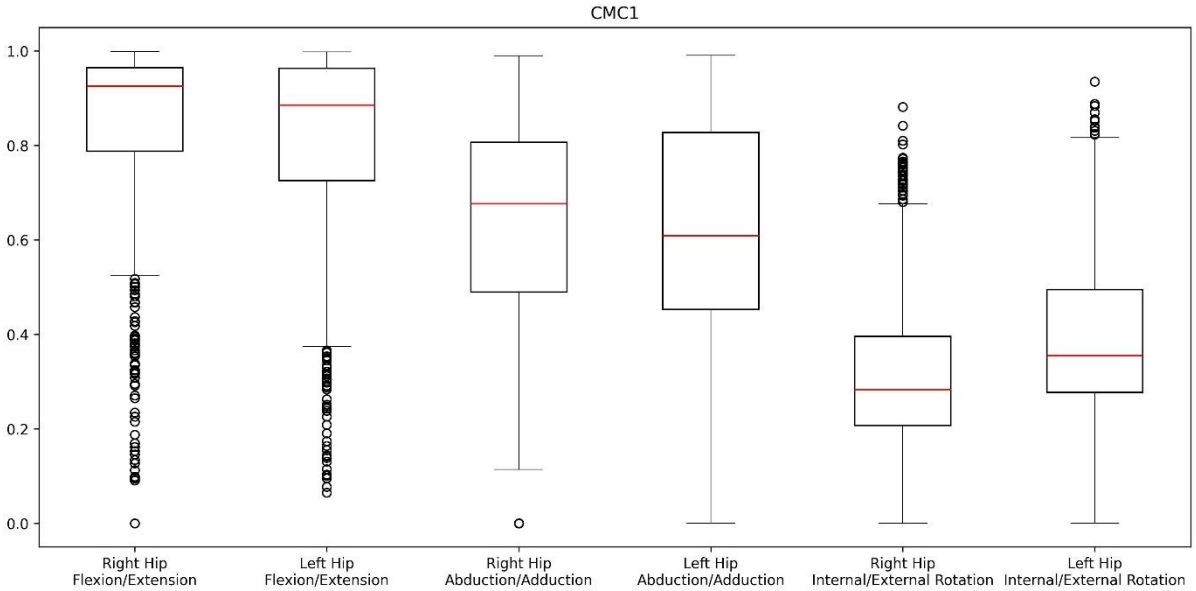


Figure 14. Box-and-whisker plots of pre-correction waveform similarity (CMC1) between IMU- and OMC-derived hip kinematics across movement planes for the right and left hips. Boxes represent the interquartile range, central lines indicate medians, and whiskers represent data variability.

4.1.4.2 Post-Correction Waveform Similarity (CMC2)

Following offset correction, waveform similarity improved substantially across all motions (*Table 7*). CMC2 values indicated excellent similarity for flexion/extension in both hips, with mean values of 0.967 for the right hip and 0.964 for the left. Accordingly, 87.4% of right hip trials and 85.6% of left hip trials exceeded the excellent threshold for this motion. Frontal plane adduction/abduction also improved markedly following offset correction, with mean CMC2 values increasing to 0.853 at the right hip and 0.876 at the left, indicating very good waveform similarity overall. In contrast, internal/external rotation remained the least similar motion plane after correction, although mean CMC2 values improved to 0.750 and 0.761 for the right and left hip, respectively. These values indicate good waveform similarity on average, but only 1.9% of right hip trials and 1.1% of left hip trials exceeded the excellent threshold, such that transverse plane tracking remained comparatively less consistent than sagittal and frontal plane motions.

Table 7. Descriptive values of post-correction waveform similarity (CMC2) between IMU- and OMC-derived hip kinematics across movement planes. The percentage of trials exceeding predefined good-to-excellent CMC thresholds are presented for each motion.

Side	Motion	CMC2 Mean ± SD	CMC2 Median (+ IQR)	CMC2 > (%)		
				0.75	0.85	0.95
Right Hip	Flex/Ext	0.967 ± 0.050	0.981 (0.969–0.988)	98.71	96.42	87.41
	Add/Abd	0.853 ± 0.121	0.886 (0.816–0.931)	86.12	65.81	17.02
	Int/Ext	0.750 ± 0.110	0.764 (0.702–0.818)	55.94	14.74	1.86
Left Hip	Flex/Ext	0.964 ± 0.056	0.980 (0.968–0.987)	98.14	95.99	85.55
	Add/Abd	0.876 ± 0.110	0.908 (0.854–0.940)	90.70	76.25	18.74
	Int/Ext	0.761 ± 0.103	0.779 (0.718–0.822)	65.24	13.45	1.14

CMC = Coefficient of multiple correlation.

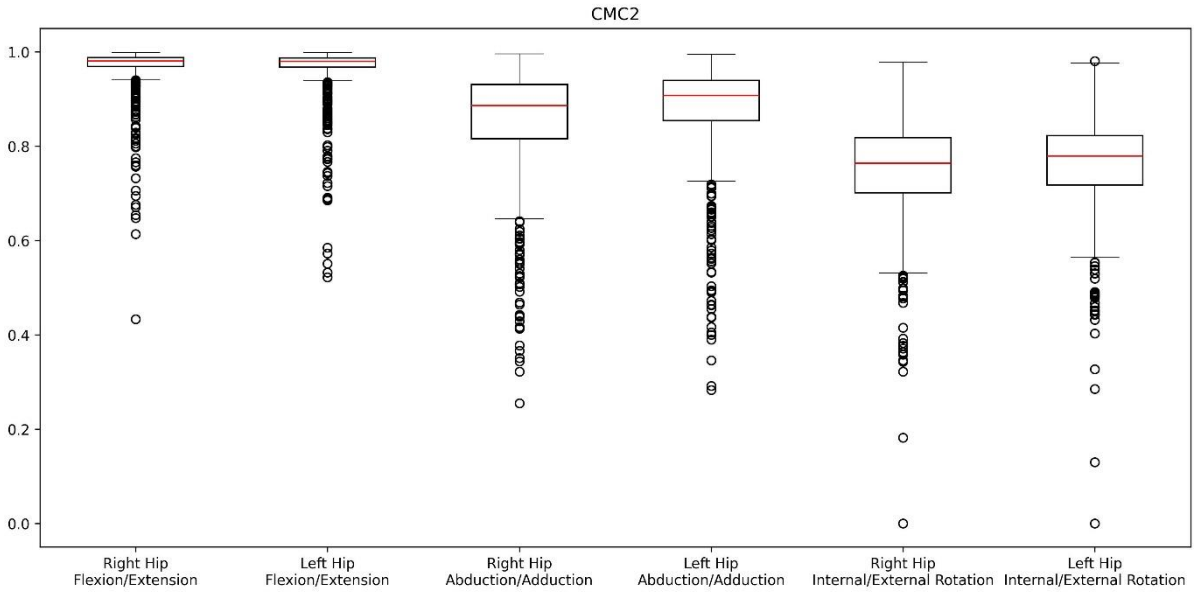


Figure 15. Box-and-whisker plots of pre-correction waveform similarity (CMC2) between IMU- and OMC-derived hip kinematics across movement planes for the right and left hips. Boxes represent the interquartile range, central lines indicate medians, and whiskers represent data variability.

4.1.5 Bland-Altman Analysis

Bland–Altman analysis demonstrated systematic differences between IMU-derived and OMC-derived hip kinematics, with results summarized in *Table 8* and visualized in *Figure 16*. Across pooled participant-trial data, joint angles for sagittal plane hip flexion/extension exhibited small negative biases, with mean differences of -1.01˚ (right) and -0.59˚ (left). Corresponding LOAs ranged from -13.48˚ to 11.47˚ and -14.27˚ to 13.09˚ for the right and left hips, respectively.

Table 8. Bland–Altman analysis of agreement between IMU- and OMC-derived hip kinematics across movement planes. Mean bias, standard deviation of differences, and 95% limits of agreement are presented for the right and left hips.

Side	Motion	Bias (˚)	SD of Differences (˚)	Upper LOA (˚)	Lower LOA (˚)
Right Hip	Flex/Ext	-1.01	6.37	11.47	-13.48
	Add/Abd	0.13	4.80	9.54	-9.28
	Int/Ext	-9.10	10.53	11.53	-29.73
Left Hip	Flex/Ext	-0.59	6.98	13.09	-14.27
	Add/Abd	-0.32	4.50	8.49	-9.13
	Int/Ext	-12.29	11.40	10.05	-34.64

SD = standard deviation. LOA = limits of agreement.

Compared with other motion planes, frontal plane adduction/abduction showed smaller absolute bias (right: 0.13˚; left: -0.32˚) and relatively narrower dispersion about the mean difference, with lower and upper LOAs of -9.28˚ to 9.54˚ for the right hip and -9.13˚ to 8.49˚ for the left hip. The most pronounced systematic differences and widest LOAs were observed in internal/external rotation for both hips. At the right hip, the mean difference was -9.10˚ with corresponding LOAs from -29.73˚ to 11.53˚, while the left hip demonstrated a mean bias -12.29 with LOAs from −34.64˚ to 10.05˚.

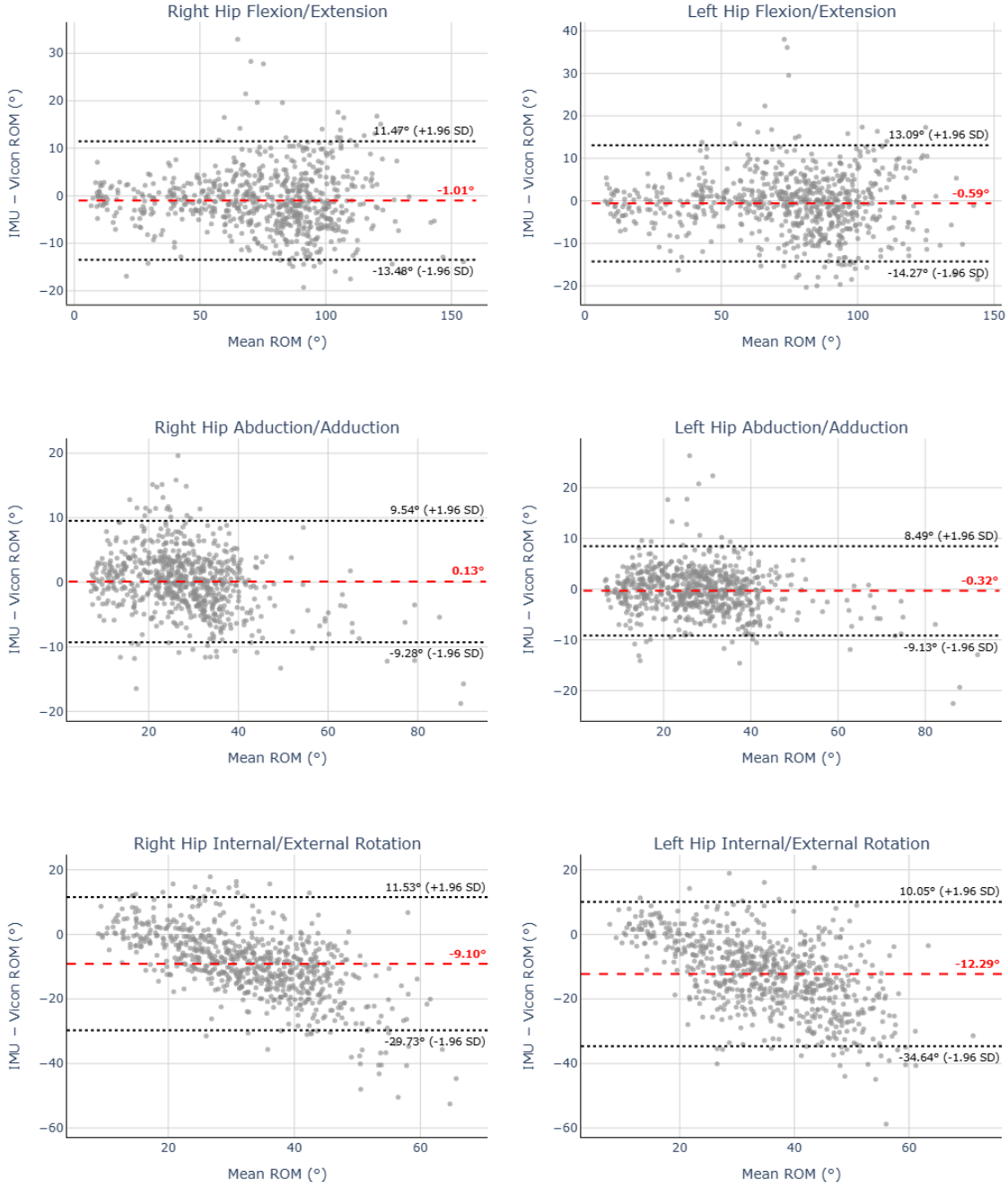
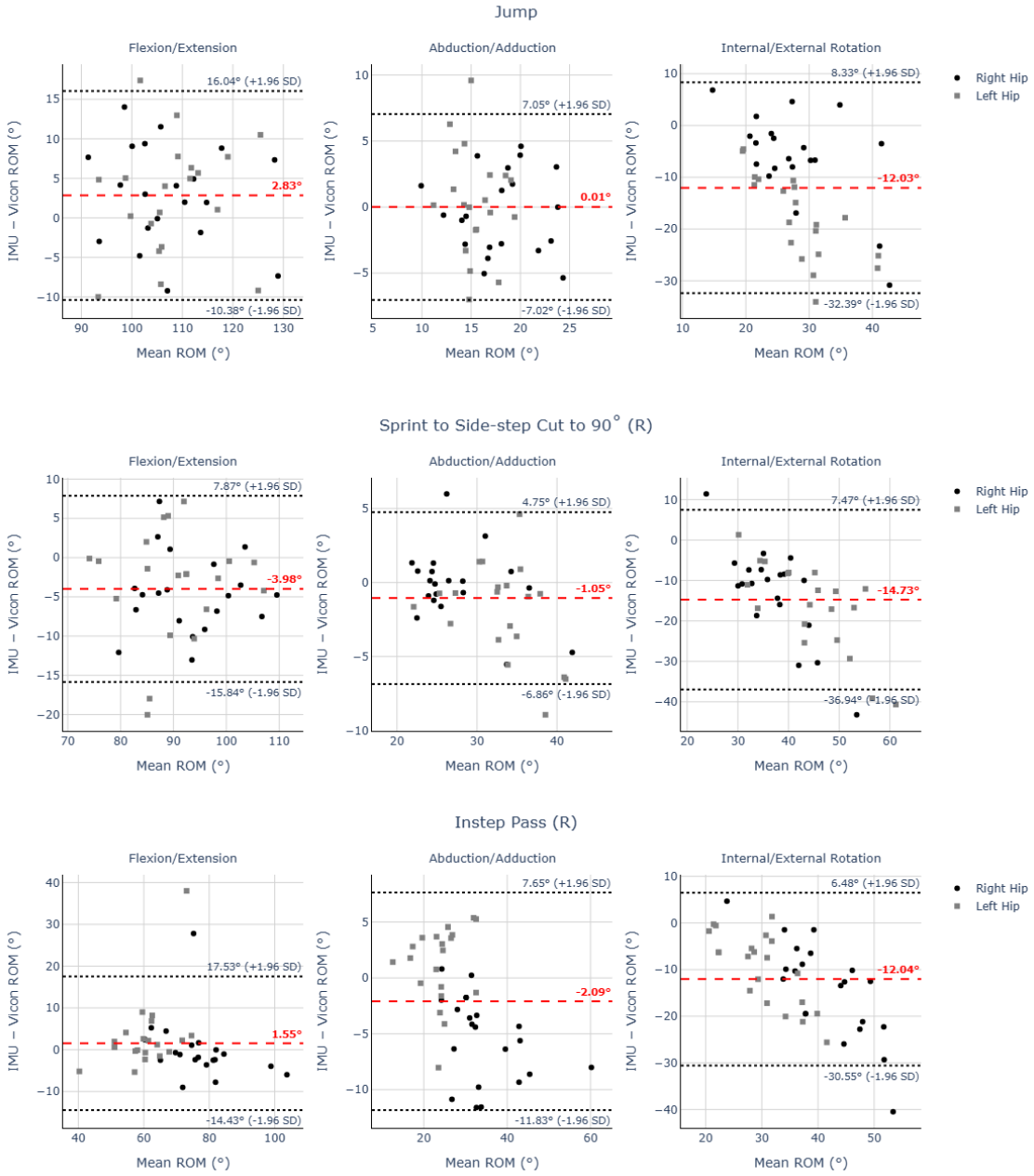


Figure 16. Bland–Altman plots demonstrating agreement between IMU- and OMC-derived hip kinematics across movement planes for the right and left hips. Red dashed lines represent mean bias, while black dotted lines indicate the 95% LOAs.

To support these findings, trial-level Bland-Altman analysis was performed across all movement tasks separately, with right and left hip measurements displayed concurrently to enable visual assessment of side-specific differences. Supplementary plots are presented in *Figure 17*, including select off-the-ball (Jump, Sprint to Side-step Cut to 90˚ (R)) and on-the-ball movements (Instep Pass (R), Instep Receive (R), Dribble to Turn (R)). Full trial-level results and a complete set of Bland-Altman plots for the remaining movements are provided in *Appendix D* and *Appendix E*, respectively.



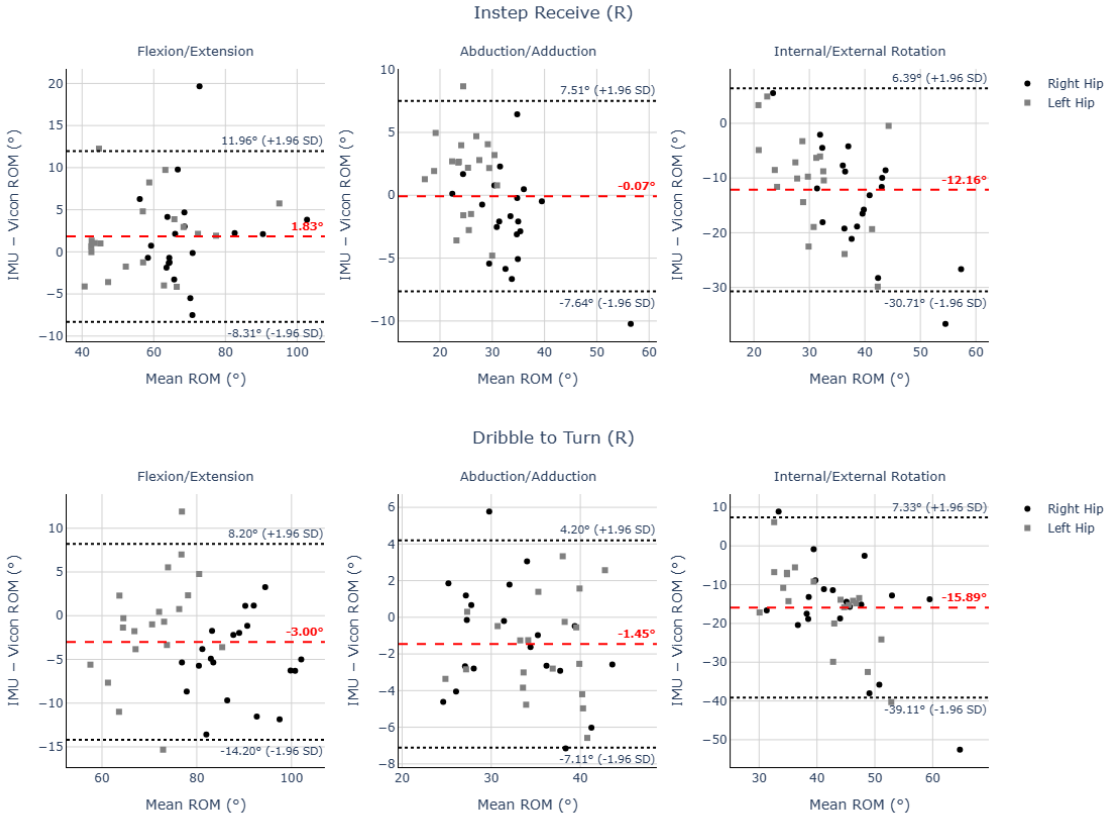


Figure 17. Supplementary trial-level Bland-Altman plots demonstrating agreement between IMU- and OMC-derived hip kinematics across movement planes during select soccer-specific tasks. Right (black circles) and left (grey squares) are presented concurrently for visual comparison of side-specific differences.

4.2 Machine-Learning Classifier

4.2.1 Classifier Evaluation

After repetition segmentation and feature extraction, the features of 2800 samples from 20 participants (140 repetitions per participant, 20 movements) were used to train and evaluate each ML classifier. As shown in *Table 9*, all classifiers demonstrated strong performance, achieving overall accuracies ≥0.912 (91.2%) and macro-averaged F1-scores ≥0.874. Among the evaluated models, XGBoost demonstrated the highest overall performance, achieving the greatest macro-averaged F1-score (0.905) and overall accuracy (0.944; 94.4%), and was therefore selected as the best-performing classifier.

XGBoost also recorded the highest values across all macro-averaged performance metrics, including precision (0.914), recall (0.899), and specificity (0.997). The mean per-fold accuracy for XGBoost was 0.944 ± 0.055, highlighting consistent classification performance across participants during LOSO evaluation. SVM demonstrated the second-best

performance, achieving a macro-averaged F1-score of 0.901 and overall accuracy of 0.937, followed by RF (F1-score = 0.892; accuracy = 0.932). Although kNN and H-SVM achieved comparable performance, both demonstrated lower macro-averaged F1-scores (kNN = 0.874; H-SVM = 0.875) and overall accuracies (0.923 and 0.912, respectively). Specificity was consistently high (0.996-0.997), reflecting the strong ability of all models to correctly reject non-target movement classes.

Table 9. Performance comparison of ML classifiers for soccer-specific movement classification. Macro-averaged F1-score, precision, recall, and specificity are provided, along with overall accuracy and mean per-fold accuracy from LOSO evaluation.

Classifier Performance Metric	kNN	RF	XGBoost	SVM	H-SVM
F1-Score	0.874	0.892	0.905	0.901	0.875
Overall Accuracy	0.923	0.932	0.944	0.937	0.912
Mean Per-Fold Accuracy (± SD)	0.923 ± 0.080	0.932 ± 0.085	0.944 ± 0.055	0.937 ± 0.074	0.912 ± 0.078
Precision	0.865	0.893	0.914	0.914	0.862
Recall	0.890	0.893	0.899	0.888	0.892
Specificity	0.996	0.996	0.997	0.996	0.996

kNN = k-Nearest Neighbors. RF = Random Forest. XGBoost = Extreme Gradient Boosting. SVM = Support Vector Machine. H-SVM = Hierarchical-SVM.

4.2.2 Best-performing Classifier Evaluation: XGBoost

A summary of the class-specific breakdown of the best-performing XGBoost classifier is presented in *Table 10*. The XGBoost model demonstrated strong class-specific performance across all 20 movement categories, with F1-scores ranging from 0.864 to 1.000. The highest classification performance was observed for Jump, which achieved perfect precision, recall, and F1-score (1.000), followed by Lateral Shuffle (F1-score = 0.973) and Submaximal Sprint to Turn (L) (F1-score = 0.975). In contrast, the lowest F1-scores were observed for Instep Receive (L) (0.864), Dribble to 90˚ Cut (R) (0.869), and Instep Receive (R) (0.882). Performance was generally comparable between right- and left-sided movement variations. For example, Sprint to Side-step Cut to 45˚ and to 90˚ achieved similar F1-scores for right (0.907, 0.939) and left (0.909, 0.046) directions, respectively, while Dribble to Turn

movements exhibited similar performance on the right side (F1-score = 0.928) compared with the left side (F1-score = 0.924).

Table 10. Class-specific performance of the XGBoost classifier for soccer-specific movement classification during model training using peak detection repetition segmentation.

Movement	F1-score	Precision	Recall
Jump	0.995	0.995	0.995
Lateral Shuffle	0.988	0.976	1.000
Submaximal Sprint to Turn (R)	0.970	0.980	0.960
Submaximal Sprint to Turn (L)	0.985	0.990	0.980
Sprint to Side-step Cut to 45˚ (R)	0.879	0.888	0.870
Sprint to Side-step Cut to 45˚ (L)	0.873	0.887	0.860
Sprint to Side-step Cut to 90˚ (R)	0.907	0.886	0.930
Sprint to Side-step Cut to 90˚ (L)	0.945	0.949	0.940
Instep Pass (R)	0.937	0.939	0.935
Instep Pass (L)	0.916	0.967	0.870
Instep Receive (R)	0.803	0.850	0.761
Instep Receive (L)	0.798	0.865	0.740
Outstep Receive (R)	0.872	0.895	0.851
Outstep Receive (L)	0.850	0.882	0.820
Dribble to 45˚ Cut (R)	0.859	0.967	0.850
Dribble to 45˚ Cut (L)	0.882	0.905	0.860
Dribble to 90˚ Cut (R)	0.860	0.892	0.830
Dribble to 90˚ Cut (L)	0.864	0.814	0.920
Dribble to Turn (R)	0.918	0.888	0.950
Dribble to Turn (L)	0.922	0.896	0.950
Other	0.984	0.971	0.998

The XGBoost classifier also showed strong subject-independent performance across the 20 LOSO folds, achieving a mean per-fold accuracy of 0.944 ± 0.055 (*Figure 18*). Classification performance was consistently high across the majority of participants, with 18 of 20 subjects achieving accuracy above 0.91. The most notable exception was P15, for which the model reported substantially reduced accuracy (0.755) relative to the mean, while P11 also demonstrated somewhat lower accuracy (0.841) than the remaining participants.

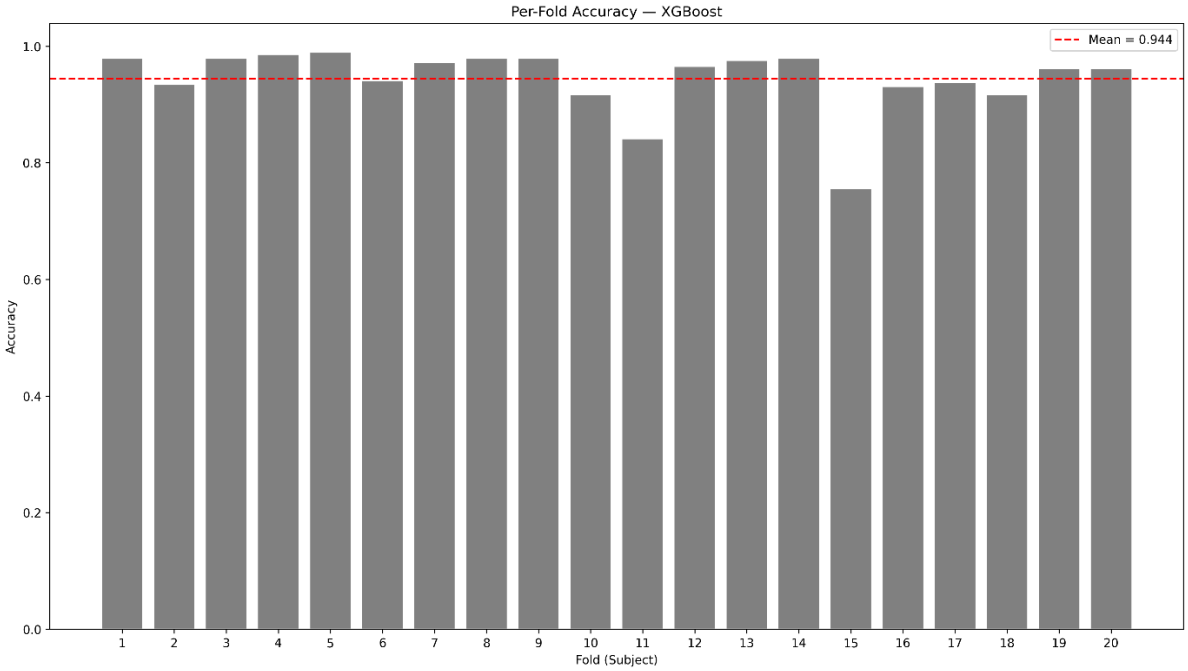


Figure 18. Subject-independent performance of the XGBoost classifier during LOSO evaluation. Classification accuracy is presented for each participant, with the overall mean per-fold accuracy indicated by the dashed red line.

Examination of the confusion matrices, presented as raw repetition counts (*Figure 19A*) and as row-normalized percentages (*Figure 19B*) demonstrated that misclassifications were primarily concentrated among kinematically similar movements, particularly within dribbling and passing/receiving actions. For example, 19 left-footed Instep Receive repetitions were misclassified as Outstep Receives, while 15 right-footed Instep Receive repetitions were misclassified as Outstep Receives. Despite these confusions, Instep Pass trials—the most frequently performed technical soccer skill—were generally classified accurately, with 174 and 186 correct predictions for left- and right-footed passes, respectively, out of 200 repetitions. Misclassifications of Instep Passes were primarily attributed to corresponding Instep Receive movements, with 6 left-footed and 7 right-footed Instep Pass repetitions incorrectly predicted as Instep Receive, while 9 left-footed Instep Pass repetitions were classified as "Other."

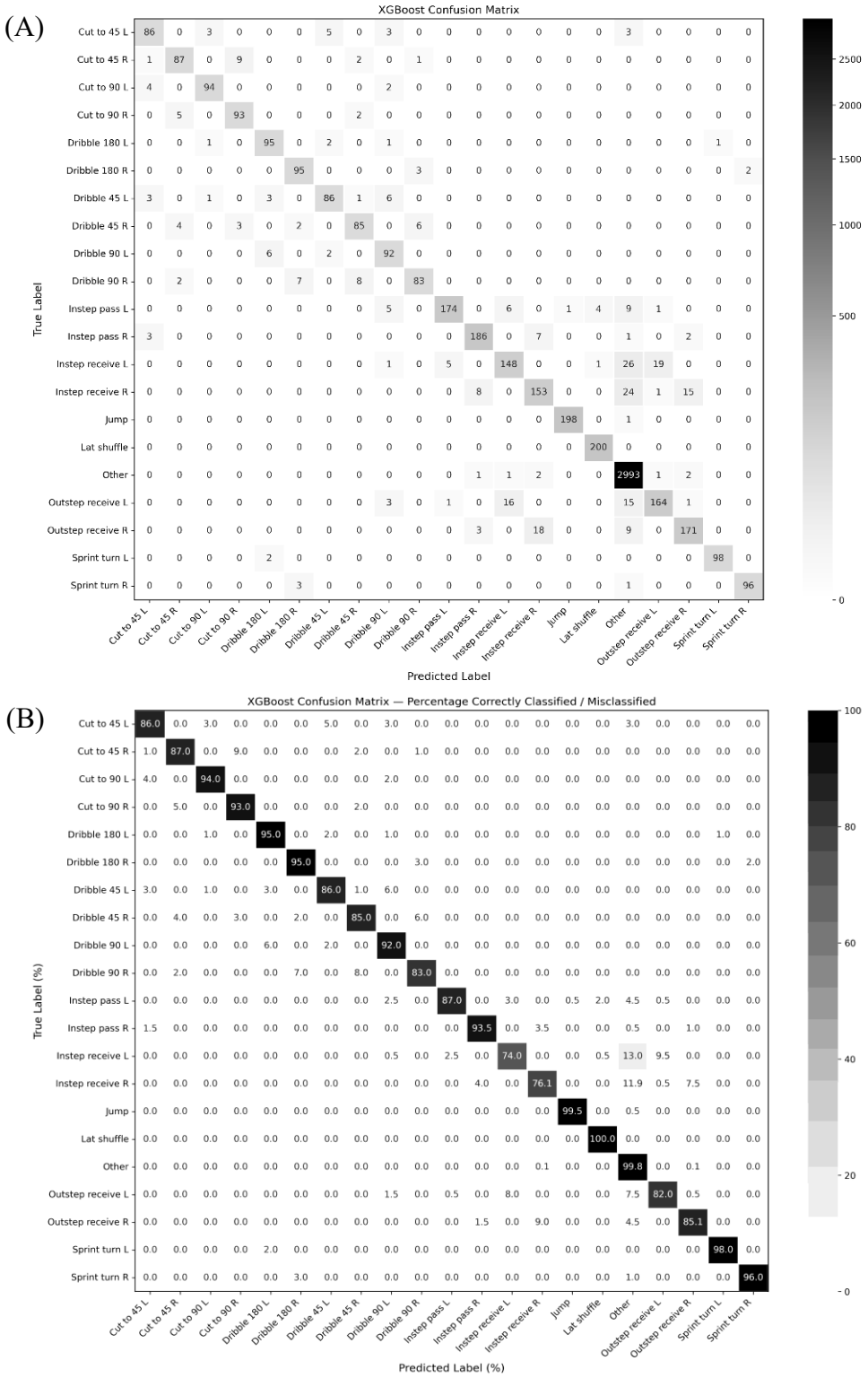


Figure 19. Confusion matrices illustrating task classification performance of the XGBoost classifier during model training LOSO evaluation, presented as (A) raw repetition counts and (B) row-normalized percentages (0–100%). Predicted and true class labels are shown on the x- and y-axes, respectively. Diagonal elements represent correctly classified movement repetitions, whereas off-diagonal elements indicate misclassifications between movement classes.

Similar patterns were observed among dribbling tasks, where errors were predominantly confined to movements with comparable change-of-direction demands. Specifically, 6 Dribble to 45˚ Cut (R) repetitions were misclassified as Dribble to 90˚ Cut (R), while 6 Dribble to 90˚ Cut (L) repetitions were misclassified as Dribble to Turn (L). Several dribbling trials were also misclassified as their corresponding off-the-ball cutting movements. For instance, 3 left- and 4 right-sided Dribble to 45˚ Cut were wrongly predicted as Sprint to Side-step Cut to 45˚ on the respective side. In contrast, Off-the-Ball movements demonstrated comparatively stronger classification performance, with Jump and Lateral Shuffle achieving near-perfect classification of all repetitions respectively, and all Sprint-based movements achieving ≥86% accuracy. The Other class, comprising non-task movement windows, was classified with high accuracy, with 2993 of 3000 repetitions correctly identified. The confusion matrices of the four remaining classifiers are presented in *Appendix F.*

4.3 XGBoost Classifier with a Sliding Window

4.3.1 Movement-Specific Classification Performance

A sliding window duration of 4 s with a 1 s step size (75.0% overlap) produced the highest macro-averaged F1-score for task movement classification and was therefore selected for the generalizability analysis. In contrast with the segmented repetition classifier evaluated in *Section 4.2.2*, the sliding window configuration generated 21,479 windows across all participants. When classifying movements, the XGBoost classifier achieved a macro-averaged F1-score of 0.759 and an overall accuracy of 0.720 (72.0%). Relative to the segmented repetition-based LOSO evaluation, these values represented reductions of 0.146 (14.6%) and 0.224 (22.4%), respectively. A movement-specific breakdown of classification performance is presented in *Table 11*, where *Δ F1-score* represents the F1-score achieved during the sliding window evaluation and that of the primary LOSO assessment. Consistent with the segmented repetition evaluation, gross locomotor movements (e.g., Jump and Lateral Shuffle) generally achieved higher classification performance than on-the-ball actions. Performance was also comparable between equivalent left- and right-sided movements, with, for example, Instep Pass achieving similar F1-scores for the right (0.828) and left (0.820) sides. The lowest classification performance was observed for Sprint to Side-step Cut to 45˚ (right = 0.561; left = 0.560). Similarly, the six dribbling classes demonstrated relatively lower performance, with F1-scores ranging from 0.588 to 0.711.

Table 11. Class-specific performance of the XGBoost classifier for soccer-specific movement classification during sliding-window evaluation using a 4 s window and 1 s step size. Change in F1-score (ΔF1-score) relative to the primary peak detection-based repetition segmentation LOSO evaluation is presented.

Movement	F1-score	Precision	Recall	Δ F1-score
Jump	0.966	0.998	0.937	-0.029
Lateral Shuffle	0.995	1.000	0.989	0.007
Submaximal Sprint to Turn (R)	0.854	0.953	0.773	-0.116
Submaximal Sprint to Turn (L)	0.800	0.987	0.673	-0.185
Sprint to Side-step Cut to 45˚ (R)	0.561	0.846	0.419	-0.318
Sprint to Side-step Cut to 45˚ (L)	0.560	0.805	0.430	-0.313
Sprint to Side-step Cut to 90˚ (R)	0.837	0.843	0.830	-0.07
Sprint to Side-step Cut to 90˚ (L)	0.767	0.881	0.679	-0.178
Instep Pass (R)	0.828	0.970	0.721	-0.109
Instep Pass (L)	0.820	0.973	0.709	-0.096
Instep Receive (R)	0.800	0.801	0.798	-0.003
Instep Receive (L)	0.780	0.818	0.746	-0.018
Outstep Receive (R)	0.887	0.951	0.831	0.015
Outstep Receive (L)	0.832	0.867	0.800	-0.018
Dribble to 45˚ Cut (R)	0.634	0.568	0.719	-0.225
Dribble to 45˚ Cut (L)	0.686	0.629	0.754	-0.196
Dribble to 90˚ Cut (R)	0.711	0.702	0.720	-0.149
Dribble to 90˚ Cut (L)	0.646	0.583	0.725	-0.218
Dribble to Turn (R)	0.588	0.893	0.439	-0.330
Dribble to Turn (L)	0.621	0.841	0.492	-0.301
Other	0.867	0.913	0.825	-0.117

Much like the segmented repetition evaluation, misclassifications during the sliding-window generalizability assessment occurred predominantly between kinematically similar movements. As shown in *Figure 20*, the greatest source of confusion was between dribbling actions differing only in cutting angle on the same side. Most notably, Dribble to Turn was frequently misclassified as Dribble to 45˚ Cut or Dribble to 90˚ Cut in the same direction, accounting for 76 and 99 windows, respectively, on the left side and 100 and 61 windows on the right side. Confusion was also observed between cutting and dribbling tasks involving the same change-of-direction angle, such as Sprint to Side-step Cut to 45˚ (L) being predicted as Dribble to 45˚ Cut (L), although these errors occurred less frequently. Similar trends were evident for passing and receiving actions with comparable movement characteristics. On the right side, 58 Instep Pass windows and 40 Outstep Receive windows were incorrectly classified as Instep Receive, while the corresponding values on the left side were 51 and 30 windows, respectively. Overall, movement-specific classification accuracy exceeded 83% for all movements except Sprint to Side-step Cut to 45˚ (left and right), Dribble to Turn (left and right), and Dribble to 90˚ Cut (R), which achieved accuracies ranging from 53.6% to 79.2%.

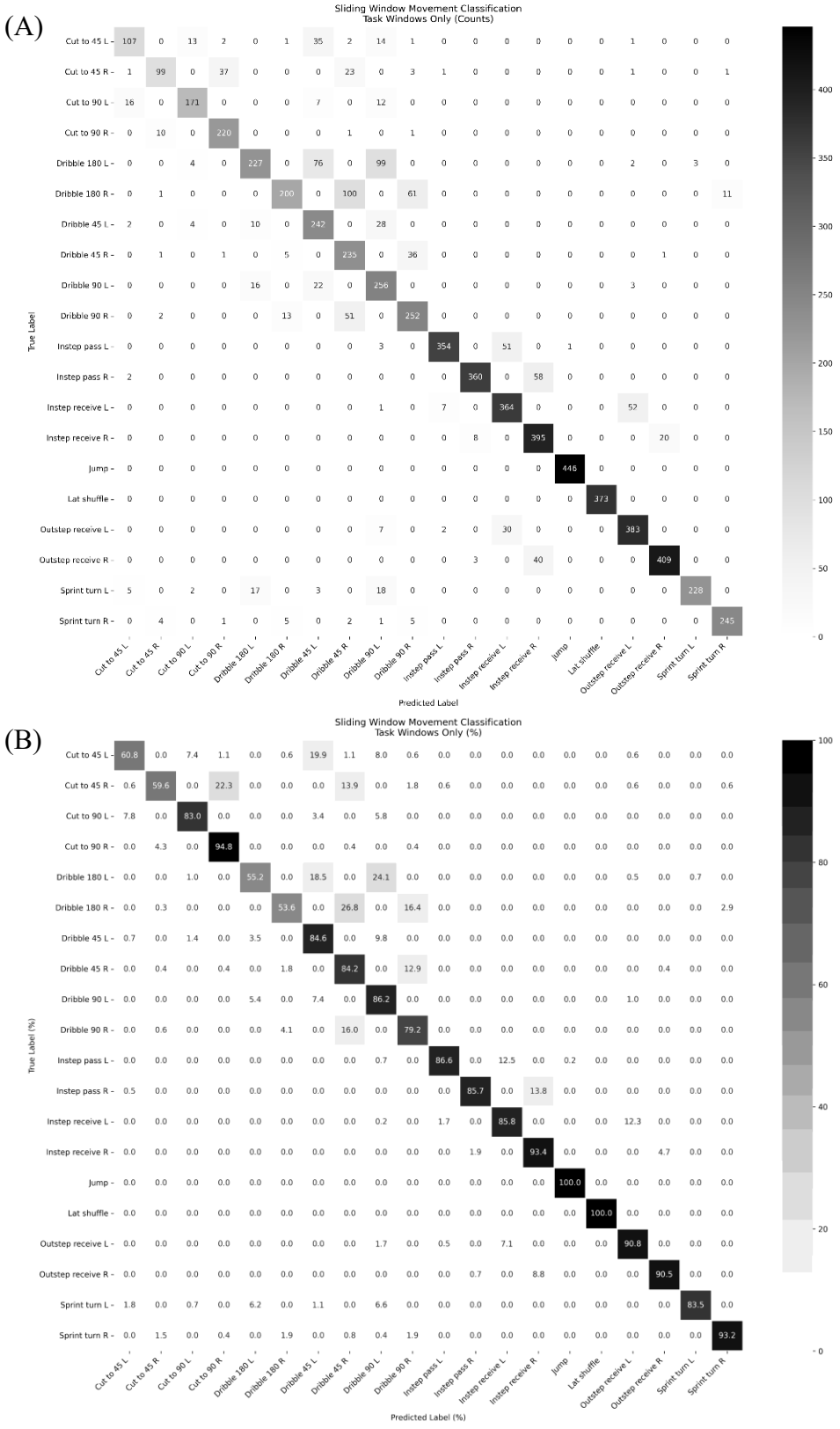


Figure 20. Confusion matrices illustrating task classification performance of the XGBoost classifier during sliding-window evaluation, presented as (A) raw window counts and (B) row-normalized percentages (0–100%). Predicted and true class labels are shown on the x- and y-axes, respectively. Diagonal elements represent correctly classified movement repetitions, whereas off-diagonal elements indicate misclassifications between movement classes.

4.3.2 Task vs. Other Classification

The classifier demonstrated strong performance in distinguishing task movements from non-target activity (*Table 11*). When evaluated as a two-class classification problem (Task vs. Other), the Other class achieved an F1-score of 0.867 (precision = 0.913, recall = 0.825). Using a confidence threshold of 0.50, the corresponding confusion matrix (*Figure 21*) shows that, of the 13,748 sliding windows labelled as Other, 11,343 were correctly identified (82.5%), whereas 2405 (17.5%) were incorrectly classified as one of the 20 task movement classes. Conversely, of the 7,731 true task movement windows, 1,082 (14.0%) were incorrectly rejected as Other, with the remaining 6,649 (86.0%) correctly retained as task movements. Overall classification accuracy for Task vs. Other was 0.838 (83.8%).

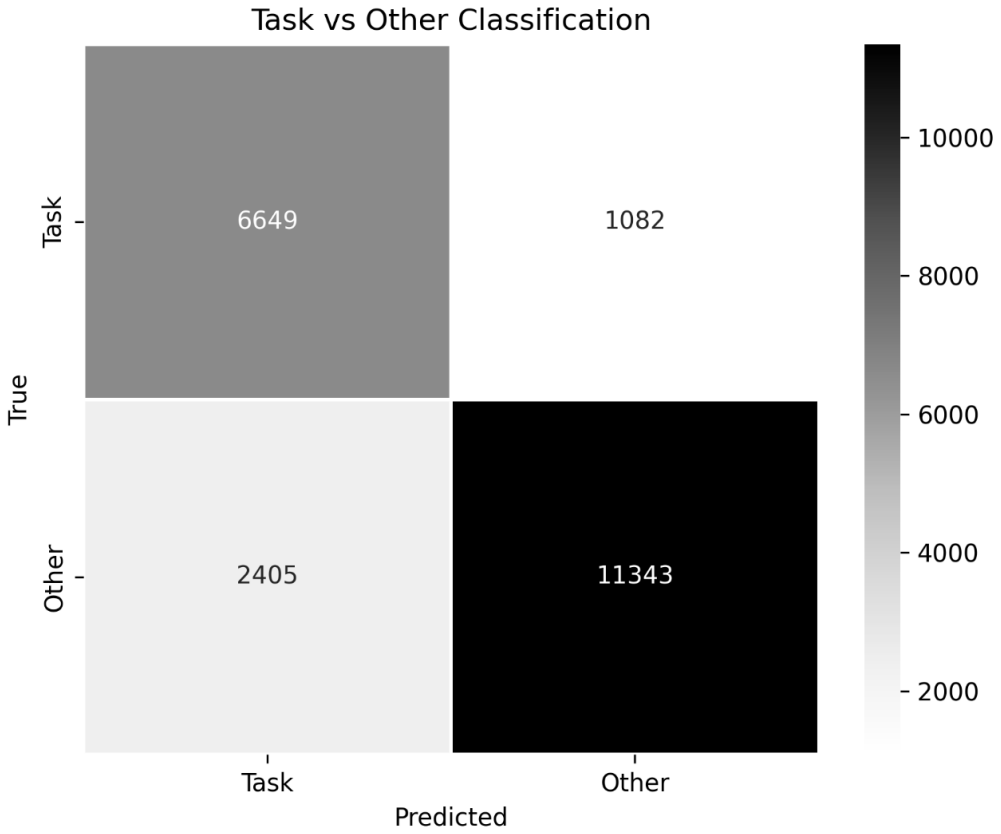


Figure 21. Confusion matrix illustrating binary classification performance of the XGBoost classifier for distinguishing Task movements from the Other class during sliding-window evaluation. Predicted and true class labels are shown on the x- and y-axes, respectively, with cell values representing the number of classified windows.

5 Discussion

This thesis aimed to validate a wearable IMU system against a gold-standard OMC system for quantifying 3D hip kinematics during a comprehensive series of soccer-specific movements. It was hypothesized that IMU-derived hip kinematics would demonstrate good-to-excellent agreement with OMC across all three planes of motion. A secondary aim was to develop an ML classifier capable of identifying several of these soccer-specific manoeuvres from IMU-derived signals, with the hypothesis that the ML classifier would distinguish between soccer-specific movement techniques with high accuracy (>90%). These objectives were motivated by a broader gap in the literature: although cam morphology and its association with symptomatic FAIS and subsequent hip OA have been strongly linked to high-impact youth sport participation, current methods have been unable to quantify how frequently, and in which specific joint positions, the hip is exposed to potentially provocative kinematic patterns associated with cam FAIS development and symptom onset during ecologically valid sporting activities.

The findings of this thesis demonstrate the feasibility of using wearable IMUs to estimate hip joint angles during complex soccer-specific techniques in a controlled setting. The first hypothesis was partially supported. The IMU system demonstrated good-to-excellent agreement with OMC for sagittal (flexion/extension) and frontal (adduction/abduction) plane hip motion across 35 movement tasks, including bilateral range-of-motion, off-the-ball, and on-the-ball actions, based on ROM and RMS error comparisons. However, larger discrepancies and greater variability were consistently observed for internal/external rotation in the transverse plane, the implications of which are discussed in detail below. Waveform similarity between systems, assessed using the CMC, followed a comparable pattern and improved substantially following offset correction.

In agreement with the second hypothesis, the 5 ML classifiers achieved strong overall classification performance across the selected subset of 20 soccer movements. Movements were selected based on two criteria: kinematic relevance to cam FAIS and symptomatic impingement, whereby the movement's peak hip flexion coincided with elevated hip adduction and internal rotation, and ecological relevance, prioritizing actions performed commonly during soccer match play or training. Among the classifiers tested, XGBoost was identified as the best-performing model. Although the XGBoost model demonstrated strong average performance at the participant level, one participant (P15) demonstrated considerably reduced classification accuracy relative to the remainder of the cohort. At the movement

level, misclassifications were concentrated among technical tasks with kinematic overlap, whereas gross off-the-ball movements were classified with near-perfect accuracy.

5.1 Validity of IMU-derived Hip Kinematics

5.1.1 Sagittal and Frontal Plane Agreement

Accurate quantification of 3D hip kinematics is fundamental to understanding movement exposures that may contribute to the development and progression of symptomatic cam FAIS through high-impact sports participation. The results of the paired-samples t-tests revealed no significant differences in ROM between the IMU and OMC systems for flexion/extension or adduction/abduction at either hip (all $p > 0.05$), indicating that the IMU system captured equivalent total joint excursion to the OMC system in these two planes. This was further supported by low RMS error (2.45˚-3.58˚) and small mean differences -1.01˚-0.13˚), suggesting that wearable IMUs can provide valid estimates of sagittal and frontal plane hip kinematics during complex soccer-specific movements. This level of agreement is particularly encouraging given that hip flexion and adduction are key components of movement patterns frequently implicated in cam FAIS.

These findings are consistent with previous validation studies demonstrating comparable hip ROM values and similarly low RMS errors during level walking, stair ascent, and squatting.[38,41,43,138] Wilmes et al.,[153] reported a larger RMS difference (8.0˚) for left hip flexion/extension during soccer-specific tasks including acceleration, deceleration, cutting (60–75˚), jumping, and instep kicking performed at three increasing intensities. Likewise, Blair et al.,[39] reported trivial differences between maximum hip extension angles measured using a full-body IMU system and a reference OMC system during a variety of kicking tasks, including instep soccer kicks. However, both studies were limited to sagittal-plane hip kinematics, preventing a comprehensive evaluation of the IMU system's ability to quantify 3D hip motion during soccer-specific activities. More broadly, prior investigations have focused on relatively simple locomotor or basic soccer tasks, in addition to heading and dribbling.[45,51,52,142,153] By evaluating 35 soccer-specific movements spanning bilateral range-of-motion, off-the-ball, and on-the-ball actions, the present study extends existing validation evidence to a substantially wider range of movement patterns representative of the kinematic demands of soccer. Moreover, many of these movements are common to other high-impact sports, such as basketball and ice hockey, suggesting that the present findings may have broader applicability to other at-risk activities.

5.1.2 Transverse Plane (Internal/External Rotation) Limitations

In contrast, ROM for internal/external rotation differed significantly between systems at both hips ($p < 0.001$). This discrepancy was accompanied by higher RMS error (R = 5.97˚; L = 6.67˚) and a substantial negative mean difference (R = -9.09˚; L = -12.28˚), indicating that the IMU system consistently underestimated hip internal/external rotation relative to OMC during soccer manoeuvres. This finding is consistent with previous validation studies investigating gait,[41] as well as change-of-direction and jumping tasks,[37] in which rotational hip kinematics demonstrated greater error than sagittal or frontal plane measurements. The present study extends these findings by demonstrating that these limitations persist during technically demanding sport-specific movements, including sprinting and dribbling with rapid directional changes. However, discrepancies between systems were generally smaller during passing and receiving tasks, implying that transverse plane accuracy may be influenced by the dynamic demands and complexity of the movement being performed. This suggests that wearable IMUs may remain a valuable tool for quantifying hip movement exposures during certain commonly performed soccer actions.

One possible explanation for the lower agreement consistently observed for internal/external rotation is that the range of motion in the transverse plane is inherently smaller than sagittal or frontal plane motion, meaning that a given absolute measurement error represents a proportionally larger error in the estimated joint angle. This may increase the relative influence of signal noise arising from factors such as soft tissue artefact, sensor movement, or from transient accelerations resulting from direct impact to the IMUs, potentially contributing to inaccuracies in segment orientation.[40] Although the effect of movement velocity on IMU measurement accuracy has produced mixed evidence,[42,49,141] faster movements may provide stronger inertial signals and therefore are not expected to reduce measurement accuracy. Rather, the complex multiplanar nature of the movements assessed in the present study may have contributed to greater errors in transverse-plane orientation estimation, consistent with previous research demonstrating reduced IMU accuracy during complex movements, particularly in the transverse plane.[46]

These findings have important implications for future applications of wearable IMUs in cam FAIS research. Positions combining hip flexion, adduction, and internal rotation are thought to promote premature contact between the proximal femur and acetabulum,[8,10,24] and so accurately quantifying the 3D profile of movements is critical. Consequently, although the present IMU configuration provides robust estimates of sagittal and frontal plane motion,

improvements in the measurement of transverse plane rotation remain necessary before wearable systems can comprehensively characterize the hip kinematic exposures most relevant to cam FAIS. Potential approaches include refinement of calibration procedures, optimization of sensor-to-segment alignment, or evaluation of the sensor fusion algorithm's ability to capture fine changes in transverse plane rotation.

The observed error in internal/external rotation limits the ability of the IMU system to directly quantify the magnitude of potentially provocative hip positions associated with cam FAIS. Nevertheless, the utility of the IMU system for the intended application does not necessarily depend on reproducing OMC-derived transverse plane angles with high absolute accuracy. Instead, a key consideration is whether the IMU preserves sufficient temporal and movement-specific information to identify when soccer techniques associated with potentially provocative hip positions occur. The time-series comparisons shown in *Figure 12* and the CMC2 data presented in *Table 7* and *Figure 14* demonstrated that, despite differences in absolute magnitude, IMU-derived waveforms generally followed the pattern of the OMC signal. This suggests that the IMU may retain information about the occurrence and timing of internal rotation and its combination with other hip motions, even when the magnitude of the rotation is under- or overestimated.

However, the wide LOAs spanning -29.73˚ to 11.53˚ for the right hip and -34.64˚ to 10.05˚ for the left hip observed for this motion indicate large variability in the magnitude of the between-system differences, as shown in *Figure 15.* A range of this magnitude indicates that, for an individual movement, the IMU-derived hip internal rotation angle could differ greatly from the OMC value, potentially resulting in the identification of provocative positions when they did not occur, or failure to identify positions that did. As such, accurately detecting individual internal rotation events or specific provocative positions in this plane from IMU data alone remains challenging and should be interpreted cautiously. In this context, the IMU setup may be more appropriately considered a tool for identifying and tracking movement exposures than for directly quantifying the absolute magnitude of potentially provocative joint positions.

This distinction is particularly relevant to the second aim of the thesis. The ML classifiers were not intended to directly estimate potentially provocative hip angles from IMU data. Instead, OMC-derived kinematics were used to identify soccer-specific movements of interest based on their kinematic relevance to cam FAIS and symptomatic impingement, while IMU-derived signals were subsequently used to classify those movement techniques.

As such, the 20 movements selected for classification represented an indirect approach to tracking potentially relevant hip exposures. In this framework, transverse plane measurement error does not necessarily mean that IMUs cannot be used to identify soccer-specific movements implicated in potentially provocative cam-FAIS hip kinematics, especially if the signal patterns associated with these techniques are generally preserved.

5.1.3 Offset Correction and Waveform Agreement

Following offset correction, the IMU system demonstrated good-to-excellent waveform agreement with OMC across all three anatomical planes, although transverse-plane agreement remained comparatively lower than in the sagittal and frontal planes. These findings suggest that much of the disagreement between systems reflected systematic differences in the definition of the zero-joint position rather than fundamental differences in the movement patterns being captured. The offset is commonly attributed to differences in calibration procedures and underlying biomechanical models between IMU- and OMC-based systems.[35,37,38,138] For example, the Xsens system defines all joints in the N-pose calibration position as 0˚, whereas Vicon reports the real anatomical joint angles assumed during the T-pose calibration position. Although the present study did not directly test whether differences in zero-position definitions accounted for the observed offsets, the improvement in waveform agreement following offset correction supports the presence of a systematic component to the disagreement. To determine whether differences in zero-position definitions are responsible for the observed offsets, future studies could directly compare the joint angles recorded during the quiet standing phase of each system's respective calibration procedure.

From a practical perspective, the offset identified in the present study cannot be directly applied to in-field settings without simultaneous OMC measurements to establish the system-to-system difference. Users applying IMUs in the field could potentially establish a standardized reference posture during calibration and interpret subsequent joint angles relative to this participant-specific neutral position; however, this would only standardize the IMU reference position rather than determine its offset relative to OMC. This reinforces that the IMU system may be most appropriately used to identify and track movement exposures only, rather than for directly measuring accurate 3D hip joint angles in real-time. Practitioners and professionals should exercise caution if directly comparing absolute joint angles obtained from different motion capture systems unless these offsets have been addressed.

Previous evaluations comparing wearable IMUs with OMC support the present findings, particularly during dynamic sporting tasks. Consistent with the results reported here, excellent agreement has been demonstrated for sagittal-plane hip kinematics during cutting and jumping manoeuvres, whereas frontal- and transverse-plane measurements have shown considerably greater variability, ranging from poor to excellent.[36,37] Notably, these authors identified offsets between IMU- and OMC-derived waveforms but did not apply offset correction, which may partially explain the comparatively lower agreement reported.

5.2 ML Classification of Soccer-Specific Movements

5.2.1 Training Classification Performance Across 20 Movements

The presented XGBoost classifier's ability to distinguish 20 distinct soccer-specific movements with an overall accuracy of 94.4% and macro-averaged F1-score of 0.905 represents a meaningful advancement beyond prior soccer skill classification work, which has largely been limited to classifying a small number of unspecific movements. Despite evaluating a greater number of more complex movement classes, the present XGBoost classifier demonstrated high overall classification performance relative to previous soccer classification studies that used a segmented repetition approach. For example, an SVM model using foot-worn IMU accelerometer data achieved a classification rate of 88.6% when distinguishing between a pass or a shot.[45] This study used a similar repetition-segmentation approach, detecting peaks that exceeded a predefined threshold and centering a 1-s window around each detected peak. Similarly, Stoeve et al.[55] used an SVM with 2-s windows centred on peaks identified using threshold-based segmentation to classify shots and passes, achieving a macro-averaged F1-score of 0.656. Overall classification accuracy was not reported in this study. Despite evaluating considerably more movement classes, the present XGBoost classifier maintained higher overall classification performance. This highlights the capability of the proposed approach to capture detailed movement patterns associated with cam FAIS-related movement monitoring from lower-limb IMU gyroscope data.

The superior performance of XGBoost compared with the alternative classifiers assessed in this study, is likely due to its gradient boosting framework, whereby each successive decision tree learns from the errors of its previous trees.[152] This improves the classifier’s ability to model non-linear relationships within the data.[152] This characteristic is particularly advantageous for the present dataset, which comprised a relatively large number of movement classes with noticeable kinematic overlap, such as the Instep Pass and Instep

Receive, or the Dribble to Cut at 45˚ and 90˚, making class boundaries less distinct. The ability of XGBoost to progressively refine these decision boundaries likely contributed to its superior classification performance relative to the other ML algorithms evaluated. Furthermore, a substantially greater number of features were extracted in the present study than in previous soccer-based classification,[45,50–52] which likely provided a more comprehensive representation of the underlying movement patterns. This increased feature space may have contributed to improved discriminative power between similar movements, which is particularly important when developing ML models intended for field-based assessment.[52]

The high classification performance observed under the segmented-trial approach demonstrates the ability of the model and extracted features to discriminate between movement techniques under controlled conditions but does not directly reflect performance during continuous field-based activity. Comparisons of generalizability to real-world soccer activity is therefore more appropriately made using the sliding-window analysis presented later in *Section 5.2.4.*

5.2.2 Sources of Misclassification

Examination of the confusion matrices demonstrated that classification errors were not randomly distributed but instead clustered among actions with similar kinematic demands or shared movement components, while gross off-the-ball movements were classified with near-perfect accuracy. Rather than indicating true classifier failure, these errors may reflect in-part the compound nature of soccer-specific techniques. For example, each outstep receive repetition required participants to first control the ball using the outside of the foot before returning a pass using the inside of the foot, mirroring the touch-and-pass sequence typical of realistic match play. Consequently, a single repetition labelled as an Outstep Receive inherently contained kinematic characteristics of two distinct technical actions, meaning these repetitions genuinely contained instep-kick-like kinematics as part of the segmented movement. Misclassification of these repetitions as Instep Passes may therefore reflect an accurate detection of features that were present within the repetition, rather than a fault of the classifier itself. Refining repetition segmentation boundaries specifically for discrete tasks, may reduce the unintended inclusion of secondary actions performed during compound soccer techniques. This could be achieved, for instance, by applying an adaptive window informed by signal decay following the identified movement peak, rather than a fixed duration.

These findings also raise a consideration for future classification work intended for ecologically valid sporting environments. Rather than assigning a single class label to a repetition, future models could explore temporal classification approaches capable of identifying sequences of consecutive soccer actions within continuous play. This would allow compound actions, such as a ball reception immediately followed by a pass, to be represented more accurately rather than forcing the entire sequence into a single movement category. Such an approach may be particularly valuable for quantifying real-world movement exposure in training and match play, where the continuous, unstructured nature of training and match play means that discrete actions of the type performed in this controlled protocol are the exception rather than the norm.

5.2.3 Participant-Level Variability

Although the XGBoost classifier demonstrated strong overall performance, inspection of individual LOSO folds revealed substantially reduced subject-independent accuracy for P15 (0.755) compared with the remaining participants (mean per-fold accuracy including P15 = 0.944 ± 0.055). Further examination of P15's movement data provided evidence of differences in movement execution compared with the more discrete and structured repetitions performed by the other participants. Specifically, Vicon observations and concurrent Vicon and IMU kinematic comparisons indicated that P15 frequently performed additional dynamic movements between repetitions, including rapid footwork during passing tasks and jogging between dribbling trials, which represent movement behaviours commonly encountered during continuous soccer training and match play. This difference is illustrated by representative Vicon frames comparing one Instep Pass (R) repetition performed by P15 and P06 (*Figure 22*). P06 was selected as the comparison participant because their LOSO fold accuracy (0.941) was closest to the mean per-fold accuracy.

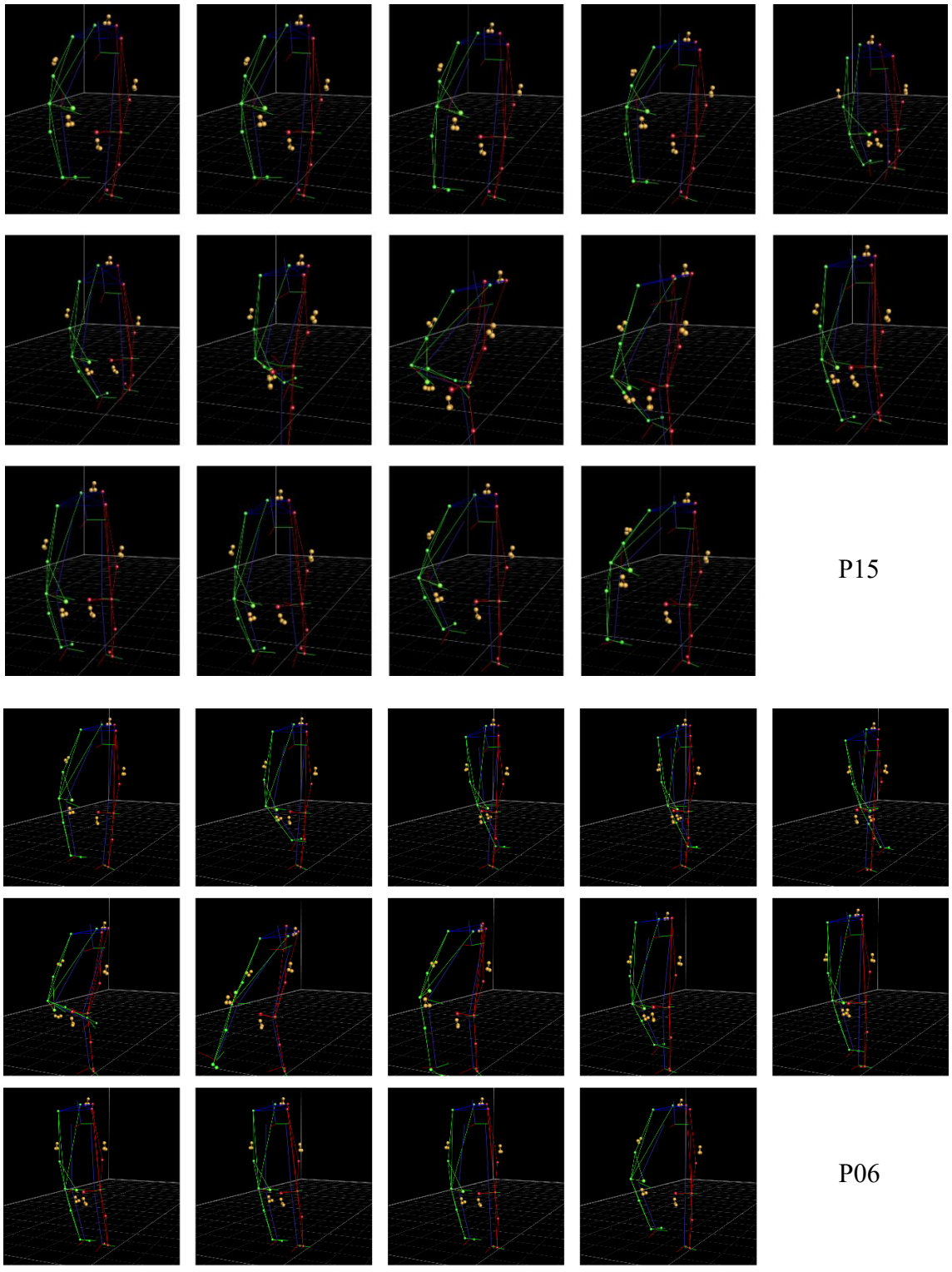


Figure 22. Representative Vicon frames demonstrating differences in movement execution and post-task activity between P15 (top) and P06 (bottom) during an instep pass (right) repetition. P15 exhibited greater non-task movement following pass completion compared with the more discrete execution observed in P06.

It is plausible that these transitional movements, that were not observed to the same extent in the other participants, increased the amount of non-task-specific movement data within the recorded trials and may have reduced the distinction between isolated repetitions and predefined movement classes. For example, Vicon and IMU traces for P15 demonstrated additional lower-limb movement variability outside of the primary instep pass execution compared to other participants, suggesting that the movement segments extracted for classification may have contained greater activity than the intended isolated repetitions. The amount of noise within data often deteriorates classifier performance.[152]

The time-normalized Vicon and IMU hip flexion/extension time-series traces for P15 and P06 completing the Instep Pass (R) are compared in *Figure 23*, further highlighting the greater non-task-specific movement variability present between repetitions within P15's data.

Importantly, the reduced performance for P15 should not be attributed to a single factor. Other participant-specific influences, including differences in movement strategy, sensor placement variability, or calibration effects may also contribute to reduced classification performance. However, recent work investigating functional sensor-to-segment calibration demonstrated that functional calibration approaches, similar to those performed for both the OMC and IMU systems in the present study, can minimize the effects of variations in IMU placement between participants, suggesting that sensor placement or calibration-related variability can be partially mitigated.[154] Nevertheless, the P15 results demonstrate that subject-independent models may exhibit participant-level fragility, where individual unseen participants may produce substantially lower performance despite high average model accuracy. This has important implications for practical use cases, where models must generalize to new athletes performing movements in ecologically valid contexts with naturally occurring variability rather than only the controlled repetitions used during model development.

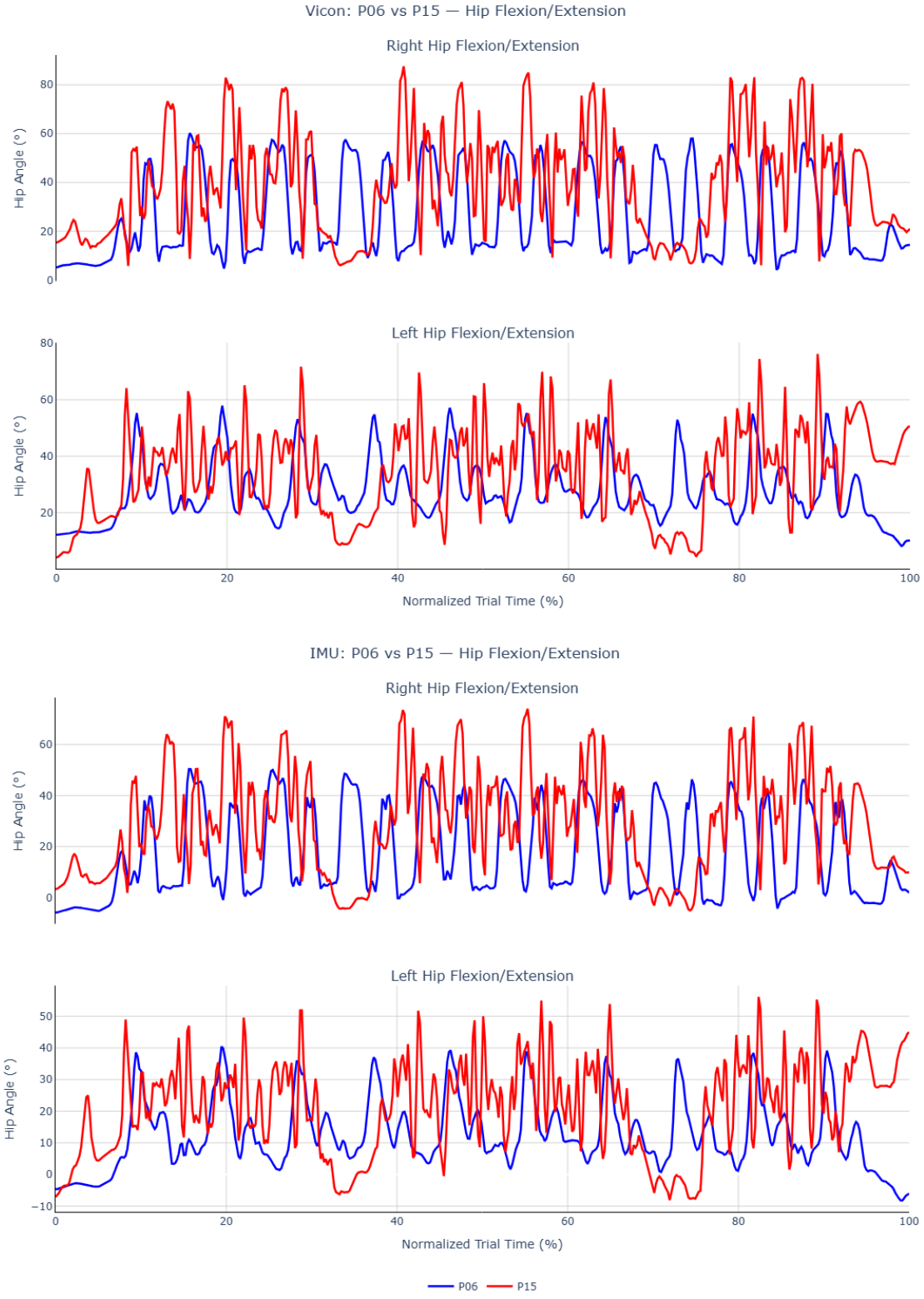


Figure 23. Right and left hip flexion/extension kinematic time-normalized time-series traces derived from Vicon OMC (top) and Xsens IMU (red) systems during an Instep Pass (R) repetition for P15 (red) and P06 (blue).

5.2.4 Model Generalizability

The XGBoost classifier demonstrated good overall performance when evaluated on continuous 4 s sliding windows, despite having been trained exclusively on segmented movement repetitions, with classification accuracy decreasing from 94.4% to 72.0% and macro-averaged F1-score declining from 0.905 to 0.759. Critically, almost no confusion occurred across left/right sides or across unrelated movement categories (e.g., dribbling misclassified as passing), indicating that the model's errors stem from genuine kinematic overlap between technique variants rather than a general breakdown in movement discrimination. Misclassification between similar motions likely reflects the shared mechanics that distinguish these actions from one another. For example, the most misclassifications occurred between dribbling actions of differing cut angle on the same side. These movements are differentiated primarily by cutting magnitude rather than gross body position, which likely makes them more difficult to separate using window-based kinematic features.

These findings align with prior work highlighting the challenges of translating laboratory-trained classifiers to realistic, continuous movement contexts. Stoeve et al.,[52] demonstrated that an SVM originally developed to distinguish two laboratory-based kicking techniques (pass vs. shot) performed poorly when expanded to a more realistic three-class problem incorporating non-kicking ("null") movements across 38 field sessions and 143 laboratory sessions. Although the original model achieved sensitivities exceeding 95% under tightly controlled laboratory conditions, classification performance for passes and shots declined markedly to 21.7% and 38.8%, respectively, once the extra “null” movement was introduced. This resulted in poor recognition of soccer actions and over-prediction of the “null” class, when the SVM trained on only laboratory data was evaluated using a sliding-window approach and real-time conditions. Moreover, Alobaid and Ramaswamy,[51] reported that a three-model, collaborative approach reached 84% classification accuracy when identifying five fundamental soccer actions (shooting, passing, heading, running, and dribbling) from IMU accelerometer data. Although the goal of this study was to recognize soccer moves in real-time, it remains unclear whether their data was collected during continuous soccer activity or under controlled conditions, which limits the direct comparability of their reported accuracy to the present sliding-window evaluation. On the other hand, Aoyagi et al.,[50] reported that an SVM achieved a macro-averaged F1-score of 0.84 when classifying a limited set of controlled soccer activities performed in sequence

using accelerometer data. F1-scores approached 90% for dribbling, passing, and shooting, but introducing additional non-skill movement classes of “Running” and “Others” reduced overall model performance by approximately 10%.

Notably, the studies evaluated considerably smaller sets of soccer actions than the 20 movements assessed here. While the present study achieved a task accuracy of 72%, some degree of performance reduction relative to these smaller-scale studies may be expected given the greater number of classes, particularly when several share overlapping kinematic characteristics, as observed between dribbling angles and receiving techniques in the present dataset. Furthermore, introducing an Other class did not produce as drastic a reduction in performance as previously reported.[52] Instead, the present classifier retained comparatively strong task classification. Viewed in this light, the present model's overall performance represents a reasonably robust outcome given the substantially greater movement diversity being discriminated.

Nonetheless, the reduction in performance observed when applying the present XGBoost classifier to continuous sliding-window data, relative to its performance on segmented training examples, highlights the challenge of generalizing feature-based classifiers beyond controlled movement trials. Models achieving high accuracy using segmented, well-defined movement examples during training will likely encounter difficulty when exposed to the greater variability and non-target activity present in unconstrained soccer environments. Addressing this gap will require comprehensive datasets collected directly during realistic training and match scenarios, thus exposing the classifier to the transitional movements and non-target activities encountered in real-world soccer. While further validation in training and match environments is required, these findings support the potential application of the model as a tool for quantifying exposure to soccer-specific movements associated with hip joint positions implicated in cam FAIS.

5.3 Limitations

Several limitations should be acknowledged when interpreting the results of this study. First, the participant cohort consisted of 20 elite-level adult soccer players. While consistent and technically proficient movement execution is desirable for between-system validation and ML model development, the relatively small cohort may limit representation of the broader movement variability present within the youth soccer population, which represents the target population for cam FAIS-related research. As such, the findings may not directly translate to

youth populations, for which differences in physical development, movement strategies, or training exposure may influence IMU-derived kinematics. External validation in adolescent soccer populations will therefore be required to establish whether the developed movement classification framework is transferable to the population in which cam morphology and FAIS-related screening applications are ultimately intended.

Similarly, the single-session laboratory protocol may not capture the full complexity of soccer-specific movement performed during training and match play. However, the controlled protocol was intentionally designed as an initial validation step to enable accurate identification and isolation of predefined movement classes before progressing towards more ecologically valid data collection. Crucially, the current protocol incorporated a larger series of soccer-specific movements than many previous IMU-based classification studies, providing an expanded foundation for future development of ML models capable of characterizing movement exposure in athletic populations. Future research should prioritize evaluation frameworks that better reflect natural sporting conditions, including continuous data collection during training and matchplay. Such assessment is important for determining whether IMU-derived kinematics and movement classification observed under controlled laboratory conditions are representative of data collected during actual soccer participation, where differences in playing surface, environmental conditions, and unrestricted motion may alter movement strategies or sensor behaviour.

The experimental protocol may also have been influenced by the fixed sequencing of movement tasks within the single session. Fatigue, learning or familiarization effects, and potential temporal changes in sensor orientation or position estimation could have influenced the kinematic characteristics of later trials. Although participants were physically fit and healthy, and substantial fatigue was therefore not expected to meaningfully affect performance, fatigue-related changes in movement execution cannot be completely excluded. Similarly, the Xsens IMUs' XKF3-hm sensor fusion algorithm is designed to compensate for sensor drift, thereby limiting the increasing orientation or position error over time.[45,136] Nevertheless, small temporal changes in sensor orientation estimation may persist and could potentially have influenced later trials. Since movement tasks were performed in a fixed sequence, these effects could have been associated with specific movement classes, and so randomizing task order across participants could provide a stronger approach for minimizing these potential effects.

Although the cohort was sex-balanced, neither validation nor classification performance was evaluated separately by sex. Therefore, potential differences in movement strategies, or anthropometric characteristics, between male and female athletes were not assessed. While cam morphology and FAIS have historically been reported more frequently in male athletes, increasing participation of female athletes in high-impact sports highlights the need to understand whether movement-based assessments generalize across sexes. This is particularly relevant given the rapid growth of women's participation in traditionally male-dominated sporting environments in North America alone, including professional ice hockey, basketball, and soccer, where exposure to high-intensity, high-impact movement patterns associated with cam morphology development may also occur. It is recommended that sex-specific models are assessed in subsequent work to ensure that emerging IMU-based approaches are applicable across diverse athletic populations.

An additional consideration is that agreement between systems was assessed using ROM, rather than discrete peak joint angles. While ROM provides useful information about the overall excursion achieved during a movement and was therefore appropriate for assessing whether Xsens and OMC captured similar movement magnitudes, it does not describe the specific joint position reached at any given point in a movement. However, reporting peak flexion, adduction, and internal rotation would provide complementary information regarding the maximum hip positions reached during each movement. This may be more relevant to cam FAIS, as greater magnitudes of hip adduction and internal rotation during athletic movements requiring substantial hip flexion have been proposed to contribute to cam FAIS progression.[24] For example, transverse plane ROM may reflect greater movement in one direction, such as external rotation, which may be less informative than peak internal rotation when considering combined hip positions associated with cam FAIS. Although peak data were recorded in the present study, they were not included in the primary analysis, as ROM was selected to provide a trial-level measure of overall movement excursion for the initial IMU validation. Nevertheless, follow-up analyses should consider peak flexion, adduction, and internal rotation alongside ROM to provide a more complete characterization of movement exposure relevant to cam FAIS progression.

A further limitation relates to the proprietary nature of the Xsens MTw Awinda IMU system. As described by Roetenberg et al.,[136] these IMUs use Xsens' proprietary XKF3-hm sensor fusion algorithm, which is specifically designed for human movement applications to provide accurate estimates of 3D three-dimensional sensor orientation. However, the specific

procedures and assumptions underlying its implementation are not fully accessible to researchers, and aspects of the system's calibration and biomechanical modelling procedures are similarly inaccessible.[133] Consequently, the contribution of individual processing steps to the observed offsets between Xsens and OMC are difficult to isolate. Differences in calibration procedures, sensor-to-segment alignment, and biomechanical model definitions may contribute to between-system discrepancies observed in the present study. Future studies comparing IMU and OMC systems could therefore benefit from evaluating alternative calibration approaches and standardized sensor-to-segment alignment procedures to determine whether agreement can be improved, particularly in the transverse plane.

Several technical considerations may also have influenced the systematic differences observed between measurement tools. Although segment orientations are represented using quaternions within the Xsens system, joint angles are subsequently extracted using an Euler angle decomposition.[136,137] Because different Euler decomposition sequences can yield different representations of the same underlying 3D segment rotation, the choice of sequence may influence the resulting joint angle estimates and, subsequently, between-system agreement. Certain Euler angle representations may also be susceptible to mathematical singularities, such as gimbal lock, depending on the selected rotation sequence, which can result in a loss of one degree of rotational freedom.[45] The present study did not evaluate the sensitivity of the results to alternative Euler angle rotation decompositions and instead extracted hip joint angles from the quaternion-derived segment orientations using the same rotation sequence applied to the OMC data, thereby standardizing the angle decomposition across systems. Nevertheless, future research could investigate whether alternative rotation sequences or orientation representations influence agreement, particularly for transverse plane motion, where the greatest between-system differences were observed.

Additionally, the seven-sensor configuration used in the present study, while appropriate for laboratory-based whole-body kinematic assessment, is relatively cumbersome for field-based application. The full configuration was required to generate the lower-body model within Xsens MVN Analyze Pro (v2021.0.1, Xsens Technologies B.V., Enschede, The Netherlands); however, not all sensors were necessary for the specific outcomes evaluated in this study. A practical implementation for continuous monitoring during soccer training and match play would likely require a reduced sensor configuration so as not to impede a player's physical or technical execution. Importantly, a streamlined sensor configuration may be feasible, given that hip joint angle estimation required only the pelvis and thigh sensors,

while thigh-derived IMU signals were sufficient for the classification of movements associated with potentially provocative hip positions in the current study. Research efforts should aim to determine an unobtrusive approach for securing a reduced sensor configuration to an athlete during soccer participation while maintaining reliable kinematic estimation and movement classification, thereby improving the practicality of field-based monitoring. For example, a novel smart sensor garment incorporating integrated IMUs has been developed to monitor lower-limb kinematics during daily training activities,[142] providing an example of a potential solution for securing IMUs during athletic activity without interfering with movement.

The ±0.25 s window used to identify simultaneous hip flexion, adduction, and internal rotation was developed specifically for the present study, as no established window for evaluating the co-occurrence of these motions during dynamic tasks was identified in the literature. Although this window provided a consistent approach for movement selection, its study-specific nature may limit the reproducibility and generalizability of the movement selection process. The extent to which a wider or narrower temporal window would alter movement selection, without including movements in which the three motions are insufficiently aligned to represent provocative cam FAIS hip positions, remains unclear. Future work should evaluate the appropriateness of this temporal window across different movement tasks and populations and, if appropriate, refine this window to better identify concurrent hip motion in all three planes.

Finally, the classifier was trained using isolated, peak-centred repetitions but evaluated on continuous sliding-window data. Consequently, the model was not exposed to partial movement data or transitions between actions, which likely contributed to reduced discrimination between actions with shared kinematic features during continuous classification. Moreover, the relatively small number of participants may also have limited the variability available for model training, despite the multiple repetitions collected from each participant. Although repeated trials from the same participant increase the number of training observations, they do not provide the same diversity as additional participants, particularly with respet to between-athlete differences in movement strategies. Future studies should investigate training models directly on continuous movement data obtained from a larger cohort, which may improve recognition of movement transitions and enhance classification between closely related soccer actions experienced during unrestricted play. Rather than requiring model development from scratch, the feature extraction and

classification pipeline presented here may serve as a viable starting point for this work. For example, features could be extracted from sliding windows using the same signal-processing approach applied here, rather than clean, segmented repetitions, with the existing XGBoost classifier then fine-tuned on this continuous data.

5.4 Conclusions

Together, these findings demonstrate the potential for wearable IMUs to support field-based assessment of the soccer-specific movements most relevant to cam FAIS. The IMU system provided valid estimates of sagittal (flexion/extension) and frontal (adduction/abduction) plane hip kinematics, which contribute to the provocative hip positions associated with symptomatic cam FAIS, across a comprehensive range of soccer-specific actions. Internal/external rotation in the transverse plane remained comparatively less accurate, highlighting a technical limitation that should be addressed before wearable setups can fully characterize the 3D hip joint exposures associated with cam FAIS risk in high-impact youth sports. Nonetheless, this does not preclude the potential use of IMUs to track exposure to soccer-specific movements associated with potentially provocative hip positions identified first through OMC.

The ML classifier's ability to accurately distinguish 20 distinct soccer movements, selected specifically for their relevance to cam FAIS through combined hip flexion, adduction, and internal rotation, represents a substantial advancement over the smaller movement sets used in prior soccer classification work. Although classification performance declined when the model was evaluated under continuous, sliding-window conditions, misclassifications were concentrated among movements sharing overlapping hip joint kinematics rather than being distributed across categories, suggesting that the extracted feature set retained discriminative capacity even under more ecologically valid testing conditions.

The combination of wearable IMUs with ML classification explored here demonstrated the feasibility of a framework to quantify and monitor sport-specific hip kinematics associated with cam FAIS risk in youth soccer athletes. Future work should focus on refining transverse plane measurement accuracy achieved by IMUs, training classifiers on continuous movement data collected during unconstrained soccer participation, and assessing validity in youth and sex-specific cohorts before application in its intended adolescent populations. Given that many of the movements assessed here are also performed frequently

in other high-impact sports with similar hip joint demands, such as ice hockey and basketball, this approach may extend beyond soccer and support movement exposure monitoring across a broader range of athletic populations at risk of cam morphology development and FAIS-related hip pathology. Ultimately, this framework represents an important step toward quantifying how frequently youth athletes are exposed to the 3D hip kinematics associated with cam FAIS during high-impact sport participation, which has previously remained difficult to measure outside controlled laboratory settings.

Since cam FAIS is posited as a precursor to premature hip OA, particularly in former elite athletes,[2–4,19]tools capable of quantifying mechanical hip exposure during youth sport may also help to support earlier identification of at-risk athletes and more timely intervention, before irreversible cartilage and labral damage accumulate. In this way, the approach developed here contributes not only to characterizing cam FAIS-related movement risk, but to the broader goal of reducing the burden of hip OA in physically active populations.

References

1. Public Health Agency of Canada. *Osteoarthritis in Canada*. 2020. Accessed February 6, 2026. https://www.canada.ca/en/public-health/services/publications/diseases-conditions/osteoarthritis.html

2. Vigdorchik JM, Nepple JJ, Eftekhary N, Leunig M, Clohisy JC. What Is the Association of Elite Sporting Activities with the Development of Hip Osteoarthritis? *American Journal of Sports Medicine*. *SAGE Publications Inc.* 2017;45(4):961-964. doi:10.1177/0363546516656359

3. Agricola R, Heijboer MP, Bierma-Zeinstra SMA, Verhaar JAN, Weinans H, Waarsing JH. Cam impingement causes osteoarthritis of the hip: a nationwide prospective cohort study (CHECK). *Ann Rheum Dis*. 2013;72:918-923. doi:10.1136/annrheumdis-2011-201643

4. Agricola R, Van Buuren MMA, Kemp JL, Weinans H, Runhaar J, Bierma-Zeinstra SMA. Femoroacetabular impingement syndrome in middle-aged individuals is strongly associated with the development of hip osteoarthritis within 10-year follow-up: a prospective cohort study (CHECK). *Br J Sports Med*. Published online September 9, 2024. doi:10.1136/bjsports-2024-108222

5. Siebenrock KA, Behning A, Mamisch TC, Schwab JM. Growth plate alteration precedes cam-type deformity in elite basketball players hip. *Clin Orthop Relat Res*. 2013;471(4):1084-1091. doi:10.1007/s11999-012-2740-6

6. Ganz R, Leunig M, Leunig-Ganz K, Harris WH. The etiology of osteoarthritis of the hip: An integrated mechanical concept. In: *Clinical Orthopaedics and Related Research*. Vol 466. Springer New York; 2008:264-272. doi:10.1007/s11999-007-0060-z

7. Nepple JJ, Vigdorchik JM, Clohisy JC. What is the association between sports participation and the development of proximal femoral cam deformity? *American Journal of Sports Medicine*. 2015;43(11):2833-2840. doi:10.1177/0363546514563909

8. Ganz R, Parvizi J, Beck M, Leunig M, Nötzli H, Siebenrock KA. Femoroacetabular Impingement: A Cause for Osteoarthritis of the Hip. In: *Clinical Orthopaedics and Related Research*. Vol 417. Lippincott Williams and Wilkins; 2003:112-120. doi:10.1097/01.blo.0000096804.78689.c2

9. Thomas Byrd JW. Femoroacetabular impingement in athletes, part 1: Cause and assessment. *Sports Health*. 2010;2(4):321-333. doi:10.1177/1941738110368392

10. Griffin DR, Dickenson EJ, O'Donnell J, et al. The Warwick Agreement on femoroacetabular impingement syndrome (FAI syndrome): An international consensus statement. *Br J Sports Med*. 2016;50(19):1169-1176. doi:10.1136/bjsports-2016-096743

11. Beck M, Kalhor M, Leunig M, Ganz R, Surgeon O, Fellow V. Hip morphology influences the pattern of damage to the acetabular cartilage FEMOROACETABULAR IMPINGEMENT AS A CAUSE OF EARLY OSTEOARTHRITIS OF THE HIP Patients and Methods. *J Bone Joint Surg*. Published online 2005. doi:10.1302/0301-620X.87B7

12. Kuhns BD, Weber AE, Levy DM, Wuerz TH. The Natural History of Femoroacetabular Impingement. *Front Surg*. *Frontiers Media S.A.* 2015;2. doi:10.3389/fsurg.2015.00058

13. Fortier LM, Popovsky D, Durci MM, Norwood H, Sherman WF, Kaye AD. An Updated Review of Femoroacetabular Impingement Syndrome. *Orthop Rev (Pavia)*. 2022;14(3). doi:10.52965/001C.37513

14. Leunig M, Ganz R. Femoroacetabular Impingement: A common cause of hip complaints leading to osteoarthritis. *Unfallchirurg*. 2005;108(1):9-17. doi:10.1007/s00113-004-0902-z

15. Smith HE, Spiker AM. Sex-Based Differences Femoroacetabular Impingement and Hip Arthroscopy. *Curr Rev Musculoskelet Med*. *Springer*. 2025;18(12):577-584. doi:10.1007/s12178-025-09988-1

16. Gosvig KK, Jacobsen S, Sonne-Holm S, Palm H, Troelsen A. Prevalence of malformations of the hip joint and their relationship to sex, groin pain, and risk of osteoarthritis: A population-based survey. *Journal of Bone and Joint Surgery*. 2010;92(5):1162-1169. doi:10.2106/JBJS.H.01674

17. Lievense AM, Bierma-Zeinstra SMA, Verhagen AP, Bernsen RMD, Verhaar JAN, Koes BW. Influence of sporting activities on the development of osteoarthritis of the hip: A systematic review. *Arthritis Care Res (Hoboken)*. *John Wiley and Sons Inc.* 2003;49(2):228-236. doi:10.1002/art.11012

18. Westermann RW, Scott EJ, Schaver AL, et al. Activity Level and Sport Type in Adolescents Correlate with the Development of Cam Morphology. *JBJS Open Access*. 2021;6(4). doi:10.2106/JBJS.OA.21.00059

19. Siebenrock KA, Ferner F, Noble PC, Santore RF, Werlen S, Mamisch TC. The cam-type deformity of the proximal femur arises in childhood in response to vigorous sporting activity. *Clin Orthop Relat Res*. 2011;469(11):3229-3240. doi:10.1007/s11999-011-1945-4

20. Tveit M, Rosengren BE, Nilsson JÅ, Karlsson MK. Former male elite athletes have a higher prevalence of osteoarthritis and arthroplasty in the hip and knee than expected. *American Journal of Sports Medicine*. 2012;40(3):527-533. doi:10.1177/0363546511429278

21. Murray RO, Duncan C. Athletic activity in adolescence as an etiological factor in degenerative hip disease. *J Bone Joint Surg*. 1971;53(3):406-419.

22. Frank JM, Harris JD, Erickson BJ, et al. Prevalence of femoroacetabular impingement imaging findings in asymptomatic volunteers: A systematic review. *Arthroscopy - Journal of Arthroscopic and Related Surgery*. *W.B. Saunders*. 2015;31(6):1199-1204. doi:10.1016/j.arthro.2014.11.042

23. Reichenbach S, Leunig M, Werlen S, et al. Association between cam-type deformities and magnetic resonance imaging-detected structural hip damage: A cross-sectional study in young men. *Arthritis Rheum*. 2011;63(12):4023-4030. doi:10.1002/art.30589

24. Weber AE, Park CS, Mayer EN, et al. *Perspective Pathomechanics Underlying Femoroacetabular Impingement Syndrome: Theoretical Framework to Inform Clinical Practice*. Vol 100. 2020. https://academic.oup.com/ptj

25. Bagwell JJ, Snibbe J, Gerhardt M, Powers CM. Hip kinematics and kinetics in persons with and without cam femoroacetabular impingement during a deep squat task. *Clinical Biomechanics*. 2016;31:87-92. doi:10.1016/j.clinbiomech.2015.09.016

26. Diamond LE, Bennell KL, Wrigley T V., Hinman RS, O'Donnell J, Hodges PW. Squatting Biomechanics in Individuals with Symptomatic Femoroacetabular Impingement. *Med Sci Sports Exerc*. 2017;49(8):1520-1529. doi:10.1249/MSS.0000000000001282

27. Fédération Internationale de Football Association. *FIFA Professional Football Report 2023*. 2024. Accessed May 15, 2026. https://inside.fifa.com/legal/news/fifa-publishes-professional-football-report-2023

28. Canadian Tire Jumpstart Charities. *State of Youth Sport in Canada: The Value and Cost of Participation*. 2025. Accessed May 14, 2026. https://jumpstart.canadiantire.ca/pages/research

29. Johnson AC, Shaman MA, Ryan TG. Femoroacetabular impingement in former high-level youth soccer players. *American Journal of Sports Medicine*. 2012;40(6):1342-1346. doi:10.1177/0363546512439287

30. Pfirrmann D, Herbst M, Ingelfinger P, Simon P, Tug S. Analysis of injury incidences in male professional adult and elite youth soccer players: A systematic review. *J Athl Train*. *National Athletic Trainers' Association Inc.* 2016;51(5):410-424. doi:10.4085/1062-6050-51.6.03

31. Carling C, Bloomfield J, Nelsen L, Reilly T. *The Role of Motion Analysis in Elite Soccer Contemporary Performance Measurement Techniques and Work Rate Data*. Vol 38. 2008.

32. Hoppe MW, Baumgart C, Polglaze T, Freiwald J. Validity and reliability of GPS and LPS for measuring distances covered and sprint mechanical properties in team sports. *PLoS One*. 2018;13(2). doi:10.1371/journal.pone.0192708

33. Shan G, Westerhoff P. Soccer: Full-body kinematic characteristics of the maximal instep Soccer kick by male soccer players and parameters related to kick quality. *Sports Biomech*. 2005;4(1):59-72. doi:10.1080/14763140508522852

34. Constantinou M, Loureiro A, Carty C, Mills P, Barrett R. Hip joint mechanics during walking in individuals with mild-to-moderate hip osteoarthritis. *Gait Posture*. 2017;53:162-167. doi:10.1016/j.gaitpost.2017.01.017

35. Benjaminse A, Bolt R, Gokeler A, Otten B. *A VALIDITY STUDY COMPARING XSENS WITH VICON*. https://commons.nmu.edu/isbs/vol38/iss1/190

36. Nijmeijer EM, Heuvelmans P, Bolt R, Gokeler A, Otten E, Benjaminse A. Concurrent validation of the Xsens IMU system of lower-body kinematics in jump-landing and change-of-direction tasks. *J Biomech*. 2023;154. doi:10.1016/j.jbiomech.2023.111637

37. Heuvelmans P, Benjaminse A, Bolt R, Baumeister J, Otten E, Gokeler A. Concurrent validation of the Noraxon MyoMotion wearable inertial sensors in change-of-direction and jump-landing tasks. *Sports Biomech*. 2025;24(2):184-199. doi:10.1080/14763141.2022.2093264

38. Al-Amri M, Nicholas K, Button K, Sparkes V, Sheeran L, Davies JL. Inertial measurement units for clinical movement analysis: Reliability and concurrent validity. *Sensors (Switzerland)*. 2018;18(3). doi:10.3390/s18030719

39. Blair S, Duthie G, Robertson S, Hopkins W, Ball K. Concurrent validation of an inertial measurement system to quantify kicking biomechanics in four football codes. *J Biomech*. 2018;73:24-32. doi:10.1016/j.jbiomech.2018.03.031

40. Dahl KD, Dunford KM, Wilson SA, Turnbull TL, Tashman S. Wearable sensor validation of sports-related movements for the lower extremity and trunk. *Med Eng Phys*. 2020;84:144-150. doi:10.1016/j.medengphy.2020.08.001

41. Teufl W, Miezal M, Taetz B, Fröhlich M, Bleser G. Validity, test-retest reliability and long-term stability of magnetometer free inertial sensor based 3D joint kinematics. *Sensors (Switzerland)*. 2018;18(7). doi:10.3390/s18071980

42. Paulich M, Schepers M, Rudigkeit N, Bellusci G. *Xsens MTw Awinda: Miniature Wireless Inertial-Magnetic Motion Tracker for Highly Accurate 3D Kinematic Applications*. www.xsens.com,

43. Poitras I, Dupuis F, Bielmann M, et al. Validity and reliability ofwearable sensors for joint angle estimation: A systematic review. *Sensors (Switzerland)*. *MDPI AG*. 2019;19(7). doi:10.3390/s19071555

44. Bastiaansen BJC, Wilmes E, Brink MS, et al. An inertial measurement unit based method to estimate hip and knee joint kinematics in team sport athletes on the field. *Journal of Visualized Experiments*. 2020;2020(159):1-8. doi:10.3791/60857

45. Schuldhaus D, Zwick C, Körger H, Dorschky E, Kirk R, Eskofier BM. *Inertial Sensor-Based Approach for Shot/Pass Classification During a Soccer Match*.

46. Lewis G, Towlson C, Roversi P, Domogalla C, Herrington L, Barrett S. Quantifying volume and high-speed technical actions of professional soccer players using foot-mounted inertial measurement units. *PLoS One*. 2022;17(2 February). doi:10.1371/journal.pone.0263518

47. Slim SO, Atia A, Elfattah MMA, Mostafa MSM. *Survey on Human Activity Recognition Based on Acceleration Data*. Vol 10. 2019. www.ijacsa.thesai.org

48. Cuesta-Vargas AI, Galán-Mercant A, Williams JM. The use of inertial sensors system for human motion analysis. *Physical Therapy Reviews*. *Taylor and Francis Ltd.* 2010;15(6):462-473. doi:10.1179/1743288X11Y.0000000006

49. Camomilla V, Bergamini E, Fantozzi S, Vannozzi G. Trends supporting the in-field use of wearable inertial sensors for sport performance evaluation: A systematic review. *Sensors (Switzerland)*. *MDPI AG*. 2018;18(3). doi:10.3390/s18030873

50. Aoyagi H, Hossain T, Yokokubo A, Lopez G. Footb Sense: Soccer Moves in Practice Environment Identification Usinga Single IMU. In: *Human Activity and Behavior Analysis: Advances in Computer Vision and Sensors: Volume 2*. CRC Press; 2024:249-266. doi:10.1201/9781032636054-16

51. Alobaid O, Ramaswamy L. A feature-based approach for identifying soccer moves using an accelerometer sensor. In: *HEALTHINF 2020 - 13th International Conference on Health Informatics, Proceedings; Part of 13th International Joint Conference on Biomedical Engineering Systems and Technologies, BIOSTEC 2020*. SciTePress; 2020:34-44. doi:10.5220/0008910400340044

52. Stoeve M, Schuldhaus D, Gamp A, Zwick C, Eskofier BM. From the laboratory to the field: Imu-based shot and pass detection in football training and game scenarios using deep learning. *Sensors*. 2021;21(9). doi:10.3390/s21093071

53. Anderson LC, Blake DJ. The Anatomy and Biomechanics of the Hip Joint. *J Back Musculoskelet Rehabil*. 1994;4(3):145-153. doi:10.3233/BMR-1994-4305

54. Harty M, Brock, Lord. *The Anatomy of the Hip Joint*.

55. El-Radi MA, Marin-Peña OR, Said HG, Tey-Pons M. Basics in hip chondrolabral lesions and state of the art. *SICOT J*. *EDP Sciences*. 2017;3. doi:10.1051/sicotj/2017040

56. Agricola R, Bessems JHJM, Ginai AZ, et al. The development of cam-type deformity in adolescent and young male soccer players. *American Journal of Sports Medicine*. 2012;40(5):1099-1106. doi:10.1177/0363546512438381

57. Claes PAM, Hanff DF, Weir A, et al. The Association Between the Development of Cam Morphology During Skeletal Growth in High-Impact Athletes and the Presence

of Cartilage Loss and Labral Damage in Adulthood: A Prospective Cohort Study With a 12-Year Follow-up. *American Journal of Sports Medicine*. Published online 2024. doi:10.1177/03635465241256123

58. Sankar WN, Nevitt M, Parvizi J, Felson DT, Agricola R, Leunig M. Femoroacetabular impingement: Defining the condition and its role in the pathophysiology of osteoarthritis. In: *Journal of the American Academy of Orthopaedic Surgeons*. Vol 21. 2013. doi:10.5435/JAAOS-21-07-S7

59. Beall DP, Sweet CF, Martin HD, et al. Imaging findings of femoroacetabular impingement syndrome. *Skeletal Radiol*. 2005;34(11):691-701. doi:10.1007/s00256-005-0932-9

60. Schuring LL, Mozingo JD, Lenz AL, et al. Acetabular labrum and cartilage contact mechanics during pivoting and walking tasks in individuals with cam femoroacetabular impingement syndrome. *J Biomech*. 2023;146. doi:10.1016/j.jbiomech.2022.111424

61. Grant AD, Sala DA, Davidovitch RI. The labrum: Structure, function, and injury with femoro-acetabular impingement. *J Child Orthop*. *Springer Verlag*. 2012;6(5):357-372. doi:10.1007/s11832-012-0431-1

62. Clohisy JC, Baca G, Beaulé PE, et al. Descriptive epidemiology of femoroacetabular impingement: A North American Cohort of patients undergoing surgery. *American Journal of Sports Medicine*. 2013;41(6):1348-1356. doi:10.1177/0363546513488861

63. Tannast M, Siebenrock KA, Anderson SE. Femoroacetabular impingement: Radiographic diagnosis - What the radiologist should know. *American Journal of Roentgenology*. 2007;188(6):1540-1552. doi:10.2214/AJR.06.0921

64. Shanmugaraj A, Shell JR, Horner NS, et al. How Useful Is the Flexion-Adduction-Internal Rotation Test for Diagnosing Femoroacetabular Impingement: A Systematic Review. *Clin J Sport Med*. 2020;30(1):76-82. doi:10.1097/JSM.0000000000000575

65. Hananouchi T, Yasui Y, Yamamoto K, Toritsuka Y, Ohzono K. Anterior impingement test for labral lesions has high positive predictive value. *Clin Orthop Relat Res*. 2012;470(12):3524-3529. doi:10.1007/s11999-012-2450-0

66. Barton C, Salineros MJ, Rakhra KS, Beaulé PE. Validity of the alpha angle measurement on plain radiographs in the evaluation of cam-type femoroacetabular

impingement. In: *Clinical Orthopaedics and Related Research*. Vol 469. Springer New York LLC; 2011:464-469. doi:10.1007/s11999-010-1624-x

67. Nötzli HP, Schmid MR, Member S, et al. *The Contour of the Femoral Head-Neck Junction as a Predictor for the Risk of Anterior Impingement*. Vol 84. 2002.

68. Ekhtiari S, Fairhurst O, Mainwaring L, Khanduja V. Current Concepts Review The Alpha Angle. *Journal of Bone and Joint Surgery*. *Lippincott Williams and Wilkins*. 2024;106(20):1910-1921. doi:10.2106/JBJS.23.01089

69. Sutter R, Dietrich TJ, Zingg PO, Pfirrmann CWA. How useful is the alpha angle for discriminating between symptomatic patients with cam-type femoroacetabular impingement and asymptomatic volunteers? *Radiology*. 2012;264(2):514-521. doi:10.1148/radiol.12112479

70. Laborie LB, Lehmann TG, Engesæter I, Eastwood DM, Engesæter LB, Rosendahl K. Prevalence of radiographic findings thought to be associated with femoroacetabular impingement in a population-based cohort of 2081 healthy young adults. *Radiology*. 2011;260(2):494-502. doi:10.1148/radiol.11102354

71. Zhou J, Melugin HP, Hale RF, et al. Sex differences in the prevalence of radiographic findings of structural hip deformities in patients with symptomatic femoroacetabular impingement. *J Hip Preserv Surg*. 2022;8(3):233-239. doi:10.1093/jhps/hnab050

72. Tsitskaris K, Sharif K, Meacock LM, et al. The prevalence of cam-type femoroacetabular morphology in young adults and its effect on functional hip scores. *HIP International*. 2012;22(1):68-74. doi:10.5301/HIP.2012.9074

73. Hack K, Di Primio G, Rakhra K, Beaulé PE. Prevalence of cam-type femoroacetabular impingement morphology in asymptomatic volunteers. *Journal of Bone and Joint Surgery*. 2010;92(14):2436-2444. doi:10.2106/JBJS.J.01280

74. Nepple JJ, Riggs CN, Ross JR, Clohisy JC. Clinical presentation and disease characteristics of femoroacetabular impingement are sex-dependent. *Journal of Bone and Joint Surgery - American Volume*. 2014;96(20):1683-1689. doi:10.2106/JBJS.M.01320

75. Clohisy JC, Knaus ER, Hunt DM, Lesher JM, Harris-Hayes M, Prather H. Clinical presentation of patients with symptomatic anterior hip impingement. In: *Clinical*

Orthopaedics and Related Research. Vol 467. Springer New York; 2009:638-644. doi:10.1007/s11999-008-0680-y

76. Stephen R, Burnett J, Rocca GJ Della, et al. *Clinical Presentation of Patients with Tears of the Acetabular Labrum*. 2006. www.aaos.org,

77. Kahlenberg CA, Han B, Patel RM, Deshmane PP, Terry MA. Time and cost of diagnosis for symptomatic femoroacetabular impingement. *Orthop J Sports Med*. 2014;2(3). doi:10.1177/2325967114523916

78. Van Klij P, Heerey J, Waarsing JH, Agricola R. The prevalence of cam and pincer morphology and its association with development of hip osteoarthritis. *Journal of Orthopaedic and Sports Physical Therapy*. *Movement Science Media*. 2018;48(4):230-238. doi:10.2519/jospt.2018.7816

79. Ganz R, Gill TJ, Gautier E, Ganz K, Krügel N, Berlemann U. *Surgical Dislocation of the Adult Hip A TECHNIQUE WITH FULL ACCESS TO THE FEMORAL HEAD AND ACETABULUM WITHOUT THE RISK OF AVASCULAR NECROSIS*. Vol 83. 2001.

80. Chaudhry H, Ayeni OR. The Etiology of Femoroacetabular Impingement: What We Know and What We Don't. *Sports Health*. 2014;6(2):157-161. doi:10.1177/1941738114521576

81. Packer JD, Safran MR. The etiology of primary femoroacetabular impingement: genetics or acquired deformity? *J Hip Preserv Surg*. 2015;2(3):249-257. doi:10.1093/jhps/hnv046

82. Pollard TCB, Villar RN, Norton MR, et al. Genetic influences in the aetiology of femoroacetabular impingement A SIBLING STUDY. *J Bone Joint Surg [Br]*. 2010;92(2):92-209. doi:10.1302/0301-620X.92B2

83. O'Rourke RJ, El Bitar Y. Femoroacetabular Impingement. In: *StatPearls*. StatPearls Publishing; 2023. Accessed April 7, 2026. https://www.ncbi.nlm.nih.gov/books/NBK547699/

84. Klit J, Gosvig K, Magnussen E, et al. Cam deformity and hip degeneration are common after fixation of a slipped capital femoral epiphysis. *Acta Orthop*. 2014;85(6):585-591. doi:10.3109/17453674.2014.957078

85. Siebenrock KA, Schwab JM. *The Cam-Type Deformity-What Is It: SCFE, Osteophyte, or a New Disease?* 2013. www.pedorthopaedics.com

86. Accadbled F, Pailhé R, Launay F, Nectoux E, Bonin N, Gicquel P. "Femoroacetabular impingement". Legg-Calve-Perthes disease: From childhood to adulthood. *Orthopaedics and Traumatology: Surgery and Research*. 2014;100(6):647-649. doi:10.1016/j.otsr.2014.03.029

87. Tannast M, Hanke M, Ecker TM, Murphy SB, Albers CE, Puls M. LCPD: Reduced range of motion resulting from extra- and intraarticular impingement hip. In: *Clinical Orthopaedics and Related Research*. Vol 470. Springer New York LLC; 2012:2431-2440. doi:10.1007/s11999-012-2344-1

88. Drawer S, Fuller CW. Propensity for osteoarthritis and lower limb joint pain in retired professional soccer players. Published online 2001.

89. Carton PF, Filan DJ. The clinical presentation, diagnosis and pathogenesis of symptomatic sports-related femoroacetabular impingement (SRFAI) in a consecutive series of 1021 athletic hips. *HIP International*. 2019;29(6):665-673. doi:10.1177/1120700018825430

90. Nepple JJ, Vigdorchik JM, Clohisy JC. What is the association between sports participation and the development of proximal femoral cam deformity? *American Journal of Sports Medicine*. 2015;43(11):2833-2840. doi:10.1177/0363546514563909

91. Lerebours F, Robertson W, Neri B, Schulz B, Youm T, Limpisvasti O. Prevalence of Cam-Type Morphology in Elite Ice Hockey Players. *American Journal of Sports Medicine*. 2016;44(4):1024-1030. doi:10.1177/0363546515624671

92. Philippon MJ, Ho CP, Briggs KK, Stull J, Laprade RF. Prevalence of increased alpha angles as a measure of cam-type femoroacetabular impingement in youth ice hockey players. *American Journal of Sports Medicine*. 2013;41(6):1357-1362. doi:10.1177/0363546513483448

93. Ayeni OR, Banga K, Bhandari M, et al. Femoroacetabular impingement in elite ice hockey players. *Knee Surgery, Sports Traumatology, Arthroscopy*. 2014;22(4):920-925. doi:10.1007/s00167-013-2598-5

94. King MG, Lawrenson PR, Semciw AI, Middleton KJ, Crossley KM. Lower limb biomechanics in femoroacetabular impingement syndrome: A systematic review and

meta-analysis. *Br J Sports Med*. *BMJ Publishing Group*. 2018;52(9):566-580. doi:10.1136/bjsports-2017-097839

95. Stull JD, Philippon MJ, Laprade RF. "at-Risk" Positioning and Hip Biomechanics of the Peewee Ice Hockey Sprint Start. *American Journal of Sports Medicine*. 2011;39(1_suppl):29S-35S. doi:10.1177/0363546511414012

96. Philippon MJ, Ho CP, Briggs KK, Stull J, Laprade RF. Prevalence of increased alpha angles as a measure of cam-type femoroacetabular impingement in youth ice hockey players. *American Journal of Sports Medicine*. 2013;41(6):1357-1362. doi:10.1177/0363546513483448

97. Siebenrock KA, Kaschka I, Frauchiger L, Werlen S, Schwab JM. Prevalence of cam-type deformity and hip pain in elite ice hockey players before and after the end of growth. *American Journal of Sports Medicine*. 2013;41(10):2308-2313. doi:10.1177/0363546513497564

98. Hanke MS, Schmaranzer F, Steppacher SD, Reichenbach S, Werlen SF, Siebenrock KA. A Cam Morphology Develops in the Early Phase of the Final Growth Spurt in Adolescent Ice Hockey Players: Results of a Prospective MRI-based Study. In: *Clinical Orthopaedics and Related Research*. Vol 479. Wolters Kluwer Health Inc; 2021:906-918. doi:10.1097/CORR.0000000000001603

99. Kellis E, Katis A. *Biomechanical Characteristics and Determinants of Instep Soccer Kick*. Vol 6. 2007. http://www.jssm.org

100. Tak I, Weir A, Langhout R, et al. The relationship between the frequency of football practice during skeletal growth and the presence of a cam deformity in adult elite football players. *Br J Sports Med*. 2015;49(9):630-634. doi:10.1136/bjsports-2014-094130

101. Gerhardt MB, Romero AA, Silvers HJ, Harris DJ, Watanabe D, Mandelbaum BR. The prevalence of radiographic hip abnormalities in elite soccer players. *American Journal of Sports Medicine*. 2012;40(3):584-588. doi:10.1177/0363546511432711

102. Bourne MN, Williams M, Jackson J, Williams KL, Timmins RG, Pizzari T. Preseason hip/groin strength and Hagos scores are associated with subsequent injury in professional Male soccer players. *Journal of Orthopaedic and Sports Physical Therapy*. 2020;50(5):234-242. doi:10.2519/jospt.2020.9022

103. Agricola R, Heijboer MP, Ginai AZ, et al. A cam deformity is gradually acquired during skeletal maturation in adolescent and young male soccer players: A prospective study with minimum 2-year follow-up. *American Journal of Sports Medicine*. 2014;42(4):798-806. doi:10.1177/0363546514524364

104. Ng VY, Ellis TJ. More than just a bump: Cam-type femoroacetabular impingement and the evolution of the femoral neck. *HIP International*. 2011;21(1):1-8. doi:10.5301/HIP.2011.6288

105. Roels P, Agricola R, Oei EH, Weinans H, Campoli G, Zadpoor AA. Mechanical factors explain development of cam-type deformity. *Osteoarthritis Cartilage*. 2014;22(12):2074-2082. doi:10.1016/j.joca.2014.09.011

106. Ng KCG, Rouhi G, Lamontagne M, Beaulé PE. Finite Element Analysis Examining the Effects of Cam FAI on Hip Joint Mechanical Loading Using Subject-Specific Geometries During Standing and Maximum Squat. *HSS Journal*. 2012;8(3):206-212. doi:10.1007/s11420-012-9292-x

107. Jorge JP, Simões FMF, Pires EB, et al. Finite element simulations of a hip joint with femoroacetabular impingement. *Comput Methods Biomech Biomed Engin*. 2014;17(11):1275-1284. doi:10.1080/10255842.2012.744398

108. Carson WG, Gasser SI. *Little Leaguer's Shoulder A Report of 23 Cases**. 1998.

109. Adams JE, Bernardino S. *Little League Shoulder Osteochondrosis of the Proximal Humeral Epiphysis in Boy Baseball Pitchers*.

110. Siebenrock KA, Wahab KHA, Werlen S, Kalhor M, Leunig M, Ganz R. Abnormal Extension of the Femoral Head Epiphysis as a Cause of Cam Impingement. *Clin Orthop Relat Res*. 2004;418:54-60. doi:10.1097/00003086-200401000-00010

111. Palmer A, Fernquest S, Gimpel M, et al. Physical activity during adolescence and the development of cam morphology: A cross-sectional cohort study of 210 individuals. *Br J Sports Med*. 2018;52(9):601-610. doi:10.1136/bjsports-2017-097626

112. Carter DR. *MECHANICAL LOADING HISTORY AND SKELETAL BIOLOGY*.

113. Zhang X, Shan G, Liu F, Yang S, Meng M. Diversity of scoring, ingenuity of striking, art of flying ' conceptual and systematical identification of soccer scoring techniques. *Physical Activity Review*. 2021;9(1):79-92. doi:10.16926/par.2021.09.10

114. Carpels T, Scobie N, Macfarlane NG, Kemi OJ. *Youth-to-Senior Transition in Elite European Club Soccer*. Vol 14. 2021. http://www.intjexersci.com

115. Kunz M. FIFA Big Count 2006: 270 million people active in football. *FIFA Magazine*. Published online July 2007:10-15. Accessed July 30, 2026. https://condorperformance.com/wp-content/uploads/2020/02/emaga_9384_10704.pdf

116. Bush M, Barnes C, Archer DT, Hogg B, Bradley PS. Evolution of match performance parameters for various playing positions in the English Premier League. *Hum Mov Sci*. 2015;39:1-11. doi:10.1016/j.humov.2014.10.003

117. Bradley PS, Carling C, Gomez Diaz A, et al. Match performance and physical capacity of players in the top three competitive standards of English professional soccer. *Hum Mov Sci*. 2013;32(4):808-821. doi:10.1016/j.humov.2013.06.002

118. Bloomfield J, Polman R, O'Donoghue P. The 'Bloomfield Movement Classification': Motion Analysis of Individual Players in Dynamic Movement Sports. *Int J Perform Anal Sport*. 2004;4(2):20-31. doi:10.1080/24748668.2004.11868300

119. Falch HN, Rædergård HG, van den Tillaar R. Effect of Approach Distance and Change of Direction Angles Upon Step and Joint Kinematics, Peak Muscle Activation, and Change of Direction Performance. *Front Sports Act Living*. 2020;2. doi:10.3389/fspor.2020.594567

120. Li J, Qian H. Biomechanical effects of different change of direction angles on lower limb joint load and injury risk in soccer players. *Sci Rep*. 2025;15(1). doi:10.1038/s41598-025-33102-7

121. Bloomfield J, Polman R, O'donoghue P. *Physical Demands of Different Positions in FA Premier League Soccer*. Vol 6. 2007. http://www.jssm.org

122. Bradley PS, Carling C, Gomez Diaz A, et al. Match performance and physical capacity of players in the top three competitive standards of English professional soccer. *Hum Mov Sci*. 2013;32(4):808-821. doi:10.1016/j.humov.2013.06.002

123. Bradley PS, Lago-Peñas C, Rey E, Gomez Diaz A. The effect of high and low percentage ball possession on physical and technical profiles in English FA Premier League soccer matches. *J Sports Sci*. 2013;31(12):1261-1270. doi:10.1080/02640414.2013.786185

124. Merlin M, Pinto A, Moura FA, da Silva Torres R, Cunha SA. Who are the best passing players in professional soccer? A machine learning approach for classifying passes with different levels of difficulty and discriminating the best passing players. *PLoS One*. 2024;19(5 May). doi:10.1371/journal.pone.0304139

125. Levanon J, Dapena J. Comparison of the kinematics of the full-instep and pass kicks in soccer. *Med Sci Sports Exerc*. 1998;30(6):917-927. doi:10.1097/00005768-199806000-00022

126. Garcia JDC, Refoyo Román I, Calleja-González J, Dellal A. Quantification and analysis of offensive situations in different formats of sided games in soccer. *J Hum Kinet*. 2014;44(1):193-201. doi:10.2478/hukin-2014-0125

127. Katis A, Kellis E. *Effects of Small-Sided Games on Physical Conditioning and Performance in Young Soccer Players*. Vol 8. 2009. http://www.jssm.org

128. Fédération Internationale de Football Association. FIFA Grassroots Manual. *FIFA Education and Technical Development.* Preprint posted online 2012. Accessed July 31, 2026. https://cdn1.sportngin.com/attachments/document/8546-2348967/FIFA_grassroots_en.pdf

129. Rana M, Mittal V. Wearable Sensors for Real-Time Kinematics Analysis in Sports: A Review. *IEEE Sens J*. 2021;21(2):1187-1207. doi:10.1109/JSEN.2020.3019016

130. Adesida Y, Papi E, McGregor AH. Exploring the role of wearable technology in sport kinematics and kinetics: A systematic review. *Sensors (Switzerland)*. *MDPI AG*. 2019;19(7). doi:10.3390/s19071597

131. Linke D, Link D, Lames M. Validation of electronic performance and tracking systems EPTS under field conditions. *PLoS One*. 2018;13(7). doi:10.1371/journal.pone.0199519

132. Rico-González M, Los Arcos A, Clemente FM, Rojas-Valverde D, Pino-Ortega J. Accuracy and reliability of local positioning systems for measuring sport movement patterns in stadium-scale: A systematic review. *Applied Sciences (Switzerland)*. *MDPI AG*. 2020;10(17). doi:10.3390/app10175994

133. Adamowicz L, Gurchiek RD, Ferri J, Ursiny AT, Fiorentino N, McGinnis RS. Validation of novel relative orientation and inertial sensor-to-segment alignment

algorithms for estimating 3D hip joint angles. *Sensors (Switzerland)*. 2019;19(23). doi:10.3390/s19235143

134. Adlou B, Wilburn C, Weimar W. Motion Capture Technologies for Athletic Performance Enhancement and Injury Risk Assessment: A Review for Multi-Sport Organizations. *Sensors*. *Multidisciplinary Digital Publishing Institute (MDPI)*. 2025;25(14). doi:10.3390/s25144384

135. Di Paolo S, Nijmeijer E, Bragonzoni L, Dingshoff E, Gokeler A, Benjaminse A. Comparing lab and field agility kinematics in young talented female football players: Implications for ACL injury prevention. *Eur J Sport Sci*. 2023;23(5):859-868. doi:10.1080/17461391.2022.2064771

136. Roetenberg D, Luinge H, Slycke P. *Xsens MVN: Full 6DOF Human Motion Tracking Using Miniature Inertial Sensors*. Vol 8. 2009. www.xsens.com,

137. Schepers M, Giuberti M, Bellusci G. Xsens MVN: Consistent Tracking of Human Motion Using Inertial Sensing. Published online 2018. doi:10.13140/RG.2.2.22099.07205

138. Zhang JT, Novak AC, Brouwer B, Li Q. Concurrent validation of Xsens MVN measurement of lower limb joint angular kinematics. *Physiol Meas*. 2013;34(8). doi:10.1088/0967-3334/34/8/N63

139. Ferrari A, Cutti AG, Garofalo P, et al. First in vivo assessment of "outwalk": A novel protocol for clinical gait analysis based on inertial and magnetic sensors. *Med Biol Eng Comput*. 2010;48(1):1-15. doi:10.1007/s11517-009-0544-y

140. Stołowski Ł, Niedziela M, Lubiatowski B, Lubiatowski P, Piontek T. Validity and Reliability of Inertial Measurement Units in Active Range of Motion Assessment in the Hip Joint. *Sensors (Basel)*. 2023;23(21). doi:10.3390/s23218782

141. Myhill N, Weaving D, Robinson M, Barrett S, Emmonds S. Concurrent validity and between-unit reliability of a foot-mounted inertial measurement unit to measure velocity during team sport activity. *Science and Medicine in Football*. Published online 2023. doi:10.1080/24733938.2023.2237493

142. Steijlen A, Burgers B, Wilmes E, et al. Smart sensor tights: Movement tracking of the lower limbs in football. *Wearable Technologies*. 2021;2. doi:10.1017/wtc.2021.16

143. Vicon Motion Systems. Vicon Plug-in Gait Reference Guide. https://help.vicon.com/space/Nexus216/11607059/Plug-in+Gait+Reference+Guide. March 19, 2023.

144. *Vicon Motion Systems-in Gait Product Guide-Foundation Notes Revision 1.0 March 2008 For Use with Plug-in Gait Version 1.9 in Vicon Nexus*. 2008. http://www.vicon.com

145. Kluyver T, Ragan-Kelley B, Pérez F, et al. Jupyter Notebooks—a publishing format for reproducible computational workflows. In: *Positioning and Power in Academic Publishing: Players, Agents and Agendas - Proceedings of the 20th International Conference on Electronic Publishing, ELPUB 2016*. IOS Press BV; 2016:87-90. doi:10.3233/978-1-61499-649-1-87

146. Wang S, Pitts J, Purohit R, Shah H. The Influence of Motion Data Low-Pass Filtering Methods in Machine-Learning Models. *Applied Sciences (Switzerland)*. 2025;15(4). doi:10.3390/app15042177

147. Ferrari A, Cutti AG, Cappello A. A new formulation of the coefficient of multiple correlation to assess the similarity of waveforms measured synchronously by different motion analysis protocols. *Gait Posture*. 2010;31(4):540-542. doi:10.1016/j.gaitpost.2010.02.009

148. Bland JM, Altman DG. Measuring agreement in method comparison studies. *Stat Methods Med Res*. 1999;8(2):135-160. doi:10.1177/096228029900800204

149. Queen R, Dickerson L, Ranganathan S, Schmitt D. A novel method for measuring asymmetry in kinematic and kinetic variables: The normalized symmetry index. *J Biomech*. 2020;99. doi:10.1016/j.jbiomech.2019.109531

150. Robinson RO, Herzog W, Nigg BM. Use of force platform variables to quantify the effects of chiropractic manipulation on gait symmetry. *J Manipulative Physiol Ther*. 1987;10(4):172-176.

151. Iranzad R, Liu X. A review of random forest-based feature selection methods for data science education and applications. *Int J Data Sci Anal*. *Springer Science and Business Media Deutschland GmbH*. 2025;20(2):197-211. doi:10.1007/s41060-024-00509-w

152. Rashidi HH, Albahra S, Robertson S, Tran NK, Hu B. Common statistical concepts in the supervised Machine Learning arena. *Front Oncol*. *Frontiers Media S.A.* 2023;13. doi:10.3389/fonc.2023.1130229

153. Wilmes E, De Ruiter CJ, Bastiaansen BJC, et al. Inertial sensor-based motion tracking in football with movement intensity quantification. *Sensors (Switzerland)*. 2020;20(9). doi:10.3390/s20092527

154. Mihy JA, Wagatsuma M, Cain SM, Hafer JF. A Functional Sensor-to-Segment Calibration Method Reduces the Effects of Varied Sensor Placement on Estimates of Segment Angular Excursion. *J Appl Biomech*. 2026;42(2):131-139. doi:10.1123/jab.2025-0073

Appendix A

Time and frequency domain features extracted from IMU signals of individual movement repetitions.

Feature	Description	Calculation
Mean	Average signal across the movement repetition	$\mu = \frac{1}{N}\sum_{i=1}^{N} x_i$
Standard Deviation	Signal variability around the mean	$\sigma = \sqrt{\frac{1}{N}\sum_{i=1}^{N}(x_i - \mu)^2}$
Peak Absolute Amplitude	Maximum absolute signal amplitude observed during the repetition	$A_{Peak} = \max(\lvert x_i \rvert)$
Skewness	Asymmetry of the signal distribution around the mean	$Skew = \frac{1}{N}\sum_{i=1}^{N}\left(\frac{x_i - \mu}{\sigma}\right)^3$
Kurtosis	Shape of the signal distribution, showing the presence of extreme values	$Kurt = \frac{1}{N\sigma^3}\sum_{i=1}^{N}(x_i - \mu)^4$
Root Mean Square (RMS)	Average magnitude of the signal	$RMS = \sqrt{\frac{1}{N}\sum_{i=1}^{N} x^2{}_i}$
Energy	Total signal power (average squared signal magnitude)	$E = \frac{1}{N}\sum_{i=1}^{N} x^2{}_i = RMS^2$
Zero-crossing Rate	Oscillatory behaviour pf the signal	$ZCR = \frac{1}{N-1}\sum_{i=2}^{N} \lvert sign(x_i) \neq sign(x_i - 1) \rvert$
Spectral Entropy	Distribution of signal power across frequencies	$H = -\sum_{k=1}^{K} P_k \ln(P_k)$
Band Power	Calculates signal power within a specific frequency range	$BP = \int_{f_1}^{f_2} P(f)df$
Magnitude	Overall signal intensity independent of motion direction	$Mag = \sqrt{x^2 + y^2 + z^2}.$
Symmetry Index	Quantifies differences between right and left limb features	$SI = \frac{Right - Left}{\lvert Right \rvert + \lvert Left \rvert}$

x_i = the i^{th} repetition; N = total number of repetitions; μ = mean signal value; σ = standard deviation; K = total number of frequency bins; k = frequency bin index; P_k = normalized power spectral density at frequency bin k; P_f = power spectral density

Appendix B

Trial-level descriptive statistics comparing hip joint ROM and RMS Error between the Xsens IMU and Vicon OMC systems during all trials.

Movement	Side	Motion	Mean Vicon ROM ± SD (°)	Mean IMU ROM ± SD (°)	Mean Difference (IMU - Vicon, °)	Mean RMS Error ± SD (°)
Squat	Right Hip	Flex./Ext.	110.74 ± 10.09	116.19 ± 9.80	5.46	4.12 ± 1.52
		Add./Abd.	19.15 ± 4.65	16.08 ± 5.76	-3.07	2.55 ± 1.62
		Int./Ext.	28.49 ± 6.85	20.05 ± 6.98	-8.44	5.63 ± 3.79
	Left Hip	Flex./Ext.	112.64 ± 9.52	116.50 ± 9.62	3.86	4.24 ± 1.21
		Add./Abd.	15.14 ± 4.58	9.96 ± 2.96	-5.19	3.49 ± 2.05
		Int./Ext.	37.24 ± 8.19	13.31 ± 3.95	-23.93	9.24 ± 3.04
Flexion/ Extension Swing (R)	Right Hip	Flex./Ext.	121.67 ± 18.63	113.49 ± 18.32	-8.18	4.71 ± 1.20
		Add./Abd.	26.05 ± 8.92	23.81 ± 9.05	-2.24	4.02 ± 2.36
		Int./Ext.	34.11 ± 10.50	31.60 ± 7.52	-2.51	9.83 ± 4.51
	Left Hip	Flex./Ext.	39.93 ± 12.78	31.66 ± 11.21	-8.27	3.52 ± 1.23
		Add./Abd.	14.87 ± 7.40	14.51 ± 6.90	-0.36	1.30 ± 0.73
		Int./Ext.	18.26 ± 7.85	17.50 ± 4.97	-0.77	5.16 ± 3.26
Flexion/ Extension Swing (L)	Right Hip	Flex./Ext.	36.95 ± 12.26	29.93 ± 12.14	-7.02	3.16 ± 1.20
		Add./Abd.	15.53 ± 8.30	15.02 ± 8.82	-0.51	1.64 ± 0.75
		Int./Ext.	20.49 ± 8.92	18.18 ± 4.92	-2.32	5.99 ± 4.09
	Left Hip	Flex./Ext.	120.12 ± 17.56	110.56 ± 18.08	-9.56	5.18 ± 1.34
		Add./Abd.	26.33 ± 9.42	25.81 ± 11.40	-0.51	3.09 ± 1.56
		Int./Ext.	38.09 ± 10.39	31.45 ± 8.90	-6.64	8.51 ± 4.60
Adduction/ Abduction Swing (R)	Right Hip	Flex./Ext.	82.08 ± 18.41	82.56 ± 15.14	0.48	3.94 ± 1.54
		Add./Abd.	71.62 ± 13.23	64.64 ± 10.69	-6.98	3.72 ± 1.02
		Int./Ext.	37.51 ± 12.29	30.57 ± 8.95	-6.94	7.47 ± 2.77
	Left Hip	Flex./Ext.	26.54 ± 8.96	27.53 ± 8.37	0.99	1.73 ± 0.59
		Add./Abd.	32.11 ± 11.43	33.30 ± 11.90	1.20	1.50 ± 0.49
		Int./Ext.	23.94 ± 10.75	24.54 ± 8.96	0.60	4.25 ± 2.11
Adduction/ Abduction Swing (L)	Right Hip	Flex./Ext.	27.93 ± 9.12	27.84 ± 9.31	-0.09	2.02 ± 0.64
		Add./Abd.	33.08 ± 9.91	36.44 ± 10.72	3.36	1.92 ± 0.82
		Int./Ext.	24.04 ± 9.98	23.03 ± 5.97	-1.02	4.03 ± 2.26
	Left Hip	Flex./Ext.	84.73 ± 18.22	84.37 ± 16.71	-0.36	4.36 ± 1.73
		Add./Abd.	73.63 ± 12.87	67.26 ± 8.43	-6.36	3.83 ± 1.55
		Int./Ext.	42.28 ± 10.73	31.37 ± 7.35	-10.91	6.96 ± 2.94
Hip Flexion (R)	Right Hip	Flex./Ext.	94.43 ± 9.23	99.03 ± 10.57	4.60	3.70 ± 1.68
		Add./Abd.	11.84 ± 3.12	19.00 ± 5.64	7.16	4.42 ± 2.00
		Int./Ext.	29.30 ± 9.29	19.49 ± 5.35	-9.81	6.33 ± 3.65
	Left Hip	Flex./Ext.	14.84 ± 5.62	12.84 ± 4.25	-1.99	2.01 ± 0.69
		Add./Abd.	10.63 ± 2.52	9.74 ± 1.88	-0.88	0.95 ± 0.42
		Int./Ext.	13.55 ± 3.78	16.67 ± 4.15	3.12	2.72 ± 1.29

Hip Flexion (L)	Right Hip	Flex./Ext.	15.25 ± 6.77	14.25 ± 5.93	-1.01	1.63 ± 0.51
		Add./Abd.	9.83 ± 2.30	9.18 ± 2.33	-0.65	1.11 ± 0.45
		Int./Ext.	12.57 ± 3.53	15.30 ± 4.42	2.74	2.99 ± 1.80
	Left Hip	Flex./Ext.	95.23 ± 8.98	99.72 ± 10.57	4.49	3.73 ± 1.37
		Add./Abd.	13.22 ± 2.84	14.81 ± 3.52	1.58	3.19 ± 1.54
		Int./Ext.	35.21 ± 9.22	18.46 ± 4.89	-16.75	7.03 ± 3.56
Transverse Plane Hip Internal/ External Rotation (R)	Right Hip	Flex./Ext.	84.18 ± 9.00	89.62 ± 9.62	5.44	2.66 ± 0.74
		Add./Abd.	22.01 ± 7.63	28.68 ± 6.39	6.67	6.05 ± 1.68
		Int./Ext.	42.31 ± 13.14	31.74 ± 5.68	-10.57	5.57 ± 2.66
	Left Hip	Flex./Ext.	13.65 ± 4.95	13.40 ± 4.81	-0.24	1.59 ± 0.50
		Add./Abd.	15.96 ± 5.51	16.57 ± 5.59	0.61	0.96 ± 0.30
		Int./Ext.	15.44 ± 6.93	13.99 ± 3.50	-1.44	2.75 ± 1.24
Transverse Plane Hip Internal/ External Rotation (L)	Right Hip	Flex./Ext.	13.49 ± 6.66	13.16 ± 6.13	-0.33	1.50 ± 0.53
		Add./Abd.	15.66 ± 6.70	16.06 ± 6.64	0.40	1.04 ± 0.40
		Int./Ext.	13.54 ± 5.08	14.09 ± 3.19	0.55	2.47 ± 0.97
	Left Hip	Flex./Ext.	82.94 ± 10.13	88.30 ± 10.18	5.36	3.03 ± 1.20
		Add./Abd.	20.36 ± 8.25	25.09 ± 7.35	4.73	5.40 ± 1.71
		Int./Ext.	45.44 ± 14.37	34.64 ± 7.20	-10.80	4.99 ± 2.55
Jump	Right Hip	Flex./Ext.	105.69 ± 11.06	108.70 ± 9.97	3.01	4.90 ± 1.74
		Add./Abd.	18.27 ± 4.36	17.88 ± 4.29	-0.40	2.06 ± 0.82
		Int./Ext.	30.95 ± 10.74	24.72 ± 5.95	-6.23	5.41 ± 3.93
	Left Hip	Flex./Ext.	106.71 ± 9.19	109.36 ± 10.07	2.65	5.12 ± 1.70
		Add./Abd.	15.25 ± 3.18	15.67 ± 2.70	0.43	2.87 ± 1.78
		Int./Ext.	37.34 ± 9.59	19.51 ± 4.11	-17.83	7.58 ± 3.11
Lateral Shuffle	Right Hip	Flex./Ext.	89.63 ± 10.61	88.85 ± 10.80	-0.77	3.35 ± 0.66
		Add./Abd.	40.70 ± 3.78	34.66 ± 4.27	-6.05	3.09 ± 0.74
		Int./Ext.	44.61 ± 12.26	28.33 ± 4.03	-16.28	5.82 ± 1.87
	Left Hip	Flex./Ext.	86.67 ± 9.35	87.11 ± 9.73	0.44	3.50 ± 0.73
		Add./Abd.	40.81 ± 5.66	35.38 ± 4.63	-5.43	3.01 ± 0.70
		Int./Ext.	47.42 ± 10.43	28.75 ± 4.42	-18.67	6.33 ± 2.05
Submaximal Sprint to Turn (R)	Right Hip	Flex./Ext.	96.43 ± 7.62	92.86 ± 7.12	-3.57	3.86 ± 0.77
		Add./Abd.	27.74 ± 5.16	27.02 ± 4.09	-0.72	2.75 ± 0.66
		Int./Ext.	43.31 ± 9.71	31.18 ± 4.38	-12.14	6.78 ± 2.17
	Left Hip	Flex./Ext.	92.95 ± 7.44	87.89 ± 7.44	-5.06	4.22 ± 0.67
		Add./Abd.	34.91 ± 4.68	32.80 ± 5.33	-2.11	2.39 ± 0.55
		Int./Ext.	51.21 ± 11.31	33.02 ± 4.70	-18.19	8.74 ± 2.76
Submaximal Sprint to Turn (L)	Right Hip	Flex./Ext.	93.86 ± 8.71	88.44 ± 7.24	-5.42	4.34 ± 0.83
		Add./Abd.	32.36 ± 5.54	30.63 ± 5.04	-1.73	2.52 ± 0.53
		Int./Ext.	44.74 ± 8.71	31.94 ± 4.33	-12.80	7.58 ± 2.35
	Left Hip	Flex./Ext.	95.19 ± 8.94	92.04 ± 8.31	-3.15	4.24 ± 0.85
		Add./Abd.	28.37 ± 4.87	26.38 ± 4.31	-1.99	2.60 ± 0.60
		Int./Ext.	46.91 ± 11.57	30.74 ± 6.48	-16.17	8.17 ± 2.59

Sprint to Side-step Cut to 45° (R)	Right Hip	Flex./Ext.	94.52 ± 11.41	91.67 ± 12.24	-2.84	3.56 ± 0.97
		Add./Abd.	27.92 ± 6.78	27.09 ± 5.66	-0.83	2.75 ± 0.78
		Int./Ext.	44.01 ± 11.17	31.63 ± 5.42	-12.38	6.95 ± 2.37
	Left Hip	Flex./Ext.	93.58 ± 12.79	91.73 ± 14.56	-1.85	3.78 ± 0.63
		Add./Abd.	32.48 ± 5.41	31.53 ± 6.14	-0.95	2.49 ± 0.69
		Int./Ext.	53.62 ± 13.63	37.89 ± 7.59	-15.73	8.65 ± 3.14
Sprint to Side-step Cut to 45° (L)	Right Hip	Flex./Ext.	90.64 ± 8.31	86.91 ± 7.91	-3.74	3.62 ± 0.67
		Add./Abd.	30.70 ± 5.04	29.51 ± 3.97	-1.19	2.67 ± 0.54
		Int./Ext.	48.26 ± 12.11	37.63 ± 5.64	-10.63	7.58 ± 2.36
	Left Hip	Flex./Ext.	93.67 ± 9.72	89.60 ± 10.43	-4.08	3.71 ± 0.64
		Add./Abd.	28.05 ± 5.16	28.93 ± 6.36	0.88	2.36 ± 0.59
		Int./Ext.	46.39 ± 12.05	33.36 ± 8.95	-13.03	7.96 ± 2.59
Sprint to Side-step Cut to 90° (R)	Right Hip	Flex./Ext.	95.41 ± 8.88	90.79 ± 8.90	-4.62	3.61 ± 0.71
		Add./Abd.	27.61 ± 5.90	27.41 ± 5.01	-0.20	2.71 ± 0.77
		Int./Ext.	43.54 ± 11.94	30.49 ± 4.09	-13.05	6.99 ± 2.28
	Left Hip	Flex./Ext.	91.94 ± 9.22	88.60 ± 9.57	-3.34	3.66 ± 0.51
		Add./Abd.	34.08 ± 5.82	32.16 ± 4.63	-1.91	2.41 ± 0.64
		Int./Ext.	52.83 ± 13.29	36.40 ± 5.96	-16.42	8.81 ± 3.09
Sprint to Side-step Cut to 90° (L)	Right Hip	Flex./Ext.	92.21 ± 8.67	88.70 ± 7.27	-3.51	3.74 ± 0.74
		Add./Abd.	33.45 ± 5.30	31.34 ± 4.47	-2.11	2.62 ± 0.56
		Int./Ext.	46.61 ± 10.54	35.01 ± 5.58	-11.60	7.49 ± 2.13
	Left Hip	Flex./Ext.	95.53 ± 9.65	91.55 ± 10.55	-3.97	3.78 ± 0.77
		Add./Abd.	27.12 ± 4.22	26.49 ± 4.12	-0.63	2.35 ± 0.59
		Int./Ext.	47.86 ± 12.28	29.28 ± 4.50	-18.58	8.12 ± 2.67
Instep Pass (R)	Right Hip	Flex./Ext.	76.16 ± 12.71	76.17 ± 10.62	0.01	3.89 ± 1.55
		Add./Abd.	37.19 ± 9.42	31.70 ± 8.04	-5.49	3.23 ± 0.97
		Int./Ext.	48.59 ± 12.06	34.25 ± 4.81	-14.34	6.13 ± 2.21
	Left Hip	Flex./Ext.	58.61 ± 7.22	61.70 ± 10.86	3.09	3.48 ± 1.57
		Add./Abd.	23.31 ± 5.06	24.61 ± 5.54	1.30	1.68 ± 0.70
		Int./Ext.	34.99 ± 9.49	25.25 ± 4.18	-9.74	5.63 ± 1.92
Instep Pass (L)	Right Hip	Flex./Ext.	60.69 ± 9.25	61.66 ± 9.76	0.97	3.66 ± 2.48
		Add./Abd.	25.92 ± 4.18	28.93 ± 3.78	3.02	1.91 ± 0.76
		Int./Ext.	31.69 ± 9.04	23.47 ± 3.97	-8.22	5.80 ± 1.65
	Left Hip	Flex./Ext.	74.65 ± 16.06	75.85 ± 13.35	1.19	4.19 ± 2.38
		Add./Abd.	41.77 ± 8.98	37.54 ± 7.88	-4.24	2.76 ± 0.72
		Int./Ext.	50.47 ± 12.14	34.29 ± 5.92	-16.19	6.89 ± 2.33
Instep Receive (R)	Right Hip	Flex./Ext.	68.59 ± 11.10	70.40 ± 11.76	1.81	3.35 ± 1.31
		Add./Abd.	34.41 ± 7.80	32.55 ± 6.05	-1.86	3.15 ± 1.17
		Int./Ext.	45.84 ± 11.74	31.93 ± 5.27	-13.91	5.37 ± 1.94
	Left Hip	Flex./Ext.	56.35 ± 14.10	58.19 ± 15.07	1.84	2.98 ± 1.33
		Add./Abd.	24.24 ± 4.40	25.96 ± 4.01	1.72	1.67 ± 0.57
		Int./Ext.	35.59 ± 9.78	25.19 ± 5.86	-10.40	5.28 ± 1.75

Instep Receive (L)	Right Hip	Flex./Ext.	54.49 ± 9.28	55.65 ± 9.04	1.16	2.87 ± 1.05
		Add./Abd.	25.65 ± 4.83	28.30 ± 3.74	2.65	1.73 ± 0.60
		Int./Ext.	30.46 ± 7.95	23.99 ± 3.52	-6.46	4.95 ± 1.50
	Left Hip	Flex./Ext.	64.30 ± 8.42	69.01 ± 8.99	4.71	3.76 ± 1.22
		Add./Abd.	35.85 ± 6.09	34.56 ± 5.69	-1.30	2.57 ± 0.65
		Int./Ext.	48.62 ± 10.91	32.94 ± 5.12	-15.68	6.23 ± 1.94
Outstep Receive (R)	Right Hip	Flex./Ext.	72.67 ± 14.22	73.09 ± 16.73	0.42	3.77 ± 1.59
		Add./Abd.	37.47 ± 5.81	37.87 ± 5.87	0.40	2.74 ± 0.81
		Int./Ext.	49.92 ± 12.73	42.96 ± 7.01	-6.96	5.90 ± 1.49
	Left Hip	Flex./Ext.	56.32 ± 18.05	58.93 ± 17.87	2.61	3.24 ± 1.76
		Add./Abd.	26.80 ± 5.16	27.96 ± 6.47	1.16	1.83 ± 0.42
		Int./Ext.	42.13 ± 13.62	26.29 ± 4.35	-15.84	6.39 ± 2.25
Outstep Receive (L)	Right Hip	Flex./Ext.	53.89 ± 9.88	55.83 ± 10.62	1.94	3.50 ± 2.77
		Add./Abd.	27.43 ± 5.19	29.88 ± 5.22	2.46	2.02 ± 0.83
		Int./Ext.	35.63 ± 8.23	24.93 ± 2.76	-10.71	5.60 ± 1.82
	Left Hip	Flex./Ext.	70.24 ± 10.31	70.07 ± 10.37	-0.17	4.09 ± 2.57
		Add./Abd.	37.49 ± 7.02	39.08 ± 7.34	1.59	2.70 ± 0.90
		Int./Ext.	47.92 ± 10.42	41.84 ± 8.64	-6.08	6.80 ± 2.18
Instep Volley (R)	Right Hip	Flex./Ext.	82.77 ± 15.40	88.09 ± 14.56	5.32	3.53 ± 1.23
		Add./Abd.	22.24 ± 6.29	26.77 ± 6.41	4.53	3.46 ± 1.48
		Int./Ext.	40.00 ± 11.96	25.30 ± 4.38	-14.70	5.13 ± 2.47
	Left Hip	Flex./Ext.	43.58 ± 10.57	45.13 ± 13.01	1.55	2.85 ± 0.93
		Add./Abd.	18.43 ± 5.38	20.73 ± 5.06	2.30	1.83 ± 0.74
		Int./Ext.	26.30 ± 8.87	21.39 ± 4.72	-4.91	5.43 ± 2.01
Instep Volley (L)	Right Hip	Flex./Ext.	42.53 ± 8.74	41.61 ± 8.23	-0.92	2.58 ± 0.54
		Add./Abd.	20.53 ± 6.72	24.51 ± 6.83	3.98	2.02 ± 0.79
		Int./Ext.	23.35 ± 6.95	21.55 ± 2.94	-1.80	4.98 ± 1.64
	Left Hip	Flex./Ext.	82.50 ± 10.92	86.09 ± 10.48	3.60	3.55 ± 1.06
		Add./Abd.	22.69 ± 6.67	23.61 ± 6.67	0.93	3.17 ± 1.48
		Int./Ext.	43.18 ± 13.22	29.10 ± 5.27	-14.07	7.03 ± 2.45
Laces Volley (R)	Right Hip	Flex./Ext.	87.44 ± 12.89	87.73 ± 12.14	0.29	3.30 ± 1.04
		Add./Abd.	16.78 ± 5.51	18.59 ± 5.36	1.81	2.69 ± 1.16
		Int./Ext.	32.21 ± 7.87	22.12 ± 2.85	-10.10	5.60 ± 2.04
	Left Hip	Flex./Ext.	42.01 ± 9.17	43.30 ± 9.42	1.29	2.57 ± 0.87
		Add./Abd.	13.98 ± 4.74	15.68 ± 5.76	1.70	1.56 ± 0.57
		Int./Ext.	24.91 ± 8.69	19.18 ± 2.84	-5.73	4.28 ± 1.81
Laces Volley (L)	Right Hip	Flex./Ext.	44.80 ± 8.45	43.51 ± 7.94	-1.30	2.58 ± 0.94
		Add./Abd.	13.82 ± 4.50	16.81 ± 5.48	3.00	1.94 ± 0.61
		Int./Ext.	23.69 ± 8.58	19.38 ± 3.28	-4.31	4.50 ± 1.72
	Left Hip	Flex./Ext.	83.00 ± 8.38	83.65 ± 7.55	0.66	3.64 ± 1.10
		Add./Abd.	18.74 ± 4.81	18.73 ± 4.48	-0.01	2.46 ± 0.96
		Int./Ext.	38.49 ± 8.47	21.56 ± 3.91	-16.93	6.56 ± 2.42

Aerial Control (R)	Right Hip	Flex./Ext.	103.89 ± 8.64	105.05 ± 7.94	1.16	3.82 ± 0.86
		Add./Abd.	33.03 ± 10.73	31.98 ± 8.55	-1.05	3.17 ± 0.97
		Int./Ext.	47.77 ± 13.48	36.76 ± 6.00	-11.01	5.67 ± 2.22
	Left Hip	Flex./Ext.	46.50 ± 9.30	48.97 ± 10.13	2.47	2.80 ± 0.93
		Add./Abd.	24.81 ± 4.60	27.03 ± 3.90	2.22	1.69 ± 0.33
		Int./Ext.	32.89 ± 8.85	27.75 ± 5.45	-5.14	4.86 ± 1.68
Aerial Control (L)	Right Hip	Flex./Ext.	48.56 ± 8.94	49.10 ± 9.03	0.54	2.99 ± 1.04
		Add./Abd.	25.17 ± 7.01	27.33 ± 6.28	2.16	1.91 ± 0.51
		Int./Ext.	29.97 ± 8.48	26.46 ± 4.23	-3.51	4.68 ± 1.59
	Left Hip	Flex./Ext.	103.09 ± 9.35	105.41 ± 8.16	2.32	4.09 ± 1.29
		Add./Abd.	35.31 ± 6.86	34.30 ± 5.34	-1.01	2.80 ± 0.66
		Int./Ext.	50.85 ± 8.82	35.90 ± 6.53	-14.95	7.07 ± 2.23
Dribble to 45° Cut (R)	Right Hip	Flex./Ext.	91.70 ± 7.96	84.97 ± 7.17	-6.73	3.82 ± 0.78
		Add./Abd.	33.09 ± 5.22	34.56 ± 5.71	1.46	2.85 ± 0.61
		Int./Ext.	50.52 ± 13.67	34.55 ± 4.92	-15.96	6.55 ± 1.85
	Left Hip	Flex./Ext.	74.88 ± 7.99	71.97 ± 8.01	-2.91	3.38 ± 0.61
		Add./Abd.	32.77 ± 5.20	33.98 ± 4.21	1.21	2.57 ± 0.56
		Int./Ext.	49.48 ± 11.93	38.91 ± 7.80	-10.57	7.63 ± 2.37
Dribble to 45° Cut (L)	Right Hip	Flex./Ext.	74.13 ± 9.40	70.56 ± 9.72	-3.57	3.46 ± 1.16
		Add./Abd.	31.88 ± 6.06	33.10 ± 5.12	1.22	2.70 ± 0.56
		Int./Ext.	46.07 ± 9.69	37.54 ± 4.80	-8.53	6.59 ± 1.73
	Left Hip	Flex./Ext.	89.61 ± 9.23	84.35 ± 10.12	-5.26	3.98 ± 1.11
		Add./Abd.	32.98 ± 6.90	33.98 ± 7.33	1.00	2.43 ± 0.57
		Int./Ext.	54.27 ± 10.58	36.83 ± 5.22	-17.44	7.20 ± 2.08
Dribble to 90° Cut (R)	Right Hip	Flex./Ext.	92.88 ± 9.84	87.96 ± 10.31	-4.92	4.02 ± 1.23
		Add./Abd.	33.27 ± 5.61	32.95 ± 6.45	-0.33	2.95 ± 0.82
		Int./Ext.	49.85 ± 12.59	35.55 ± 5.23	-14.30	6.45 ± 2.01
	Left Hip	Flex./Ext.	77.82 ± 8.41	75.30 ± 9.29	-2.52	3.62 ± 1.04
		Add./Abd.	36.20 ± 6.11	36.25 ± 6.17	0.05	2.56 ± 0.62
		Int./Ext.	52.96 ± 12.16	34.99 ± 5.34	-17.98	7.80 ± 2.43
Dribble to 90° Cut (L)	Right Hip	Flex./Ext.	74.48 ± 11.87	71.83 ± 13.02	-2.65	3.34 ± 0.89
		Add./Abd.	34.62 ± 4.74	33.42 ± 4.08	-1.20	2.58 ± 0.50
		Int./Ext.	46.87 ± 10.13	34.31 ± 4.69	-12.56	6.74 ± 1.92
	Left Hip	Flex./Ext.	91.69 ± 8.51	86.15 ± 7.99	-5.54	3.77 ± 0.95
		Add./Abd.	35.04 ± 8.68	33.97 ± 8.31	-1.06	2.37 ± 0.62
		Int./Ext.	50.72 ± 12.00	35.40 ± 7.18	-15.32	7.17 ± 2.30
Dribble to Turn (R)	Right Hip	Flex./Ext.	91.05 ± 7.78	86.08 ± 8.17	-4.98	3.93 ± 0.93
		Add./Abd.	32.94 ± 6.41	31.71 ± 5.48	-1.23	2.78 ± 0.60
		Int./Ext.	52.60 ± 13.33	36.13 ± 7.12	-16.47	6.42 ± 2.03
	Left Hip	Flex./Ext.	71.47 ± 6.50	70.45 ± 8.89	-1.02	3.61 ± 0.84
		Add./Abd.	36.36 ± 5.12	34.68 ± 5.34	-1.68	2.39 ± 0.48
		Int./Ext.	48.79 ± 11.17	33.49 ± 4.90	-15.31	7.86 ± 2.57
Dribble to Turn (L)	Right Hip	Flex./Ext.	69.30 ± 6.47	67.87 ± 7.05	-1.43	3.71 ± 0.90
		Add./Abd.	34.87 ± 7.60	33.53 ± 5.66	-1.34	2.61 ± 0.61
		Int./Ext.	43.34 ± 8.49	33.04 ± 4.21	-10.30	6.90 ± 1.75
	Left Hip	Flex./Ext.	90.92 ± 5.87	86.54 ± 5.48	-4.38	4.16 ± 0.92
		Add./Abd.	35.56 ± 5.03	35.27 ± 5.47	-0.29	2.55 ± 0.67
		Int./Ext.	54.33 ± 13.97	38.95 ± 6.52	-15.38	7.31 ± 2.46

Appendix C

Estimated marginal means from linear mixed models assessing the effect of motion type on RMS error for right and left hip kinematics.

Right Hip Motion	Estimate (RMS Error, °)	SE	95% CI		z	*p*-value
			Lower	Upper		
Flex./Ext.	3.45	0.268	2.92	3.97	10.03	< 0.001
Add./Abd.	2.69	0.268	2.16	3.22	12.85	< 0.001
Int./Ext.	5.97	0.268	5.45	6.50	22.26	< 0.001
Left Hip Motion	**Estimate (RMS Error, °)**	**SE**	**95% CI**		**z**	***p*-value**
			Lower	**Upper**		
Flex./Ext.	3.58	0.284	3.02	4.13	8.62	< 0.001
Add./Abd.	2.45	0.284	1.89	3.01	12.60	< 0.001
Int./Ext.	6.67	0.284	6.11	7.22	23.47	< 0.001

SE = standard error. CI = confidence interval. Estimate = estimated marginal mean RMS (root mean square) error. $\alpha = 0.05$.

Appendix D

Trial-level Bland–Altman analysis descriptive statistics for agreement between Xsens IMU and Vicon OMC systems during all trials.

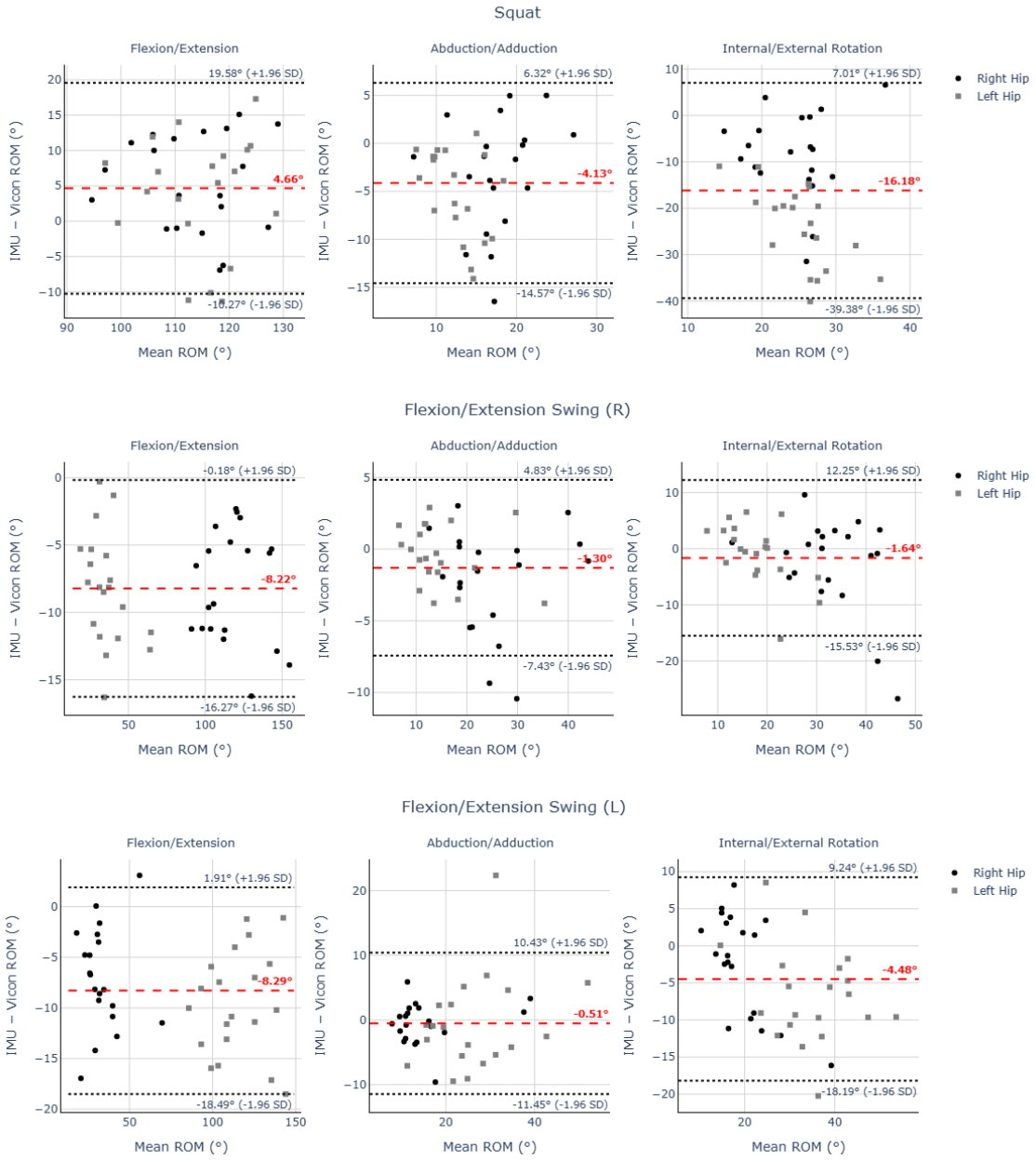
Trial	Motion	Bias (°)	SD of Differences (°)	Upper LOA (°)	Lower LOA (°)
Squat	Flex./Ext.	4.66	7.62	19.58	-10.27
	Add./Abd.	-4.13	5.33	6.32	-14.57
	Int./Ext.	-16.18	11.83	7.01	-39.38
Flexion/ Extension Swing (R)	Flex./Ext.	-8.22	4.10	-0.18	-16.27
	Add./Abd.	-1.30	3.13	4.83	-7.43
	Int./Ext.	-1.64	7.09	12.25	-15.53
Flexion/ Extension Swing (L)	Flex./Ext.	-8.29	5.20	1.91	-18.49
	Add./Abd.	-0.51	5.58	10.43	-11.45
	Int./Ext.	-4.48	7.00	9.24	-18.19
Adduction/ Abduction Swing (R)	Flex./Ext.	0.74	5.17	10.86	-9.39
	Add./Abd.	-2.89	5.74	8.36	-14.15
	Int./Ext.	-3.17	12.24	20.82	-27.16
Adduction/ Abduction Swing (L)	Flex./Ext.	-0.23	4.87	9.33	-9.78
	Add./Abd.	-1.50	6.97	12.16	-15.16
	Int./Ext.	-5.96	10.78	15.16	-27.09
Hip Flexion (R)	Flex./Ext.	1.30	5.22	11.53	-8.93
	Add./Abd.	3.14	5.38	13.68	-7.40
	Int./Ext.	-3.35	10.36	16.97	-23.66
Hip Flexion (L)	Flex./Ext.	1.74	5.17	11.87	-8.39
	Add./Abd.	0.47	3.38	7.08	-6.15
	Int./Ext.	-7.01	11.89	16.29	-30.31
Transverse Plane Hip Internal/ External Rotation (R)	Flex./Ext.	2.60	4.67	11.76	-6.56
	Add./Abd.	3.64	5.67	14.74	-7.46
	Int./Ext.	-6.00	10.24	14.06	-26.07
Transverse Plane Hip Internal/ External Rotation (L)	Flex./Ext.	2.51	5.22	12.75	-7.73
	Add./Abd.	2.56	7.63	17.52	-12.39
	Int./Ext.	-5.13	10.23	14.93	-25.18
Jump	Flex./Ext.	2.83	6.74	16.04	-10.38
	Add./Abd.	0.01	3.59	7.05	-7.02
	Int./Ext.	-12.03	10.39	8.33	-32.39
Lateral Shuffle	Flex./Ext.	-0.17	4.53	8.71	-9.04
	Add./Abd.	-5.74	3.16	0.45	-11.92
	Int./Ext.	-17.48	10.11	2.33	-37.28

Submaximal Sprint to Turn (R)	Flex./Ext.	-4.32	5.63	6.71	-15.35
	Add./Abd.	-1.42	3.12	4.71	-7.54
	Int./Ext.	-15.16	10.79	5.97	-36.30
Submaximal Sprint to Turn (L)	Flex./Ext.	-4.29	6.10	7.67	-16.24
	Add./Abd.	-1.86	2.92	3.86	-7.57
	Int./Ext.	-14.49	11.11	7.30	-36.27
Sprint to Side-step Cut to 45˚ (R)	Flex./Ext.	-2.35	6.22	9.84	-14.54
	Add./Abd.	-0.89	3.60	6.17	-7.95
	Int./Ext.	-14.05	9.19	3.96	-32.06
Sprint to Side-step Cut at 45˚ (L)	Flex./Ext.	-3.91	4.43	4.76	-12.58
	Add./Abd.	-0.15	3.70	7.10	-7.41
	Int./Ext.	-11.83	10.43	8.62	-32.28
Sprint to Side-step Cut to 90˚ (R)	Flex./Ext.	-3.98	6.05	7.87	-15.84
	Add./Abd.	-1.05	2.96	4.75	-6.86
	Int./Ext.	-14.73	11.33	7.47	-36.94
Sprint to Side-step Cut to 90˚ (L)	Flex./Ext.	-3.74	5.64	7.31	-14.79
	Add./Abd.	-1.37	3.51	5.51	-8.25
	Int./Ext.	-15.09	10.66	5.81	-35.99
Instep Pass (R)	Flex./Ext.	1.55	8.15	17.53	-14.43
	Add./Abd.	-2.09	4.97	7.65	-11.83
	Int./Ext.	-12.04	9.45	6.48	-30.55
Instep Pass (L)	Flex./Ext.	1.08	8.91	18.54	-16.38
	Add./Abd.	-0.61	5.42	10.01	-11.23
	Int./Ext.	-12.20	10.31	8.01	-32.41
Instep Receive (R)	Flex./Ext.	1.83	5.17	11.96	-8.31
	Add./Abd.	-0.07	3.87	7.51	-7.64
	Int./Ext.	-12.16	9.46	6.39	-30.71
Instep Receive (L)	Flex./Ext.	2.94	6.61	15.88	-10.01
	Add./Abd.	0.68	3.61	7.76	-6.41
	Int./Ext.	-11.07	10.71	9.92	-32.06
Outstep Receive (R)	Flex./Ext.	1.52	7.12	15.48	-12.45
	Add./Abd.	0.78	2.57	5.82	-4.26
	Int./Ext.	-11.40	13.19	14.46	-37.26
Outstep Receive (L)	Flex./Ext.	0.88	9.00	18.52	-16.75
	Add./Abd.	2.02	3.18	8.25	-4.21
	Int./Ext.	-8.40	9.43	10.09	-26.88
Instep Volley (R)	Flex./Ext.	3.44	4.77	12.78	-5.91
	Add./Abd.	3.42	4.61	12.46	-5.63
	Int./Ext.	-9.81	10.19	10.16	-29.77

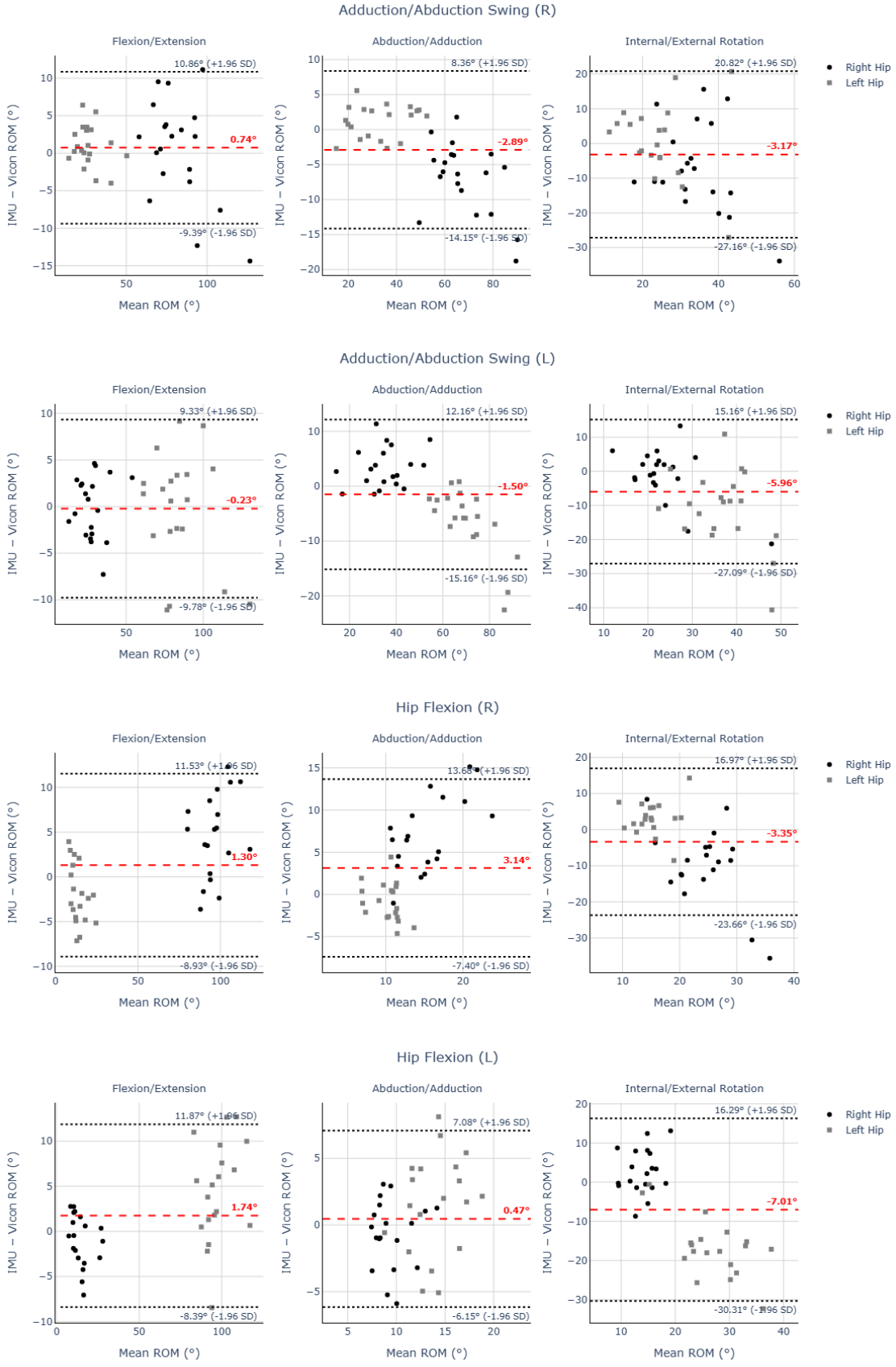
Instep Volley (L)	Flex./Ext.	1.34	4.63	10.41	-7.73
	Add./Abd.	2.45	4.97	12.19	-7.28
	Int./Ext.	-7.94	10.84	13.31	-29.18
Laces Volley (R)	Flex./Ext.	0.79	4.21	9.04	-7.46
	Add./Abd.	1.75	3.38	8.38	-4.87
	Int./Ext.	-7.91	7.79	7.34	-23.17
Laces Volley (L)	Flex./Ext.	-0.32	3.64	6.80	-7.45
	Add./Abd.	1.49	3.31	7.98	-4.99
	Int./Ext. Rotaion	-10.62	10.35	9.67	-30.91
Aerial Control (R)	Flex./Ext.	1.81	5.51	12.62	-8.99
	Add./Abd.	0.58	3.51	7.46	-6.29
	Int./Ext.	-8.07	9.93	11.39	-27.54
Aerial Control (L)	Flex./Ext.	1.43	6.25	13.68	-10.82
	Add./Abd.	0.58	4.08	8.57	-7.42
	Int./Ext.	-9.23	9.54	9.47	-27.94
Dribble to 45˚ Cut (R)	Flex./Ext.	-4.82	5.58	6.12	-15.75
	Add./Abd.	1.34	3.32	7.85	-5.17
	Int./Ext.	-13.27	11.97	10.19	-36.73
Dribble to 45˚ Cut (L)	Flex./Ext.	-4.42	6.19	7.71	-16.54
	Add./Abd.	1.11	2.89	6.78	-4.56
	Int./Ext.	-12.99	9.63	5.90	-31.87
Dribble to 90˚ Cut (R)	Flex./Ext.	-3.72	7.18	10.35	-17.78
	Add./Abd.	-0.14	3.30	6.34	-6.61
	Int./Ext.	-16.14	11.60	6.61	-38.88
Dribble to 90˚ Cut (L)	Flex./Ext.	-4.10	5.21	6.11	-14.30
	Add./Abd.	-1.13	3.11	4.97	-7.23
	Int./Ext.	-13.94	9.35	4.40	-32.27
Dribble to Turn (R)	Flex./Ext.	-3.00	5.71	8.20	-14.20
	Add./Abd.	-1.45	2.89	4.20	-7.11
	Int./Ext.	-15.89	11.85	7.33	-39.11
Dribble to Turn (L)	Flex./Ext.	-2.90	4.44	5.80	-11.60
	Add./Abd.	-0.81	4.07	7.16	-8.79
	Int./Ext.	-12.84	10.30	7.34	-33.02

Appendix E

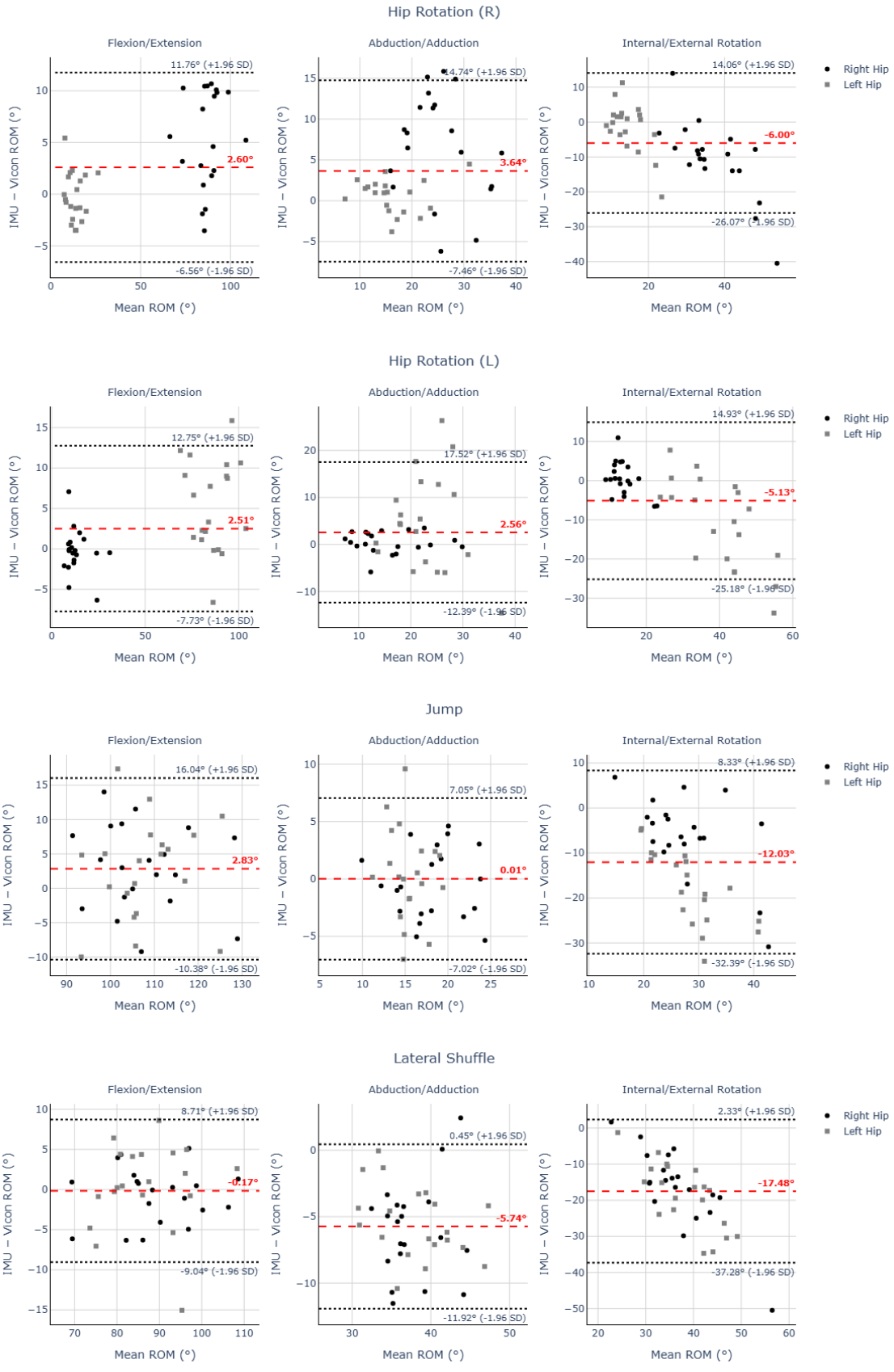
Bland–Altman plots assessing agreement between Xsens IMU and Vicon OMC systems for all remaining movements. Each panel presents the difference between IMU- and Vicon-derived ROM (IMU-Vicon) plotted against the mean of the two measures, with mean bias (red dashed line) and 95% LOAs (black dotted lines) shown for the right and left hip.



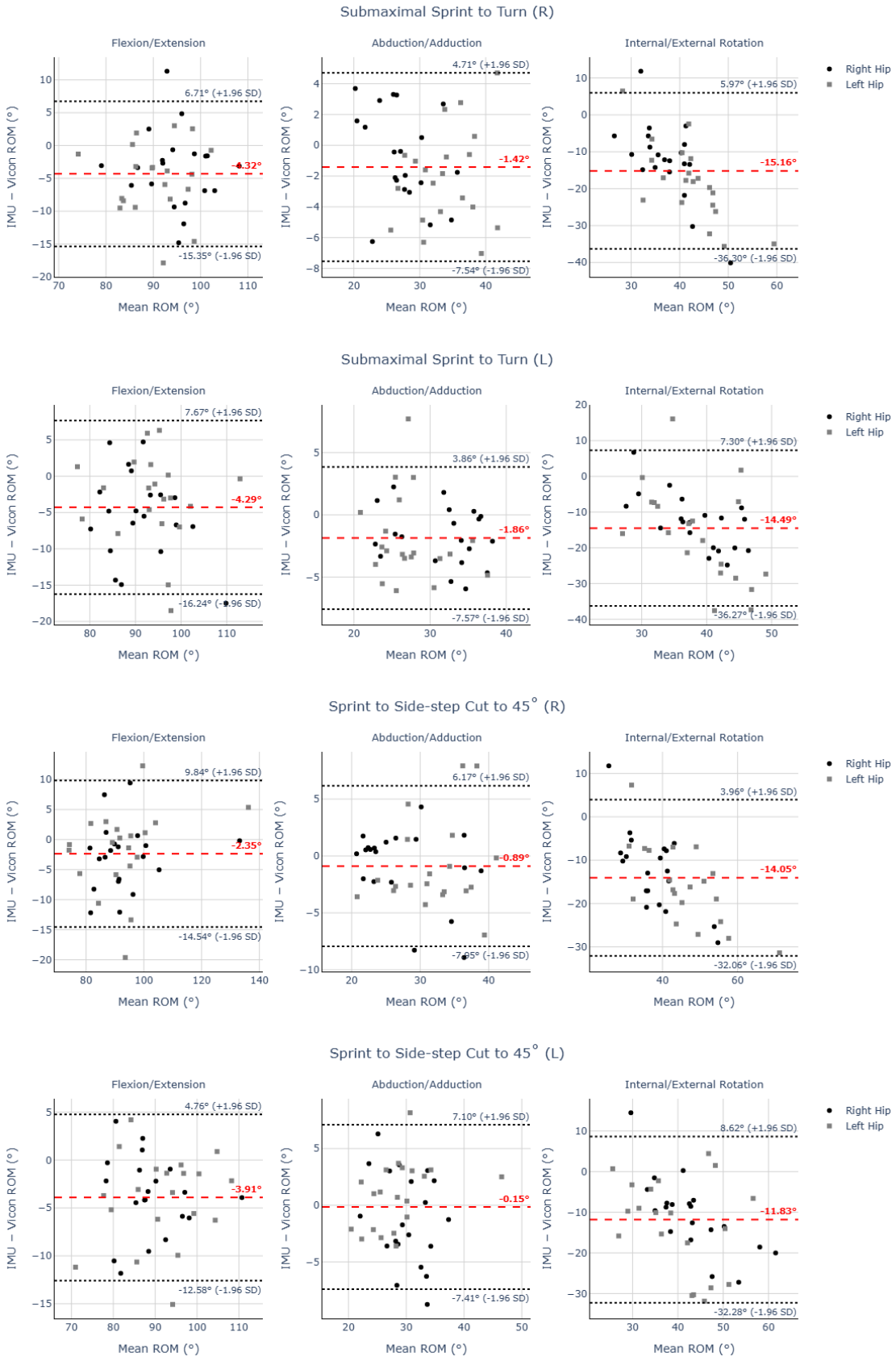
Squat, Flexion/Extension Swing (R/L)



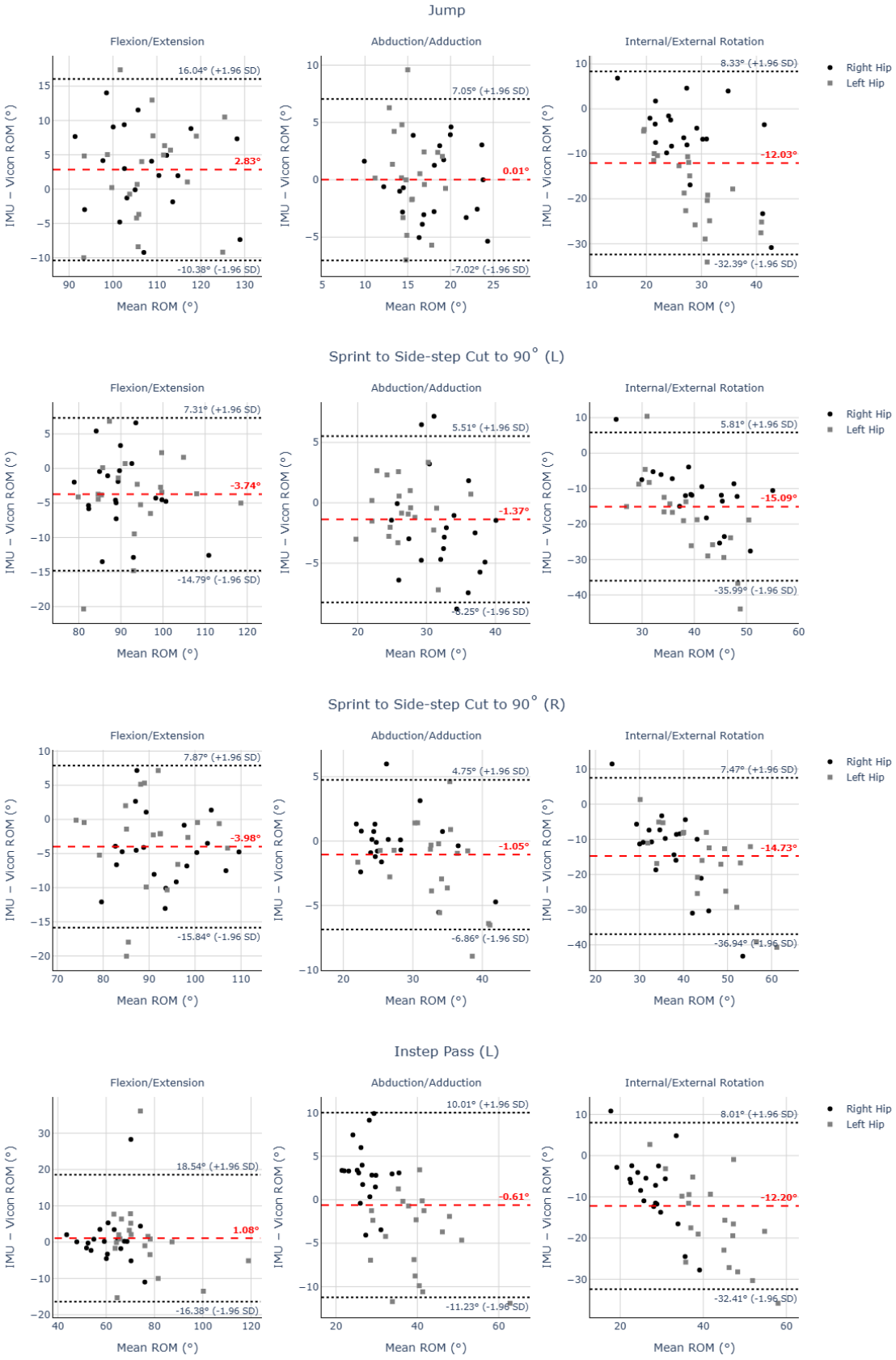
Adduction/Abduction Swing (R/L), Hip Flexion (R/L)



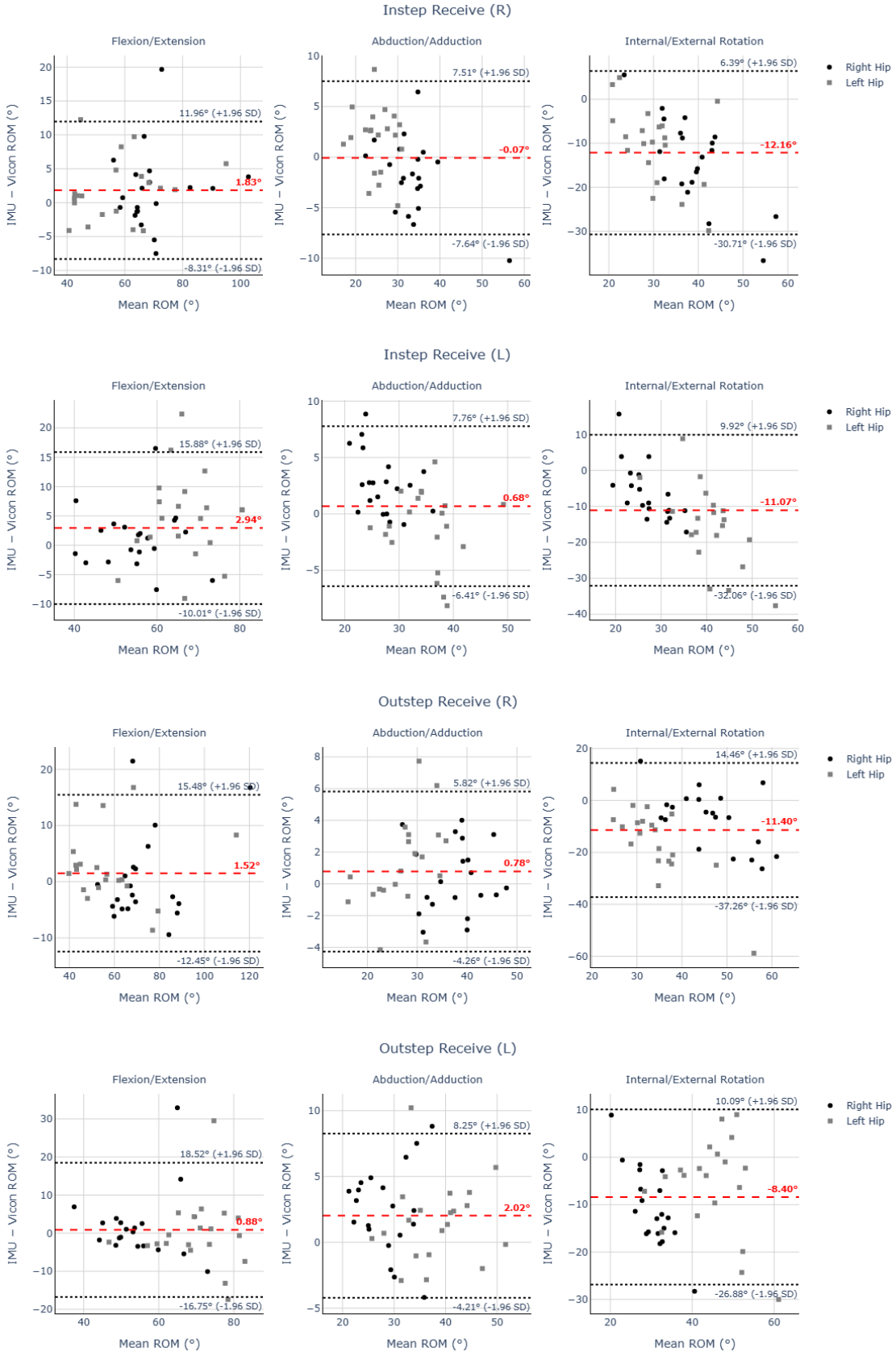
Transverse Plane Hip Internal/External Rotation (R/L), Jump, Lateral Shuffle



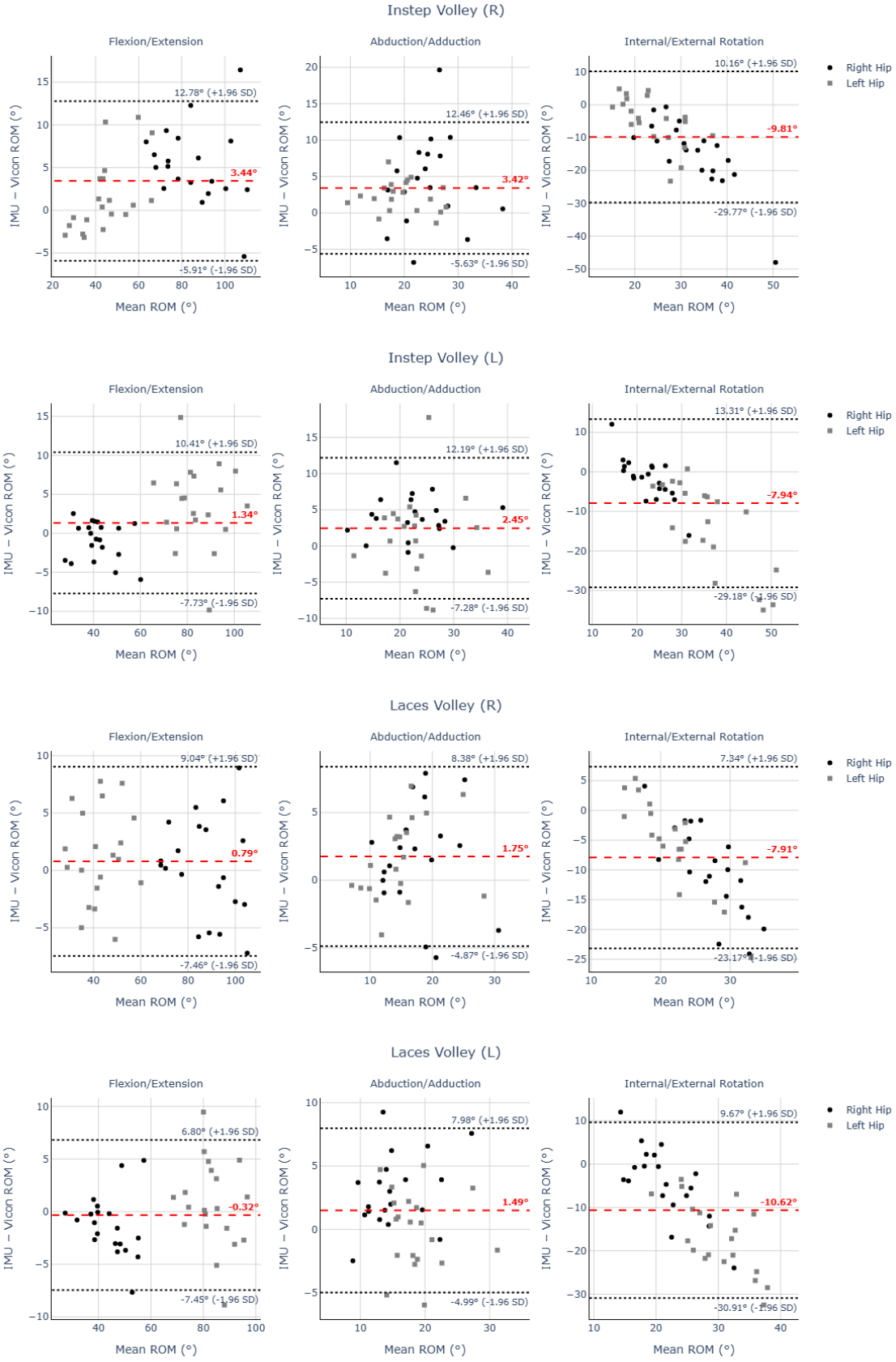
Submaximal Sprint to Turn (R/L), Sprint to Side-step Cut to 45˚ (R/L)



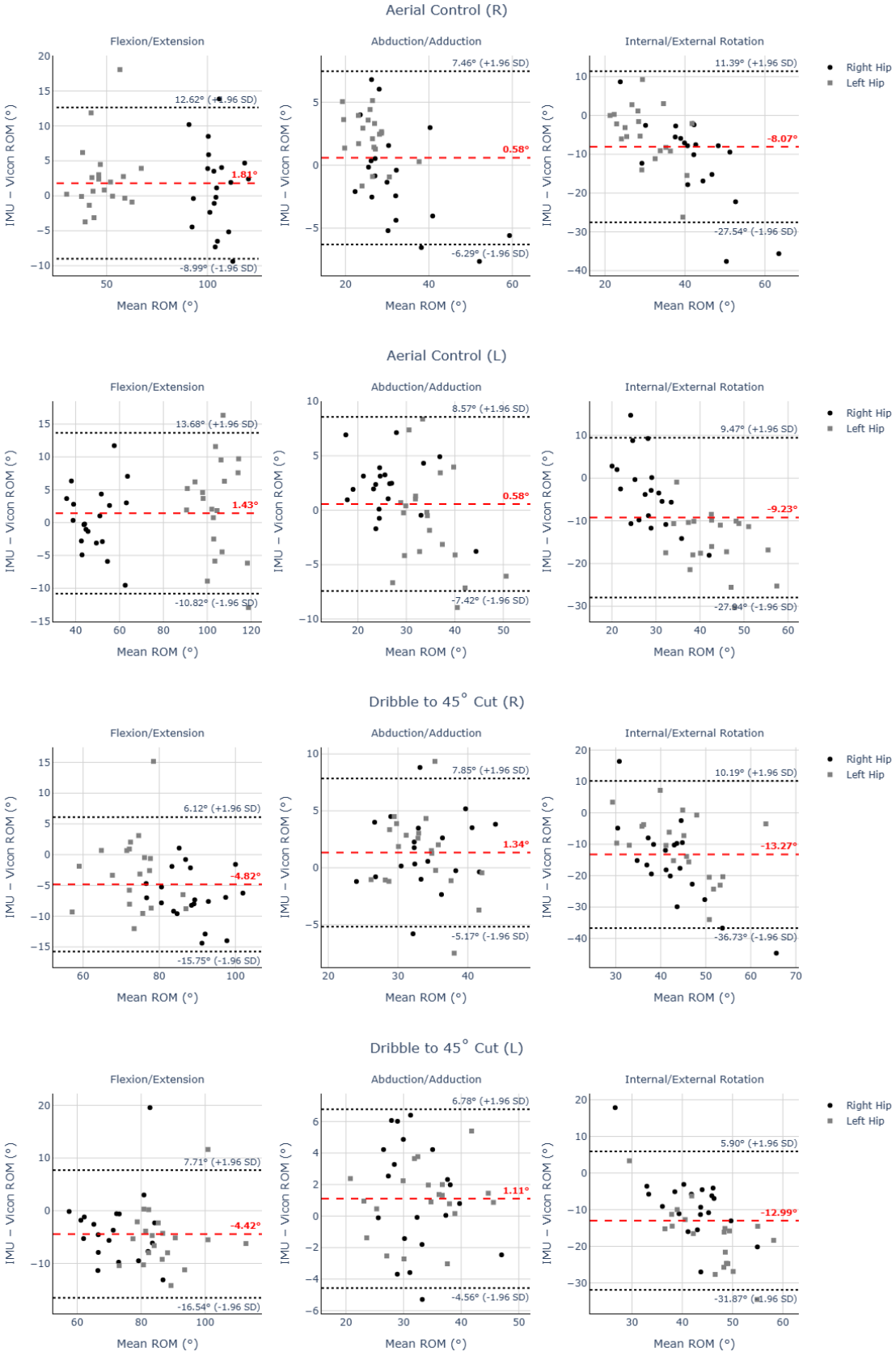
Sprint to Side-step Cut to 90˚ (R/L), Instep Pass (R/L)



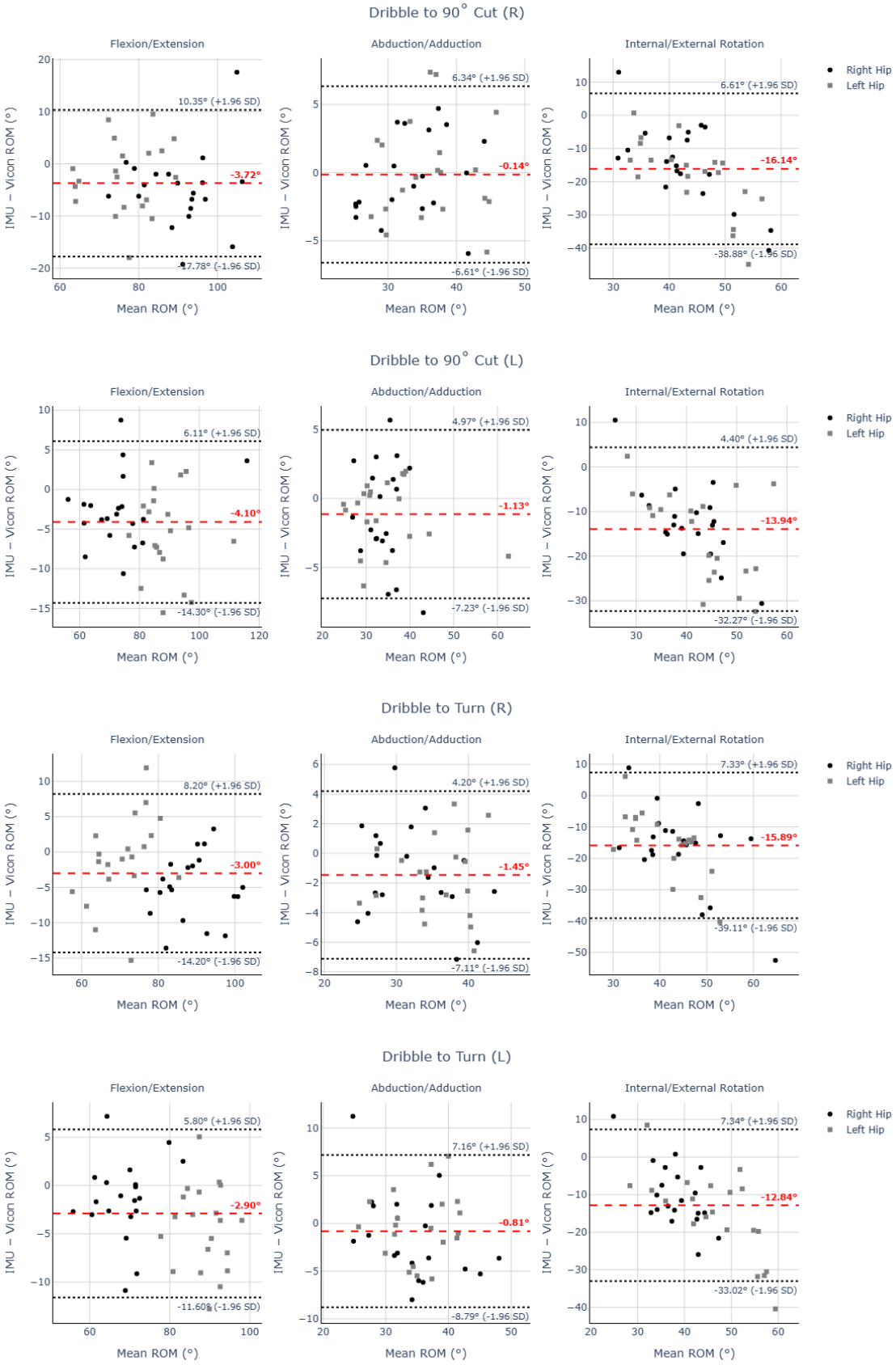
Instep Receive (R/L), Outstep Receive (R/L)



Instep Volley (R/L), Laces Volley (R/L)



Aerial Control (R/L), Dribble to 45˚ Cut (R/L)

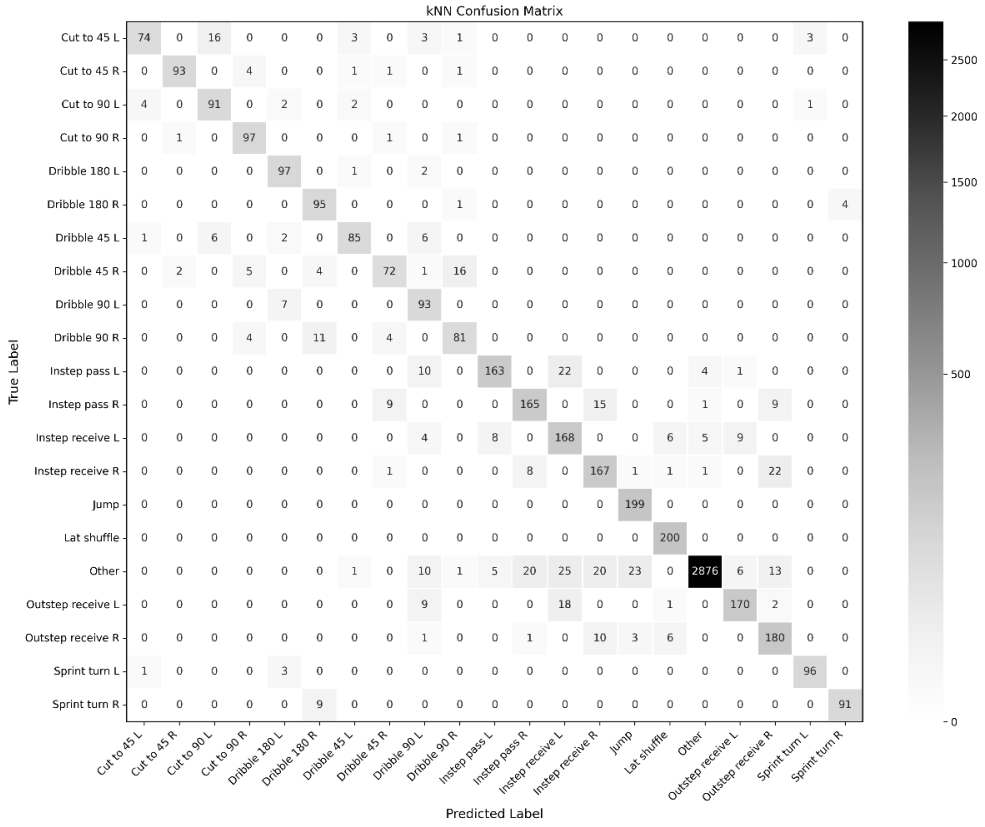


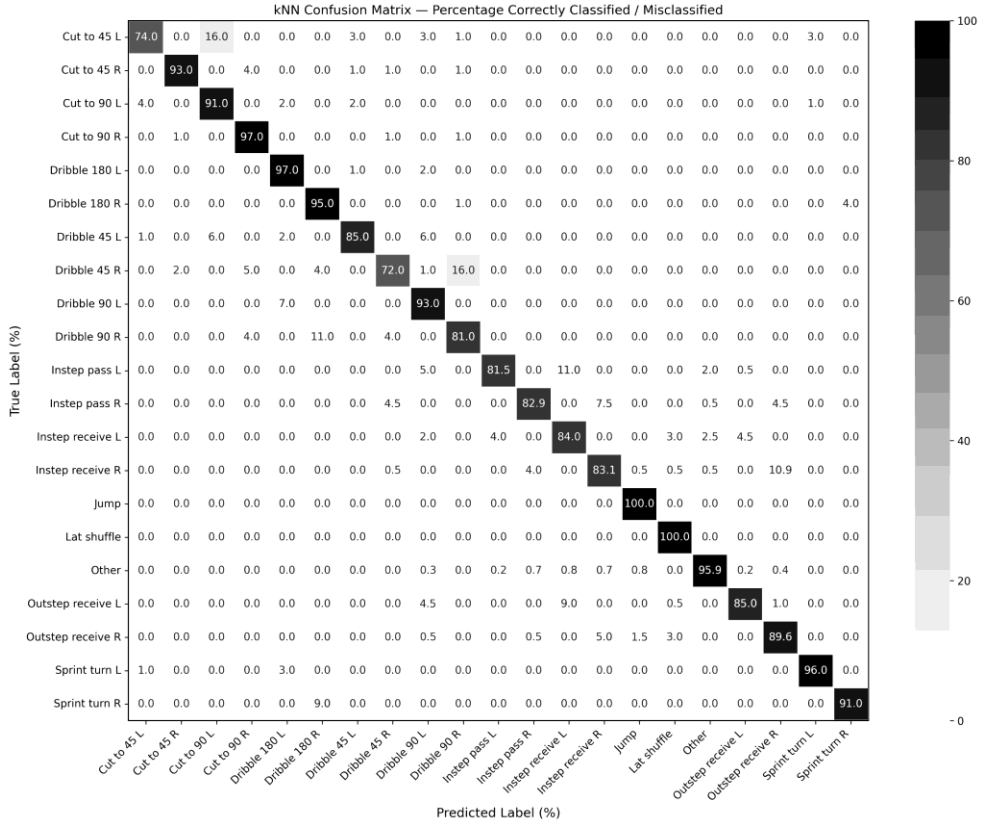
Dribble to 90˚ Cut (R/L), Dribble to Turn (R/L)

Appendix F

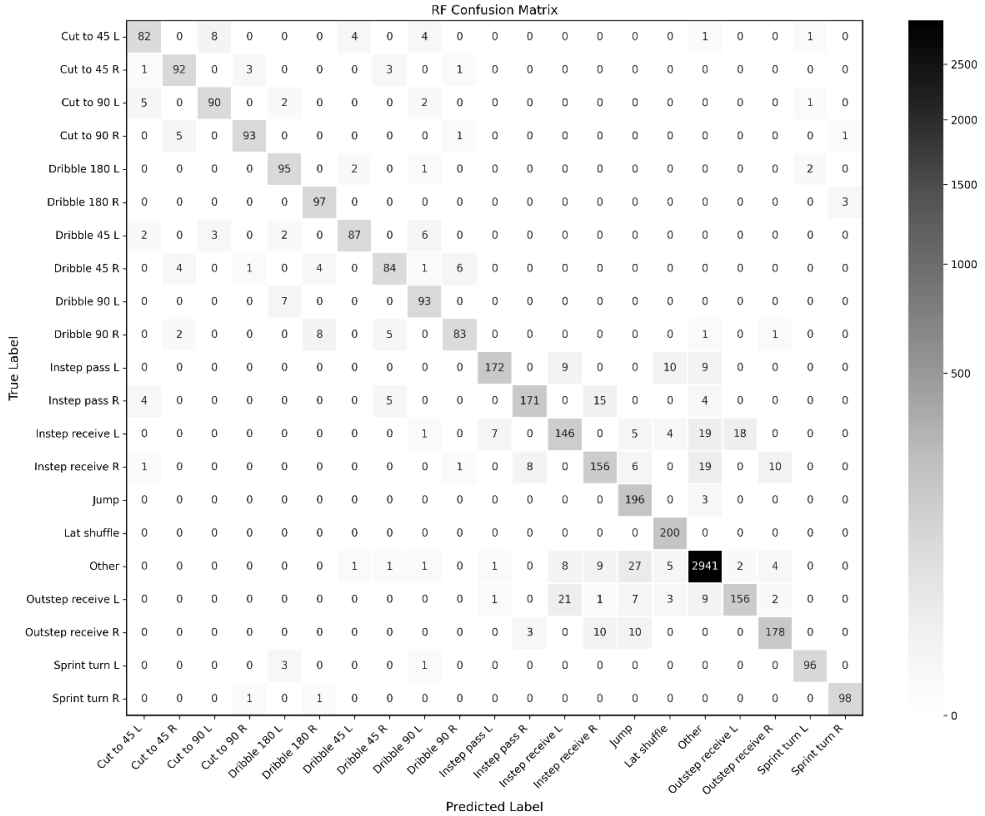
Confusion matrices for the remaining four classifiers evaluated, presented as both raw repetition counts (A) and row-normalized percentages (B). XGBoost is not presented.

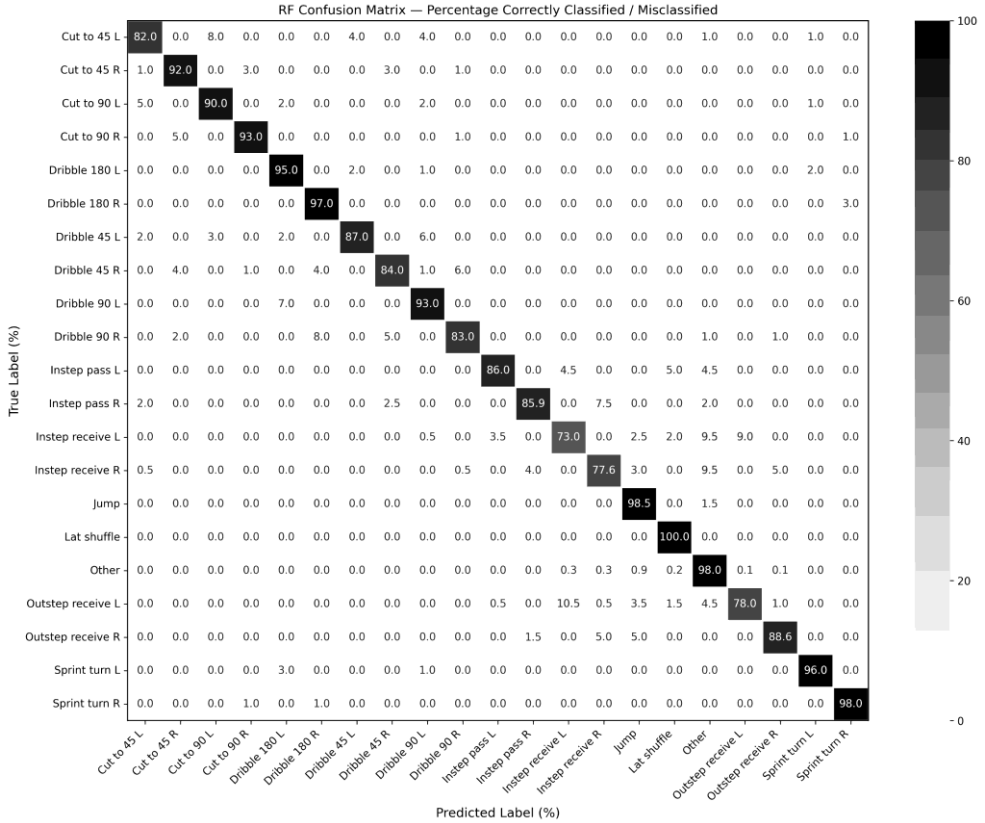
kNN



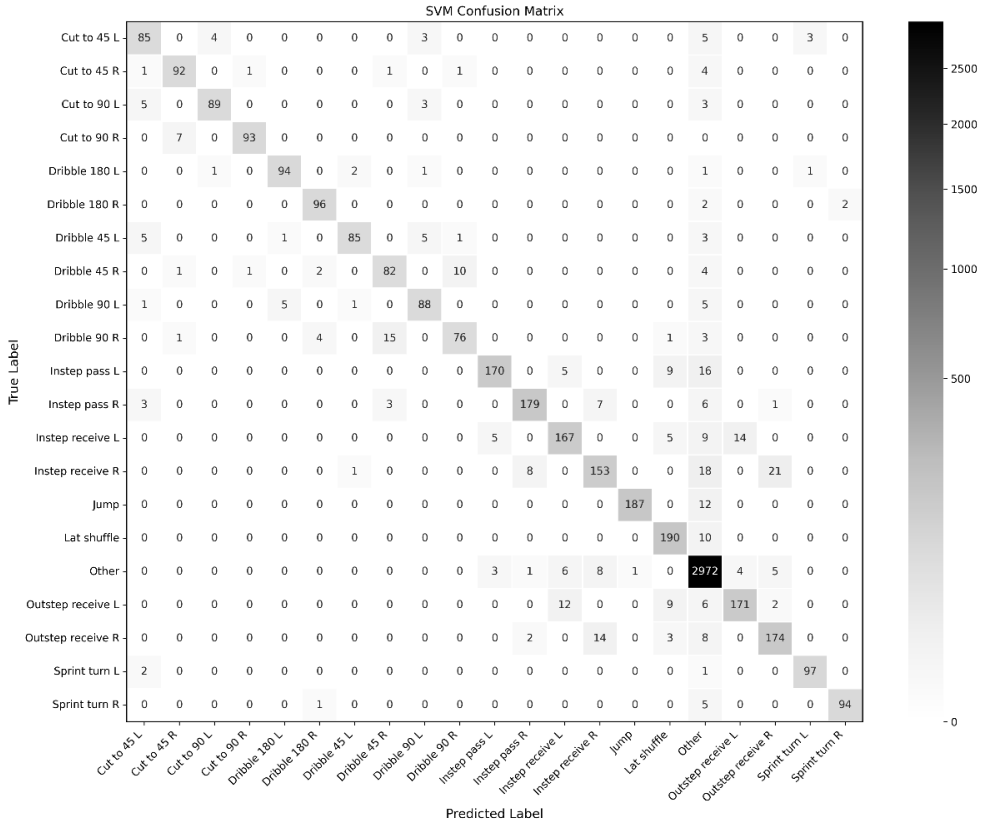


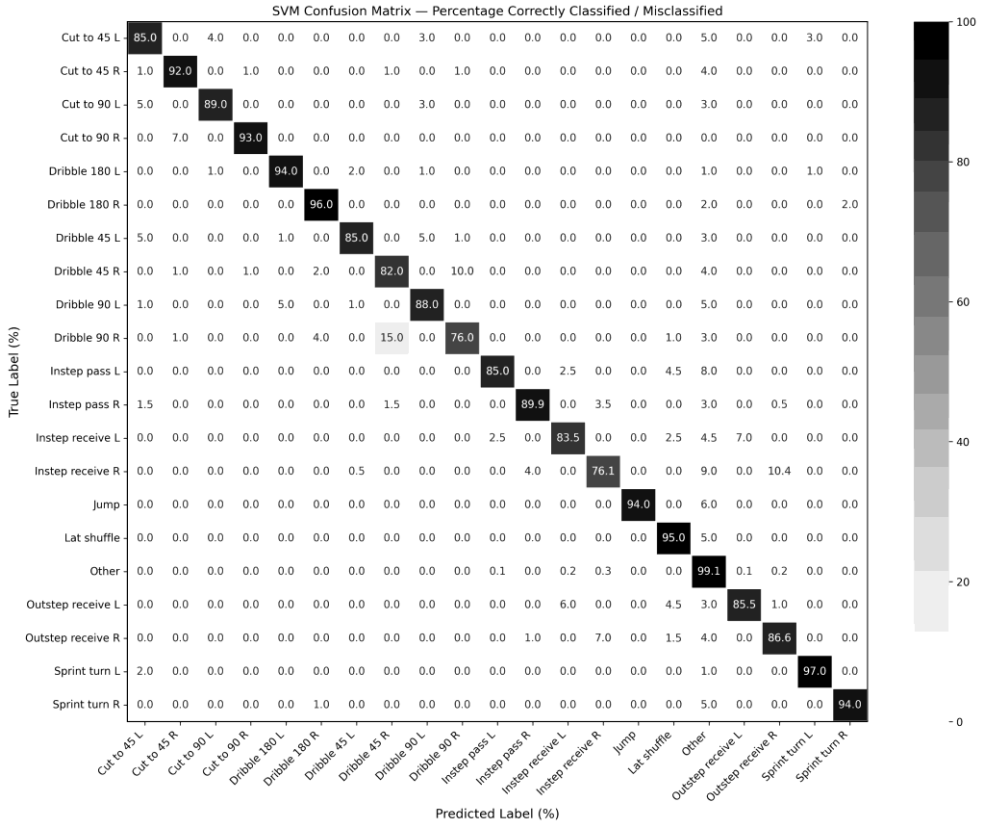
Random Forest



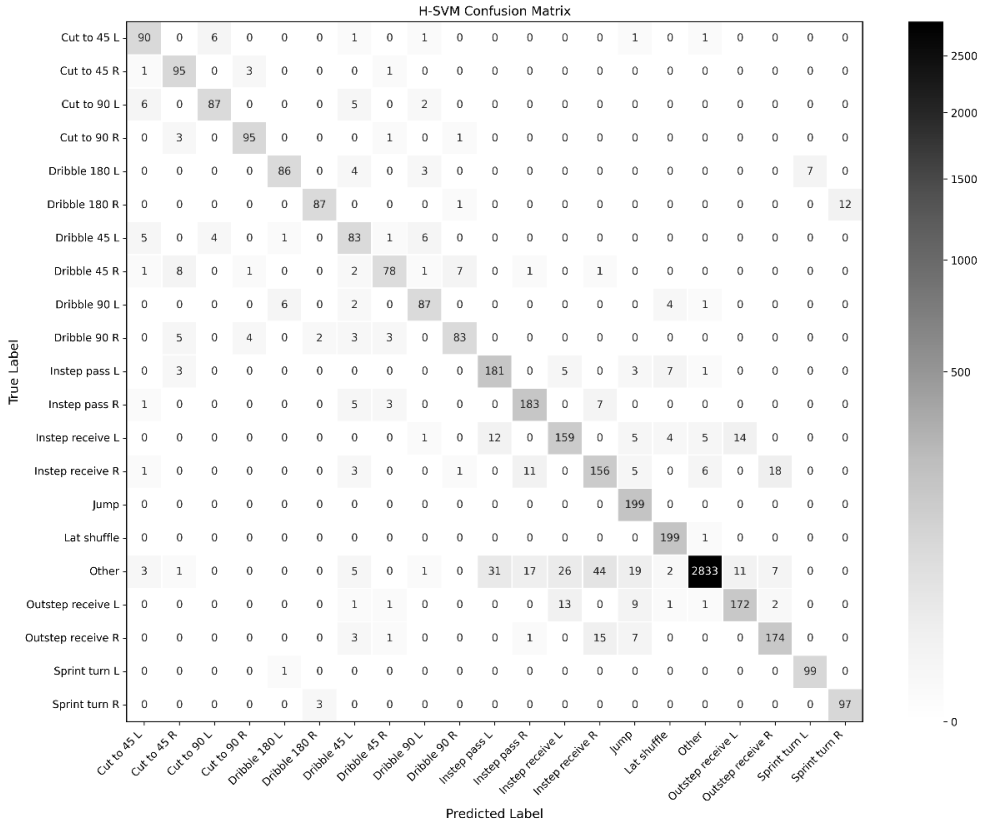


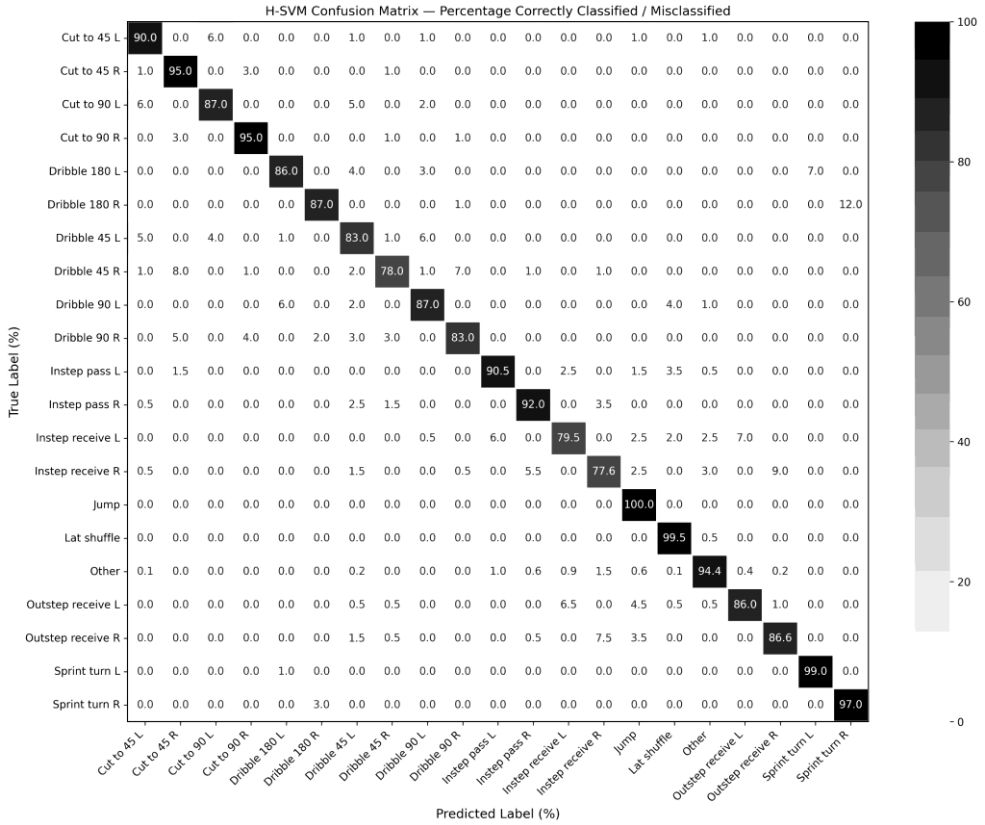
SVM


SVM Confusion Matrix
True Label
Predicted Label
Cut to 45 L
Cut to 45 R
Cut to 90 L
Cut to 90 R
Dribble 180 L
Dribble 180 R
Dribble 45 L
Dribble 45 R
Dribble 90 L
Dribble 90 R
Instep pass L
Instep pass R
Instep receive L
Instep receive R
Jump
Lat shuffle
Other
Outstep receive L
Outstep receive R
Sprint turn L
Sprint turn R
2500
2000
1500
1000
500
0


SVM Confusion Matrix — Percentage Correctly Classified / Misclassified
True Label (%)
Predicted Label (%)
Cut to 45 L
Cut to 45 R
Cut to 90 L
Cut to 90 R
Dribble 180 L
Dribble 180 R
Dribble 45 L
Dribble 45 R
Dribble 90 L
Dribble 90 R
Instep pass L
Instep pass R
Instep receive L
Instep receive R
Jump
Lat shuffle
Other
Outstep receive L
Outstep receive R
Sprint turn L
Sprint turn R
100
80
60
40
20
0

H-SVM


H-SVM Confusion Matrix
True Label
Predicted Label
Cut to 45 L
Cut to 45 R
Cut to 90 L
Cut to 90 R
Dribble 180 L
Dribble 180 R
Dribble 45 L
Dribble 45 R
Dribble 90 L
Dribble 90 R
Instep pass L
Instep pass R
Instep receive L
Instep receive R
Jump
Lat shuffle
Other
Outstep receive L
Outstep receive R
Sprint turn L
Sprint turn R
2500
2000
1500
1000
500
0


H-SVM Confusion Matrix — Percentage Correctly Classified / Misclassified
True Label (%)
Predicted Label (%)
Cut to 45 L
Cut to 45 R
Cut to 90 L
Cut to 90 R
Dribble 180 L
Dribble 180 R
Dribble 45 L
Dribble 45 R
Dribble 90 L
Dribble 90 R
Instep pass L
Instep pass R
Instep receive L
Instep receive R
Jump
Lat shuffle
Other
Outstep receive L
Outstep receive R
Sprint turn L
Sprint turn R
100
80
60
40
20
0